EXPLORING THE ROLE OF DNA DAMAGE, NUCLEOTIDE EXCISION REPAIR, AND CIRCADIAN RHYTHM ON CELLULAR RESPONSE TO PLATINUM-BASED DRUGS

Courtney M. Vaughn

A dissertation submitted to the faculty at the University of North Carolina at Chapel Hill in partial fulfillment of the requirements for the degree of Doctor of Philosophy in Curriculum in Genetics and Molecular Biology in the School of Medicine.

Chapel Hill
2020

Approved by:

Dale Ramsden

Aziz Sancar

Mauro Calabrese

Julie Blatt

David Hsu

ABSTRACT

Courtney M. Vaughn: Exploring the role of DNA damage, nucleotide excision repair, and circadian rhythm on cellular response to platinum-based drugs
(Under the direction of Aziz Sancar)

Platinum-based drugs are a mainstay of solid tumor treatment and act by inducing bulky DNA adducts which should ultimately result in cell death. Unfortunately, these drugs have serious side effects and rates of resistance are high; for example about half of colorectal tumors are platinum-resistant. Understanding the molecular mechanisms of resistance could help maximize efficacy by providing targets to counter drug resistance. The overall purpose of this project is to comprehensively characterize the role of DNA intrastrand adduct formation, nucleotide excision repair, circadian rhythm, and the interplay of these processes in tumor and normal tissue response to platinum-based chemotherapy. To achieve this, we used novel methods to measure repair rates, amounts, and genome-wide patterns at single-nucleotide resolution of multiple tumor models. In a panel of 10 colorectal cancer cell lines, we demonstrate that nucleotide excision repair is not an essential component of platinum resistance as all cell lines have similar nucleotide excision repair efficiencies despite the varying responses. Damage formation, however, may partially dictate oxaliplatin response as lower damage levels correlate with oxaliplatin resistance. While all oxaliplatin-resistant cell lines in this study showed low levels of platinum induced adducts, oxaliplatin sensitive cell lines showed more variation. We next sought to address factors that may lead to this variable damage formation and response in sensitive cell lines. Notably, we

identify a large DNA amplification, containing many cancer related transcripts, specific to the sensitive cell lines with low initial damage. Additionally, damage repair in normal and xenograft tissues appear to oscillate throughout a 24 hour period indicating that treatment timing impacts the platinum-DNA adduct formation. The studies described in this dissertation improve our understanding of the role of DNA damage formation and nucleotide excision repair in response to platinum-based chemotherapy and provide a foundation for understanding how circadian rhythms may impact these factors.

To my grandma for providing constant inspiration and my grandpa for his unwavering belief in me.

ACKNOWLEDGEMENTS

First and foremost, I would like to thank Professor Aziz Sancar for his mentorship and for challenging and inspiring me to constantly improve. I am also very grateful for the support from and discussions with all members of the Sancar laboratory. In particular, I would like to thank Drs. Christopher P. Selby, Laura Lindsey-Boltz, and Yanyan Yang for their guidance through this project. I am also grateful for the collaboration and conversations with the Hsu laboratory. My committee provided helpful feedback and encouragement on my project and pushed me to think more critically, thank you! I am extremely appreciative of Dr. Julie Blatt who served as my clinical mentor the past three years and helped me to see the clinical importance of the work we do. This exposure has been essential to my development as a physician scientist and has shown me the immense impact one person can make.

I have benefitted greatly from being a part of the UNC MD-PhD program and the Genetics and Molecular Biology Curriculum. Thank you to Toni Darville, Mohanish Deshmunk, Alison Regan, Carol Herion, and Amber Brosius for all of your support and for your confidence in me. Thank you to Jeff Sekelsky, Jonathan Cornett, Cara Marlow, and to my GMB colleagues for making graduate school such an enjoyable experience. To the UNC Pediatric Hematology-Oncology group, thank you for letting me be a part of your family and for the immense amount that you have taught me about caring for people. I am incredibly appreciative to the many colleagues and mentors throughout my education who have shaped who I am as a scientist and person.

To my friends, thank you for being such positive constants in my life. To my family, I could not have done this without you. Thank you for all of the love and encouragement at every step leading to this.

TABLE OF CONTENTS

LIST OF TABLES

LIST OF FIGURES

LIST OF ABBREVIATIONS

6-4 PP: 6-4 pyrimidine-pyrimidone photoproducts

CPD: Cyclobutane pyrimidine dimer

NER: Nucleotide Excision Repair

NTS: Non-transcribed strand

RPKM: reads per kilobase per million total reads

TES: Transcription end site

TS: Transcribed strand

TSS: Transcription start site

UV: Ultraviolet

CHAPTER 1: INTRODUCTION[1]

The work in this thesis explores the molecular response to platinum-based drugs, specifically focusing on nucleotide excision repair, circadian rhythm, and the interplay of these two processes. This introduction will present each of these topics individually first and will then explore the work that has been done linking them together.

1.1 Platinum based drugs: mechanisms and resistance

Platinum-based drugs are a mainstay of solid tumor treatment and are used to treat a wide array of cancers including lung, liver, colorectal, testicular, ovarian, head and neck, and cervical cancers (5-7). Cisplatin, the first generation platinum-based chemotherapy, was first approved by the FDA in 1978 and continues to be an effective therapy option. Unfortunately, platinum based drugs are very toxic and patients receiving these treatments can experience numerous side effects including severe emesis, nephrotoxicity, ototoxicity, and neurotoxicity (8). While numerous cisplatin analogues have been tested for anticancer properties, oxaliplatin and carboplatin are the only other platinum-based drugs approved for clinical use by the FDA.

Platinum-based drugs work by creating Pt-d(GpG) adducts with the platinum atom covalently bonding to the N7 nitrogen in adjacent guanines. Once this damage is

[1] Section 1.2 “Nucleotide Excision Repair”, 1.3 “Nucleotide excision repair, cancer, and platinum response” and 1.4.2 “Circadian rhythm control of NER” are reproduced from a chapter written by Courtney Vaughn and Aziz Sancar in an upcoming book . 4. Vaughn, C., and Sancar, A. (2020) Mechanisms and Maps of Nucleotide Excision Repair. in *DNA Damage, Repair, and Disease* (LLoyd, R. S., and Dizdaroglu, M. eds.), Royal Society of Chemistry, London. pp , 4. Ibid.

recognized, the cell can either repair the damage through nucleotide excision repair, ignore the damage through translesion synthesis, or initiate stress signals to induce cell death (5-7). In addition to these intrastrand adducts, platinum-based drugs induce very low levels of interstrand crosslinks and have been shown to induce reactive oxygen species which can in turn damage the DNA.

Despite their common use and effectiveness of platinum complexes, many patients have tumors that are intrinsically resistant to platinum-based drugs and still more will develop resistance. In order for platinum based drugs to induce cell death, the drug must enter the cell, undergo biotransformation, and damage the DNA. The cell must then respond with the correct stress pathways (5). Altering any one of these steps may change how a cell responds to the treatment. A better understanding of the mechanisms of resistance to platinum-based drugs may help us develop better treatment plans for patients. The following sections cover our understanding of the molecular mechanisms of platinum resistance.

1.1.1 Drug Influx/Efflux

Transport of cisplatin, and other platinum-based drugs across the plasma membrane can vary between cells and this variation can lead to differences in platinum-DNA adduct levels. Cells with decreased influx and/or increased efflux of cisplatin will have decreased drug accumulation in the cell leading to lower levels of DNA damage and in turn, less cell death. It is thought that the primary method by which cisplatin enters the cell is passive diffusion. This is supported by the fact that cisplatin uptake directly correlates with cisplatin concentration. Additionally this uptake is not inhibited by platinum analogues which would compete for active transporters (9). It is further

supported by a more recent study that used a stopped-flow kinetic method with lipid vesicles which showed that cisplatin can passively diffuse through cell membranes but that this is regulated by the chloride concentration of the extracellular fluid. Chloride concentration influences cisplatin transport as cisplatin is trapped in the cytoplasm due to dissociation of its chloride ligands. The authors further claim that, given the prominence of passive diffusion of cisplatin, alterations in membrane transport protein for the drug will not be a significant mechanism of resistance (10). A comparison of a cisplatin sensitive non-small cell lung cancer and its derivative cisplatin resistant cell line found that there was no difference in cisplatin uptake (11). In contrast, a number of transporters have been shown to influence influx and efflux of platinum-based drugs. For example, the copper influx transporter CTR1 is implicated in cisplatin resistance and studies have shown that deletion of the *CTR1* gene leads to reduced levels of cisplatin within a cell for the same dose and leads to an increase in cisplatin resistance (12). The human organic cation transporters OCT1 and OCT2 may be involved in oxaliplatin resistance as cells transfected with these genes display increased intracellular oxaliplatin and increased cell death. This was further supported by showing that an OCT inhibitor could attenuate this effect in the OCT transfected cells (13). Once within the cell, platinum-based drugs must enter the nucleus. Knockdown of nucleoporin p62 (NUP62) has been shown to decrease drug sensitivity to cisplatin in ovarian cancer cell lines. This effect can be mitigated by ectopic expression of NUP62 (14).

1.1.2 Cellular Pharmacodynamics

Biotransformation and sequestration

Once within the cell, platinum-based drugs must be hydrolyzed in order achieve their reactive form. This process depends on the release of chloride ions and thus occurs preferentially within cells as opposed to in the blood given the lower intracellular concentration of chloride compared with extracellular chloride concentration (5,15). Once hydrolyzed, cisplatin is an electrophile; while cisplatin will primarily target nitrogen groups in DNA, it can react with other nucleophiles in the cell. Sulfurs can compete with the nitrogen atoms in DNA for interactions with the platinum-based drugs (16). Additionally, availability of purine nucleotides may influence cellular response to cisplatin. Mutations that lead to constitutive activity in both the salvage and *de novo* purine nucleotide biosynthesis increase resistance to cisplatin (17). Melnikov el al proposed that cisplatin can form adducts between ribosomes and messenger RNA, thus inhibiting mRNA translocation and protein synthesis (18). Thus platinum sensitivity can vary between cells based on the levels of alternative interacting partners for the drug.

Adduct formation

We have shown that platinum-induced damage occurs uniformly across the genome in human lymphocyte cells (19). When examined more closely, it appears that DNA confirmation and protein binding can play a role in platinum-induced adduct formation. Platinum-based drugs preferentially form guanine-guanine adducts and cisplatin preferentially damages runs of consecutive guanines (20). In addition to sequence effects, there are claims that DNA conformation may play a role in platinum-induced DNA damage formation (20,21). Higher mutation rates are found both in

actively bound transcription factor binding sites and in the DNA minor groove facing the histone (22,23). However, this increase in mutation rate may be more due to a decrease in repair capacity at these sites since repair machinery would be blocked from the DNA (1,22-24). DNA-protein interactions may also play a role in platinum-induced damage formation. Binding of SP1 family proteins to DNA may enhance adduct formation by bending the DNA to enable increased binding of cisplatin (20).

While DNA is the primary target for platinum-based drugs, factors that influence the biotransformation and activation of the drug along with alternative binding partners may impact how cells respond to the therapy. Additionally, the accessibility of DNA based on chromatin changes may change the platinum-DNA interaction and which damage sites remain in the genome.

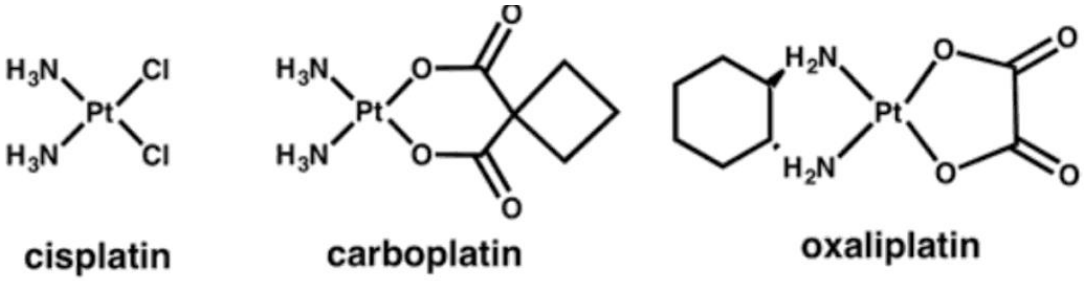

Figure 1.1 (9): Chemical structures of cisplatin, carboplatin, and oxaliplatin (9).

1.1.3 Cellular Response to Cisplatin

1.1.3.1 Signaling pathways

Interactions between cisplatin and the MAPK pathway may play a role in the sensitivity of a cell to cisplatin. Cisplatin has been shown to dissociate cRaf from MEK1 thus inhibiting the pathway and promoting cell death. However, cisplatin resistant cells in turn show higher levels of MAST1 which can replace cRaf to reactivate the MAPK pathway and allow for continued cancer cell proliferation. Treating cells and xenografts

with a combination of cisplatin and a MAST1 inhibitor can re-sensitize these model tumors to cisplatin (25). Low concentrations of cisplatin have been shown to augment activation of ERK1/2 in an ovarian cancer cell line. Furthermore, inhibiting ERK1/2 with protein inhibitor increases the sensitivity of the cells to low dose cisplatin (26). This pattern has also been shown in breast cancer cell lines, where resistance to cisplatin was shown to correlate with increased ERK phosphorylation. Inhibiting this phosphorylation increased the sensitivity of cells to cisplatin. This relationship appeared to be modulated by FEN1 flap endonuclease (27). Inhibiting the MAPK pathway has also been shown to increase sensitivity to cisplatin in an osteosarcoma cell line (28) and HeLa cells (29). In short, activation of the MAPK/ERK pathway appears to correlate with increased resistance to cisplatin (25,27,28,30). Many additional signaling pathways have been implicated in cancer response, include the JNK pathway, NFκB signaling, PD-L1 signaling, ATM, and cell cycle and checkpoints (30-38).

1.1.3.2 Translesion Synthesis

When replication machinery encounters DNA damage, permissive polymerases can bypass the lesion through translesion synthesis. This enables the cell to continue replicating despite the damage, avoiding the need for the cell to send stress signals to induce cell death. Studies have shown that Pol ζ and Pol η can bypass cisplatin-induced di-guanine adducts (39). Further analysis of these polymerases show that the most efficient bypass of these lesions occurs with Pol η inserting a dCTP opposite the 3' guanine of the damage and a four subunit Pol ζ extending the primers (39). A comparison between a cisplatin sensitive non-small cell lung cancer cell line and its derivative cisplatin resistant cell line showed that, while cisplatin uptake and damage

removal were the same between groups, the resistant cell line had increased expression of Pol η, a translesion synthesis polymerase, following cisplatin treatment as compared to the sensitive cell line. The resistant cell line could be re-sensitized to cisplatin by knocking down Pol η (11). Pol η has also been shown to bypass platinum-induced damage and genetic mutations in Pol η can cause increased sensitivity to cisplatin, carboplatin, and oxaliplatin (40). Similarly, cisplatin resistant melanoma cell lines had increased expression of the translesion synthesis polymerase, Pol ζ, following cisplatin treatment. Knocking down Pol ζ in these cells significantly increased sensitivity to cisplatin (41). RAD6, and E2 ubiquitin-conjugating enzyme, is required for translesion synthesis. Knocking down or pharmacologically inhibiting RAD6B restores sensitivity to both cisplatin and oxaliplatin resistant cells. This interaction is mediated by a decrease in translesion synthesis foci in the RAD6B depleted cells (42). Overall, the ability to ignore platinum-induced DNA damage appears to be an important factor in resistance to platinum-based drugs.

Cells can also respond to platinum-DNA adducts by repairing the damage. Platinum induced intrastrand DNA adducts are solely repaired by nucleotide excision repair. The next section will go into more details of the mechanism of nucleotide excision repair.

1.2 Nucleotide Excision Repair

Nucleotide excision repair (excision repair) is the process by which helix-distorting DNA lesions and bulky adducts, such as those induced by UV (ultraviolet

light), cisplatin, cigarette smoke, and aflatoxin, are removed from the genome.(43) The UV-induced DNA cyclobutane dimers (CPDs) and 6-4 pyrimidine-pyrimidone photophroduct (6-4PP), and cisplatin-induced DNA lesions are most commonly formed between adjacent nucleotides on the same strand. Mechanisms for resolving these damages were first suggested by studies that showed bacterial factors could partially resolve the negative effects of UV irradiation if exposed to visible light (44,45). These studies led to the discovery of the direct repair enzyme, photolyase, in *E. coli*. Photolyases are enzymes that when activated by blue light cleave UV-induced DNA damage into two adjacent, normal thymine bases.(46-48) Following UV irradiation, *E. coli* cells exposed to blue light eliminated thymine-thymine dimers, while *E. coli* cells kept in the dark maintained the same level of these adducts. Surprisingly, when glucose was added to the suspension buffer, both *E. coli* cells exposed to blue light and cells kept in the dark exhibited thymine-thymine dimer removal with increased levels of dimers present in small DNA fragments and decreased levels found in bulk chromosomal DNA (49-53). Additionally, small gap synthesis was observed in both *E. coli* and mammalian cells following UV irradiation (52,54). These studies illuminated another repair mechanism that involved the excision of these dimers from genomic DNA, later described as nucleotide excision repair.

The general process of nucleotide excision repair follows 5 steps: (1) bulky adduct damage is first recognized; (2) dual incisions are made on the 5′ and 3′ end of the damage creating a small oligodeoxynucleotides containing the damage; (3) the excised oligodeoxynucleotide is released from the DNA; (4) the remaining gap in the DNA is filled in by repair synthesis; and (5) the newly synthesized DNA is ligated. [43,55-

[59] Of note, while this general process is conserved through evolution, proteins specific to excision repair are not conserved from prokaryotes to eukaryotes.(43) This chapter will cover the specific mechanisms of these steps in mammalian cells, methods for mapping where this repair occurs, the consequences of inadequate repair, and the role of excision repair in disease.

1.2.1 Mammalian Nucleotide Excision repair

1.2.1.1 Global Repair

Human excision repair requires sixteen proteins incorporated into six repair factors to accomplish this as shown in Figure 1.2(1,43,60). Excision repair in humans is initiated by XPC, RPA, and XPA recognizing damage and recruiting the TFIIH repair complex. XPC acts as a molecular matchmaker, using energy from hydrolyzing ATP to bring the factors together into a complex. The TFIIH repair complex includes the helicases XPB and XPD. XPB and XPD help with damage recognition through kinetic proofreading using energy from ATP hydrolysis and unwind DNA to create a repair bubble of about 25 base pairs surrounding the DNA lesion (61-64). XPC then dissociates from the repair complex. This is followed by the recruitment of XPF and XPG which make the 5′ and 3′ incisions respectively. In humans, the 5′ incision is made nineteen to twenty-two bases away from the damage, while the 3′ incision is made five to six bases away from the damage creating an excised oligodeoxynucleotides length of twenty-four to thirty (57,61,63,65,66).

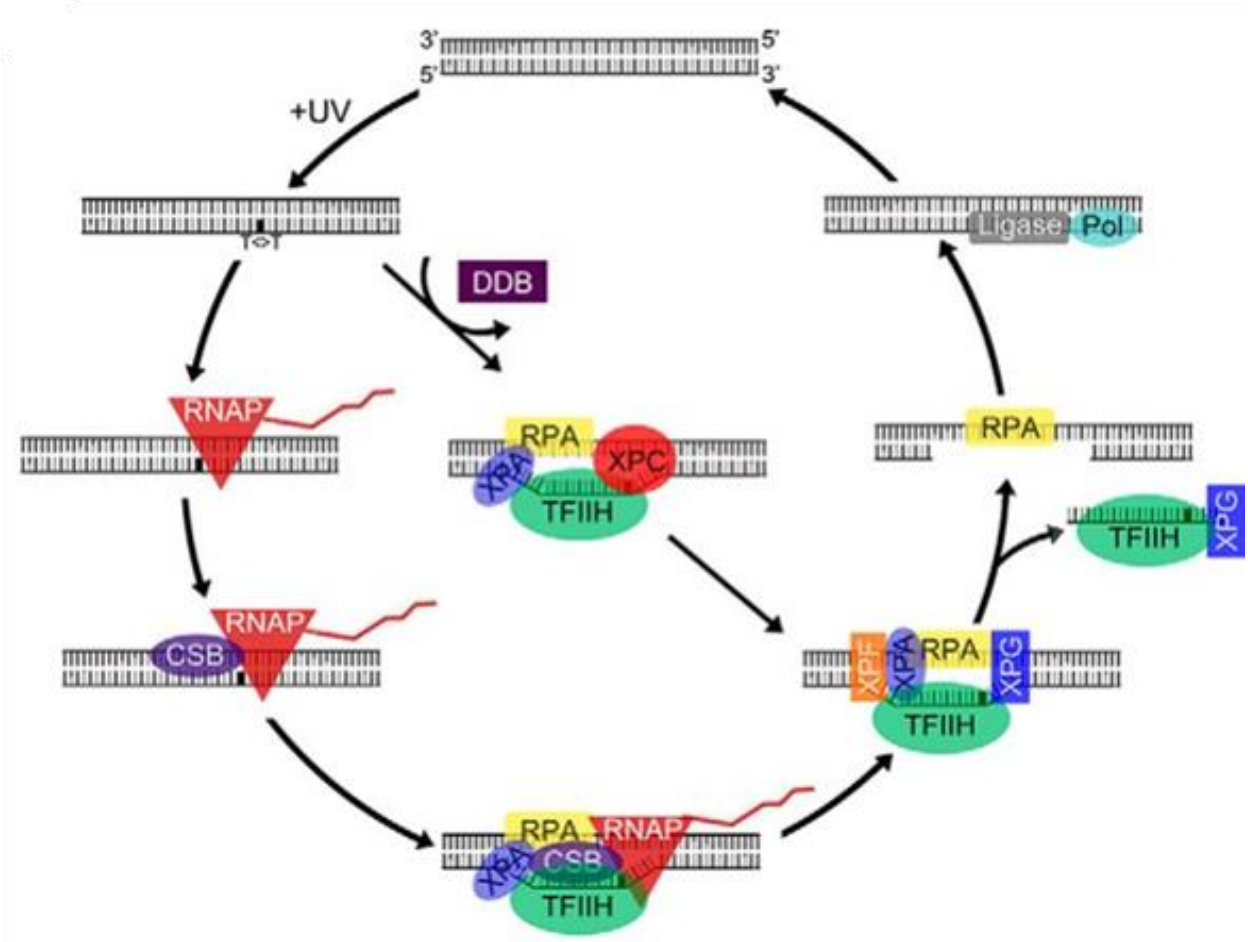

Figure 1.2(1): The molecular mechanism of mammalian NER. DNA is damaged and the damage is recognized either by stalled RNA polymerase and CSB (transcription coupled repair, outer circle) or with the help of an accessory protein (global repair, inner pathway). The damaged DNA is excised in an approximately 26 base pair long oligodeoxynucleotide. The excised oligodeoxynucleotide is released in complex with repair proteins. The gap is filled in with repair synthesis and ligated (1).

The excised oligodeoxynucleotide is then released in complex with TFIIH; this complex is stable for about ten minutes *in vivo* (67). Once TFIIH dissociates from the excised oligodeoxynucleotide, the oligodeoxynucleotide is then degraded by nucleases (67-73). Following the release of the damaged DNA, DNA polymerases fill in the gap in the DNA with repair synthesis. The specific DNA polymerase used for repair synthesis in human cells depends on the cell cycle stage. In proliferating cells, DNA pol δ/ε fill in the gap, while in non-proliferating cells, other polymerases such as DNA pol κ/λ

complete this task (61,63,74). The size of the repair patch is the same size as the gap left following release of the excised oligodeoxynucleotide. This indicates that nick translation is does not occur during this process.(75) Rarely, Exo I extends the excision gap by over twenty additional nucleotides. The single stranded DNA at this gap is covered and protected by RPA and will serve as a signal for ATR checkpoint kinase.(76) After ligation of the repaired patch by either DNA ligase I or the XRCC1-ligase3 complex, the process of excision repair is complete.(61,63,77)

1.2.1.2 Transcription-Coupled Repair

NER can also be transcription coupled in humans in a process depicted by the outer circle of Figure 1.2 (1). RNA polymerase II forms a stable RNA pol II-RNA-DNA complex similar to the complex formed in *E. coli*. While in *E. coli* Mfd is the essential factor to recruit repair factors to the stalled RNA polymerase, in humans transcription coupling of repair is coordinated by the CSB translocases, aided by CSA protein. (19,78,79) When CSB recognizes a stalled RNA polymerase II, it prevents backtracking of the polymerase. It also promotes forward translocation on non-damaged templates such as pause-inducing repetitive A-tract sequences. Likewise, the binding CSB to RNA polymerase II promotes transcriptional bypass of less bulky DNA lesions. The binding of CSB to RNA polymerase II alters the protein interaction landscape of the polymerase. This facilitates the recruitment of excision repair factors and promote subsequent repair of the damaged DNA (80). Of note, when TCR occurs in mammalian cells, XPC is not involved in the repair process.(19,78,79)

1.2.2 Excision Repair Sequencing

XR-seq uses our ability to capture all the small pieces of the excised oligodeoxynucleotides released during excision repair through immunoprecipitations with highly specific antibodies to identify the precise location and relative amount of excision repair throughout the genome. This process can be used to determine what factors influence repair, how repair changes over time, and if repair patterns correlate with response to a damaging agent.(19,24,81)

1.2.2.1 XR-seq method

The ability to isolate the excised oligodeoxynucleotides by immunoprecipitation (IP) of the TFIIH complex created the foundation for mapping repair events throughout the genome at single nucleotide resolution. The detailed protocol has been published [82], and the general procedure is depicted in Figure 1.3.The first step of the XR-seq protocol is to treat cells with a damaging agent (such as UV or cisplatin) and, following a designated incubation time, cells are lysed by homogenization. The lysis procedure and IP antibodies vary depending on the organism being studied. For mammalian cells or

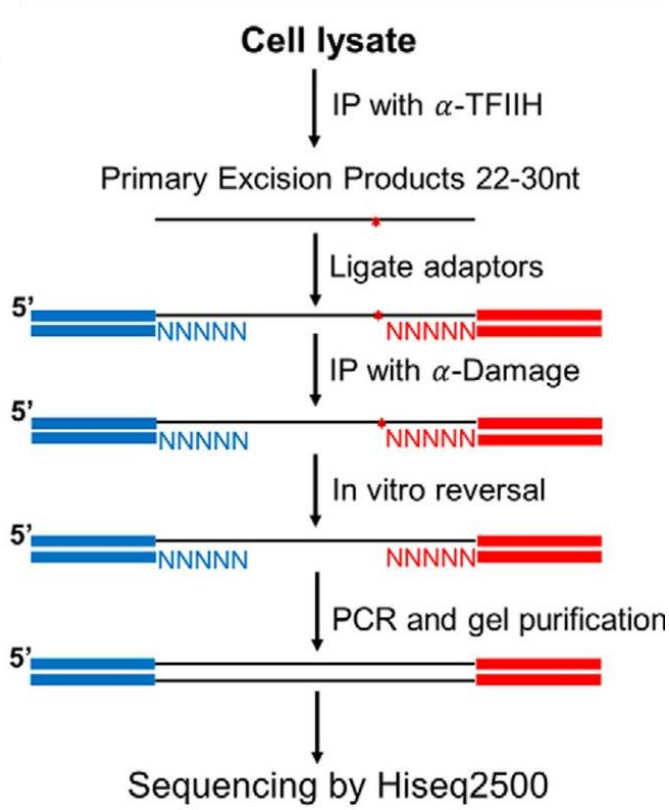

Figure 1.3 (1): XR-seq is conducted by exposing cells to a damaging agent, lysing cells, conducting an IP for repair proteins to extract the excised oligodeoxynucleotides, and purifying and amplifying the oligodeoxynucleotides.

tissue, it is important that the lysis buffer does not contain sodium dodecyl sulfide or any other protein-denaturing factors, as the first IP uses antibodies against repair proteins to purify the excised oligodeoxynucleotides. The excised oligodeoxynucleotides are then eluted and adapters ligated to the oligodeoxynucleotides. Following this step, the excised oligodeoxynucleotides are purified further through a damage IP to ensure that only DNA fragments containing damage are prepared for sequencing. The damage is then reversed to allow for PCR amplification of the excised oligodeoxynucleotides. These samples are then sequenced with NGS. These reads can then be aligned to the genome to show exactly where repair occurs. The excision repair maps show that there are regions of high repair and low repair and can lead to better understanding of what genetic, genomic, and epigenetic features influence repair. The maps also can show repair at specific loci, enabling more thorough studies of how driving mutations occur.(82)

1.3 Nucleotide excision repair, cancer, and platinum response

1.3.1 Xeroderma Pigmentosum

Human excision repair proteins are named for the human disease xeroderma pigmentosum (XP). XP is a hereditary disease that makes patients highly sensitive to UV light with an approximately 5,000-fold increase in sunlight-induced skin cancer compared to people without this disease. In 1968, James Cleaver discovered that these patients were defective in NER.(83) Seven of the key excision repair factors, XPA through XPG, were identified by studying the mutations present in XP patients. The increased risk for skin cancer in these patients is attributed to the inefficient excision repair capacity.(83-85)

1.3.2 Excision repair and tumor response to cisplatin

1.3.2.1 Repair gene variants and alterations in gene expression

Polymorphisms in genes coding for excision repair proteins are reported to be predictive of tumor response to platinum treatment in esophageal cancer cells (86), non-small cell lung cancer (87-90), and in multiple other cancers (91). A number of other variants in genes encoding excision repair factors have been identified as indicators of cancer prognosis and/or treatment response; however, the genes that significantly correlate with outcomes vary between screens, even in similar patient populations. For example, in a screen of 25 single nucleotide polymorphisms (SNPs) in eight excision repair genes, variants in *ERCC1* (Excision Repair Cross-Complementation Group 1) and *XPC* or their regulatory regions correlated with survival in non-small cell lung cancer patients (88). In a separate screen of 173 SNPs in 27 excision repair genes, Song et. al. claim that polymorphisms in *XPA* and *ERCC6* (CSB) were associated with progression free survival in non-small cell lung cancer patients, while polymorphisms in *ERCC6* correlated with overall survival (89). In a third screen of 17 SNPs in eight excision repair genes, only a SNP in *XRCC1* correlated with survival, while *ERCC1* and *ERCC3* (XPB) correlated with platinum response.(90) Interestingly, despite their inclusion in all screens, variants in *ERCC1* and *XPC* were only shown to correlate with survival in one study.

Increased expression and activity of excision repair proteins is reported to correlate with platinum resistance in many cancers including ovarian (92,93), testicular (94), lung (95-97), melanoma (98), nasopharyngeal (99-101), pancreatic (102), and colorectal cancer (91,103). However, similar to the studies on genetic variants, the

correlations can be inconsistent between studies of similar patient populations. High *ERCC1* mRNA expression in non-small cell lung cancer tumor cells has been shown to correlate with poor disease-free survival in patients, independent of treatment with a platinum agent (104). Likewise, non-small cell lung cancer patients with low *ERCC1* expression levels benefitted more from cisplatin treatment than patients with high *ERCC1* expression levels (105). In patients with gastric cancer who were treated with surgery alone, low *ERCC1* mRNA correlated with longer overall survival. However, *ERCC1* mRNA levels could not serve as a prognostic factor for patients with breast cancer.(104) In a cohort of head and neck squamous cell carcinoma patients, it was found that there was no significant correlation between expression levels of *ERCC1*, *XPA*, or *XPF* and overall survival. However, when the cohort was broken down based on the site of the tumor, it was found that *ERCC1* expression correlated with survival in patients with oral cavity tumors, while *XPA* expression correlated with survival in patients with oropharyngeal tumors(101). In a comparison of platinum-sensitive and platinum-resistant gastric cancer cell lines, it was found that the platinum-sensitive cell line had lower levels of *XPC* leading to impaired repair and higher induction of cell death.(106) The mRNA levels of twelve DNA repair and multi-drug resistance genes were tested for correlation with cisplatin resistance and it was found that abundance of *ERCC2* (XPD), *XPA*, and *XRCC1* correlated with cisplatin resistance.(107) In effort to better account for the complexity of the repair pathways, Kang et al(108) determined a molecular score for DNA damage repair pathways based on expression levels of 23 platinum-repair related genes. Higher scores on this molecular panel correlated with improved survival and response rate.

1.3.2.2 Repair capacity

A number of studies have explored the platinum sensitizing effect of knocking down expression levels of genes encoding excision repair factors. Knocking down *CSB* in either a prostate or colorectal cancer cell line, increased tumor cell sensitivity to cisplatin, independent of p53 or mismatch repair status.(109) Furthermore a CRISPR/Cas9 screen identified transcription-coupled excision repair as a protective mechanism against cisplatin-induced cell death.(110) Likewise, knocking down both *ERCC1* and *XPF* lead to decreased repair of cisplatin-induced DNA damage and increased cisplatin-induced cell death in non-small cell lung cancer cell line.(111) Small molecule inhibitors of ERCC1-XPF also decreased DNA repair and increased cytotoxicity following treatment with cisplatin in lung cancer cell lines.(112)

Despite the studies linking excision repair efficiency to response to platinum-based drugs, there are a number of confounding factors in this connection. Most excision repair proteins serve multiple functions and do not act alone. A study on neuroblastoma cells showed that resistance to platinum-based drugs is likely related to mechanisms preventing platinum from binding to DNA and mechanisms that inhibit the downstream cell death signaling. The study also showed that resistance is not directly dependent on enhanced DNA repair capacity.(113) Furthermore a comparison between a cisplatin-sensitive non-small cell lung cancer and its cisplatin-resistant derivative cell line showed that there was no difference in platinum-induced DNA damage removal between the two cell lines.(11) A recent review on the topic pointed out more inconsistencies in our current understanding of the role of repair as a mechanism of

resistance. It called for new studies to examine repair with a more definite method than those used in previous experiments.(114)

Overall, while deficiencies in excision repair can increase susceptibility to cancer, the role of excision repair in a tumor cell's response to cisplatin and its derivatives is still unclear.

1.4 Circadian rhythm

1.4.1 Mechanism of circadian rhythm

The molecular circadian rhythm is a transcription-translation feedback loop comprised of two transcriptional activators, Clock and BMal1 and their inhibitors, Cryptochrome (Cry) 1 and 2 and Period (Per) 1 and 2. Clock and Bmal1 activate the transcription of *Cry1*, *Cry2, Per1,* and *Per2* by forming a heterodimer and binding the E-box element in Cry and Per promoters. Once transcribed, the *Cry* and *Per* transcripts are translated into proteins which heterodimerize and ultimately enter the nucleus. Once in the nucleus, the Cry-Per complexes inhibit Clock and Bmal1 from activating transcription. Inhibiting transcriptional activation by Clock and Bmal1 in turn decreases the expression levels of Cry and Per which ultimately attenuates the inhibition of the Clock-Bmal1 activator complex allowing the cycle to start again (Figure 1.4). This entire process takes approximately 24 hours (115-122). The circadian rhythm regulates cell processes as the expression of approximately 10% of genes in a given cell are regulated by Clock-Bmal1 transcriptional activation (123). Thus as the activity of Clock and Bmal1 oscillates throughout the 24 hour cycle, so too does the expression of any gene under their control.

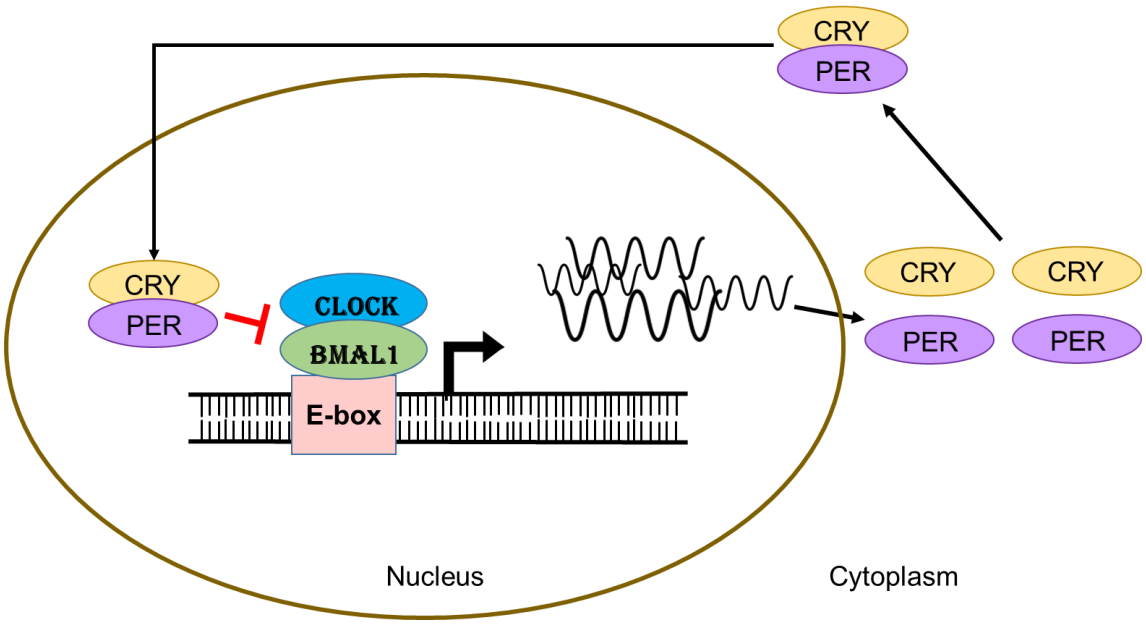

Figure 1.4: The molecular circadian clock. The Clock and BMal1 heterodimer binds E-box domains in the promoter regions of clock controlled genes, including Cry and Per, and activates their transcription. Once translated into proteins, Cry and Per form an inhibitory complex, enter the nucleus, and inhibit Clock and Bmal1. This in turn decreases transcription of Cry and Per, reducing the inhibition of Clock and Bmal1 and allowing the process to start again.

In mammals, the molecular clock in each cell is synchronized, creating tissue- and organism- wide rhythms. These rhythms are synchronized by signals released from the suprachiasmatic nucleus (SCN) in the hypothalamus. The SCN serves as the master clock, synthesizing information from environmental input, such as presence or absence of light through connections with retinal ganglion cells, and releasing signals to regulate the molecular clock in peripheral tissues (115,124). While many cellular and physiologic processes are regulated by the circadian rhythm, we will focus on the connection between circadian rhythm and nucleotide excision repair.

1.4.2 Circadian rhythm control of NER

XPA, a rate limiting protein in nucleotide excision repair (125), is under circadian control in mice. This means that the expression of the *XPA* gene is controlled by the

core circadian clock transcription translation feedback loop, oscillating with a 24 hour period (125-127). The studies that defined this pattern show that XPA gene expression peaks at 5pm and troughs at 5am (see top left panel of Figure X.7). Total excision repair oscillates in the same manner (126). Furthermore, TCR of a circadian controlled gene fluctuates following the oscillatory expression pattern of the gene (128).

Given that excision repair is the sole repair mechanism for UV damage in mouse skin cells and that UV exposure can induce invasive skin tumors, it follows suit that exposure to UV at different circadian times would lead to different effects on tumorigenesis. If this connection is true, UV exposure at times of lower levels of excision repair would lead to increased numbers of tumors compared to mice treated at times of higher levels of NER. To test if the cyclical pattern of excision repair had a physiological impact, mice were exposed to UV irradiation at either 5am (minimum repair) or 5pm (maximum repair). Decreased excision repair efficiency does appear to increase risk of tumor development in response to UV. As shown by Gadammedhi et al in the top right and bottom panels of Figure 1.5, mice exposed to UV at the minimum excision repair time-point had a 4-5 fold increase in invasive skin carcinoma development compared to mice treated in the maximum excision repair time-point. It is still unclear if excision repair is under circadian control in humans. Thus, future studies are needed to determine if response to bulky-adduct formation varies depending on the time of day in humans (2).

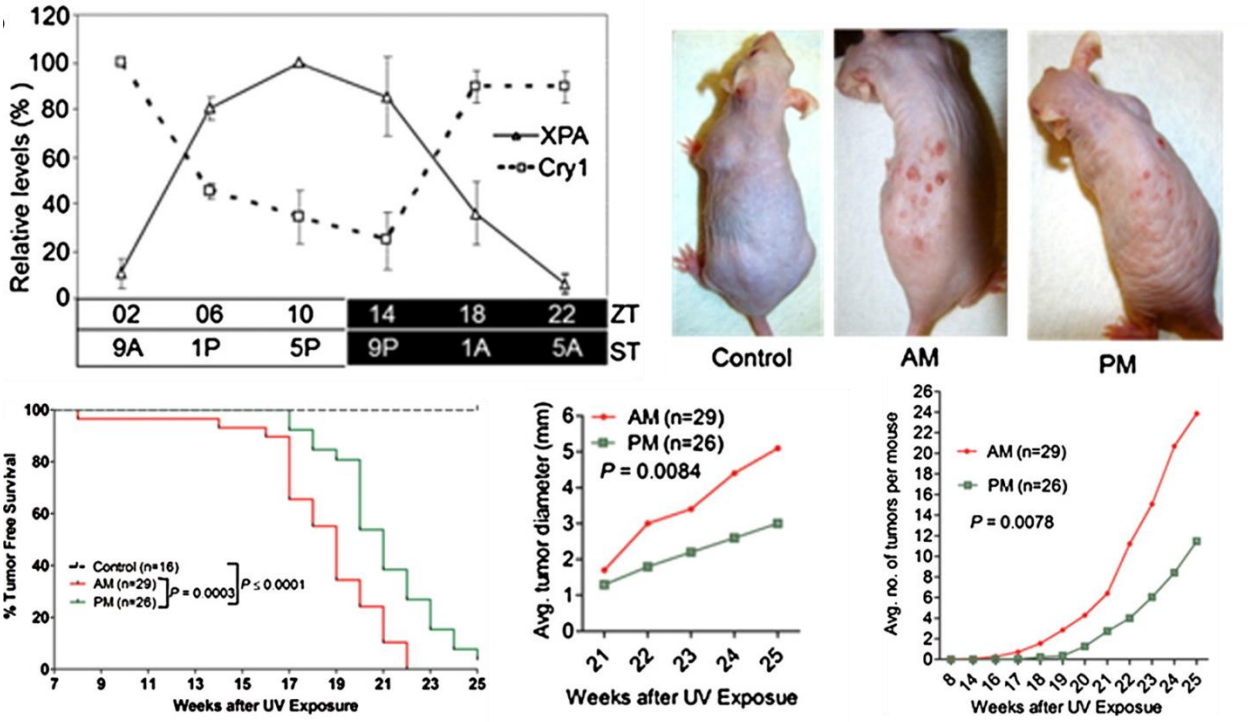

Figure 1.5 (2): XPA is under circadian control (top left) and is antiphase with cryptochrome, a core circadian factor. Mice exposed to UV in the morning develop more and larger tumors than mice exposed to UV in the evening (top right and bottom) (2).

1.5 Study rationale

Despite numerous studies exploring the role of nucleotide excision repair in directing platinum response, it remains unclear if improved repair efficiency is an essential factor in conferring resistance. Additionally, while we understand how some physiologic cues may alter nucleotide excision repair efficiency, it is still unclear how these regulators impact the response of tissues to platinum- based drugs. We aim to better understand the role of repair in platinum response both by characterizing repair in cell lines with varying responses to platinum-based drugs and by profiling how alterations in repair efficiency within the same tissue, controlled by circadian rhythm, direct changes in response to platinum-based drugs. To this end, we used the key methods of studying nucleotide excision repair (chapter 2) and compared damage

formation and repair in platinum sensitive and platinum resistant colorectal cancer cell lines (chapter 3). We then use this repair data to further explore factors that lead to differing responses to similar damage levels in chapter 4. In chapter 5, we use patient derived xenografts and to understand how environmental cues impact repair and platinum response. This model also enables us to test if the findings from our cell line work are recapitulated in an organism. Overall, this project aims to improve our understanding of the molecular response to platinum-based drugs and to begin to apply these mechanisms to creating more effective treatment plans for patients.

1.6 Thesis Contributions

The work described in this thesis involved essential collaborations. For chapter 2 the original excision assay protocol was provided by Dr. Yanyan Yang in our lab. In chapter 3, the initial oxaliplatin repair kinetics experiments were conducted by Dr. Christopher Selby and set the foundation for that project. Chapters 3 and 4 utilized the High Throughput Sequencing Facility at UNC to conduct NextGeneration sequencing on our XR-seq libraries. Additionally, original XR-seq analysis pipelines from Drs Sheera Adar, Ogun Adebali, and Yanyan Yang as well as skills learned from the Practical RNA Sequencing course taught by Drs Mauro Calabrese, Hemant Kelkar, and Joel Parker proved essential in the analysis of XR-seq data. The PDXs and cell lines used in chapter 5 were created and provided by the Hsu lab (Wayne Glover and Gabrielle Rupprecht). The PDX and mouse tissue collection were conducted jointly by Dr. Yanyan Yang and myself. Blood samples from the chronotoxicity studies in chapter 5 were processed by the Animal Histopathology and Laboratory Medicine core facility to obtain blood urea nitrogen and serum creatinine levels.

CHAPTER 2: OPTIMIZATION OF THE EXCISION ASSAY

2.1 Introduction

The initial studies of the mechanism of nucleotide excision repair involved "*in vitro*" experiments using labeled, damaged substrate and either cell free extract or purified proteins. To better understand nucleotide excision repair within a cell, the "*in vivo*" excision assay (here on referred to as the excision assay) was first described in 2013 (67). This method was expanded on and converted to a non-radioactive method in 2014 (129). The excision assay has been used to better understand nucleotide excision repair in cells and to characterize differences in repair over time, between different cell or tissue types, and between varying damaging agents (129-134).

The excision assay enables us to visualize the amount of repair occurring in a cell. Briefly, this is done by extracting, labeling, and imaging the excised oligomer released during nucleotide excision repair. More specifically, the excision assay starts by treating cells with a damaging agent and allowing cells a set amount of time to repair. Following the repair incubation, cells are lysed and spun down. The soluble fragment is then used for an immunoprecipitation with an antibody against a nucleotide excision repair protein complexed with the excised oligomer or against the DNA damage itself.

After eluting the IP, the excised oligomer is purified and labeled with radioactivity. The sample is purified again and then run on a sequencing gel for imaging.

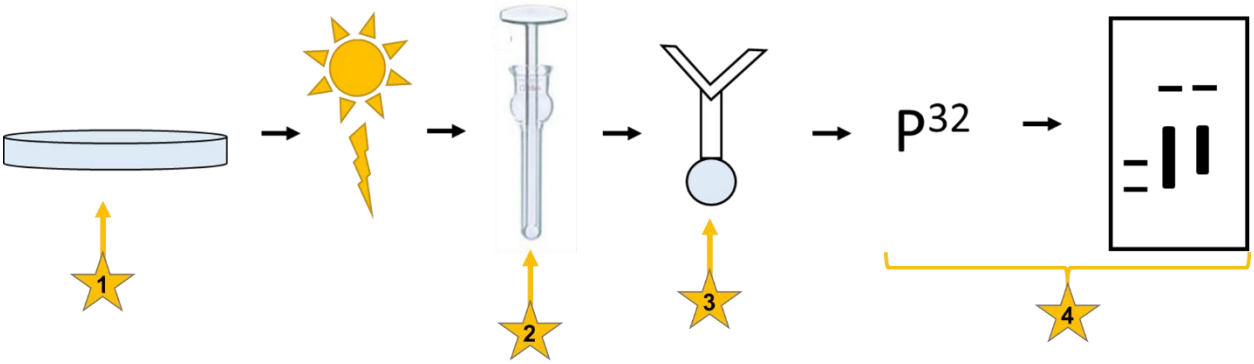

Figure 2.1: General schema of the excision assay protocol with stars and arrows indicating critical points of variation (listed in the introduction). In brief, cells are plated and allowed to grow to 100% confluence. Plates of cells are then treated with a damaging agent, and lysed via homogenization. The soluble fragment of the lysed cells is then used for an immunoprecipitation with antibodies against the repair factors. The excised oligomers are then eluted, purified, and labeled with radioactivity. Labeled samples are then run on a sequencing gel, exposed to a phosphor-imager, screen, imaged, and quantified.

While this method has proven useful, its use as a qualitative or semi-quantitative assay rather than a quantitative assay limits the breadth of its use. Within this protocol, the critical points for variation are (1) the damaged cell line input, (2) the cell lysis, (3) the immunoprecipitation, and (4) radiolabeling and quantification of the samples (Figure 2.1). We aimed to better characterize the efficiency of these steps and to identify ways to make the excision assay more quantitative.

2.2 Methods

2.2.1 Excision Assay Protocol (67,68)

Cell treatment:

1. Treat cells with desired damaging agent (ie UV or platinum) and return to the incubator for repair incubation.

a. If treating with UV, wash cell plates with room temperature PBS and remove all PBS immediately prior to treatment to remove any UV absorption by the media. Add fresh media to the plates immediately following treatment.
b. If treating with a platinum, dissolve the drug in DMSO to be a 20mM solution and then dilute into the media in the cell plates accordingly for the desired dose. Platinum damage does not produce a strong signal on excision assay, so start by scaling up the number of plates you use. It is also recommended to include a UV treated plate as a positive control- treat with 20J/m^2 and leave the cells for 30 minutes before following the rest of the protocol.

2. After the designated repair incubation, place the plates on ice, wash with cold PBS, add about 5mL of cold PBS to each plate, and use a cell scraper to collect cells from the plate into a falcon tube (15mL or 50mL depending on the number of plates used).

Low Molecular Weight DNA Isolation

3. Transfer the cells into a 15 ml tube (use 50 ml tube for large scale) and pellet them by centrifugation at 2,500 rpm for 4 min (5 min for 50 ml tube).
4. Discard the supernatant and re-suspend the cells in 0.5mL ice cold Buffer A/per plate
5. Incubate them in ice for 10 min.
6. Transfer the re-suspended cells to an ice-cold dounce homogenizer/tissue grinder and lyse them on ice with 80 strokes using a *tight* plunger (carefully remove small pieces connective tissue).

7. Transfer the lysed cells into 1.7 ml (or 2 ml) tube and pellet the chromatin fraction by centrifugation for 30 min at 14,000 rpm in the 4 ^{o}C cold room.
8. Take out the supernatant and put it into a new 15 ml tube (or 1.7mL if it will fit).

Immunoprecipitation with anti-TFIIH antibody

9. Add 8 µL anti-XPG and 10µL RNaseA (Sigma R4642) per plate into the supernatant
10. Add 12.5 µL/per plate of IgG of blocked protein A/G PLUS-agarose (Santa Cruz sc2003) in Buffer A (50%) and incubate overnight. (The beads should be washed and blocked by 0.2 mg/ml BSA and re-suspended in Buffer A as 50% slush before using it.)

For blocking the beads:

A. Spin down the original beads (1:3) at 2, 000 rpm for 2 min.
B. Wash the beads 2 times using Buffer A.
C. Re-suspend beads in 500 µL or 1 ml Buffer A.
D. Add 2% volume of 10 mg/ml BSA and incubate at 4 ^{o}C for 2-3 hrs.
E. Wash the beads 2 times using Buffer A.
F. Re-suspend beads in the same volume of Buffer A.
G. Store the BSA blocked beads at 4 ^{o}C.

11. Put the samples onto the rotator and rotate overnight at 4^{o}C
12. Spin down the beads at 2, 800 rpm for 1 min and discard the supernatant.
13. Wash the beads 2 times with 1 ml of Buffer A and 2 times with 1 ml of Buffer B at 4 ^{o}C. (*Rotate at 4°C for 5 min each wash*)
14. Remove all the supernatant at the last wash.
15. Prepare 400uL Buffer C with 2fmol spike-in 50mer DNA per sample

16. Add 200 µL Buffer C to each sample and incubate at 65 ^{o}C for 10 min to elute the DNA. (Vortex the sample every 1-2 min)
17. Spin down the beads at 3, 500 rpm for 1 min, transfer the supernatant into a new EP tube, add 2µL proteinase K to eluted DNA and incubate at 55 ^{o}C for 10 min.
18. At the same time repeat steps 21 and 22: Add 200 µL Buffer C to each sample, incubate at 55 ^{o}C for another 10 min and spin down.
19. Transfer the 200 µL eluted DNA into the tube containing 200 µL eluted DNA and 2 µL Proteinase K.
20. Incubate at 65 ^{o}C for another 10 min.

DNA isolation

21. Add 1 volume of phenol-chloroform and vortex briefly.
22. Centrifuge at 14,000 rpm for 5-7 min and transfer the upper layer into a new EP tube.
23. Repeat steps 21 and 22.
24. Add 0.11 volume of 3M NaAc (pH5.2) and mix well before adding 2.5 volume of cold 100% ethanol and 1 µL Glycogen.
25. Invert several times to mix it and put the tubes at -20 ^{o}C overnight.
26. Centrifuge at 14,000 rpm for 30 min in the cold room to pellet the DNA.
27. Remove the residue liquid carefully and air dry the pellet. (A*void over drying; the pellet should not become clear*)

Radio-labelling

28. Label purified DNA by TdT enzyme and ^{32}P-cordycepin:
    a. Dissolve the sample in 5 uL molecular grade water with 1mg/mL BSA

b. For each sample add 1 uCi ^{32}P-cordycepin, 1 uL TdT, 5 uL TdT buffer, 5uL $CoCl_2$, and 34 uL molecular grade water with 1mg/mL BSA (*pre-making this mix for all samples and store on ice to ensure equal amounts of reagent between all samples. Add TdT and ^{32}P-cordycepin just before addition of labeling mix to samples*)
c. Incubate purified DNA and labeling at 37 ^{o}C for 90 min.

29. Add 1 volume of phenol-chloroform and vortex for a few seconds
30. Centrifuge at 14,000 rpm for 4 min and transfer the upper layer into a new EP tube.
31. Repeat steps 29 and 30
32. Add 2.5 volume of 100% ethanol, 0.11 volume of 3M NaAc.
33. Invert several times to mix it and put the tubes at -20 ^{o}C overnight.
34. Centrifuge at 14,000 rpm for 30 min in the cold room to pellet the DNA.
35. Remove the residue liquid carefully and air-dry the pellet. (*avoid over drying*)
36. Dissolve the pellet with 6 µL loading buffer.
37. Heat it at 90 ^{o}C for 1 min.
38. Immediately place samples on ice after denaturation.
39. Once samples have cooled, centrifuge all samples briefly and place back on ice.
40. Load the samples and radio-labeled marker on a large 10% gel with urea (after pre-run for >30min).
41. Run the gel at 25-35W (2000V, 35mA) until the blue dye is 5-8 cm from the bottom then raise to 60W until the blue dye is 1-3 cm from the bottom. Stop running and transfer the gel to filter paper, wrap it.
42. Dry the gel for ~90 minutes and expose it to phosphoimager overnight.

43. Scan and image the gel on the Typhoon detection system. Signal can be measured using ImageJ software.

Solutions

A. Buffer A (25 mM Hepes pH 7.9, 100 mM KCl, 12 mM $MgCl_2$, 0.5 mM EDTA, 2 mM DTT, 12.5% glycerol, 0.5% NP-40) put in 4 degree.
B. Buffer B (25 mM Hepes pH 7.9, 100 mM KCl, 12 mM $MgCl_2$, 0.5 mM EDTA, 2 mM DTT, 12.5% glycerol, 1% NP-40) put in 4 degree.
C. Buffer C (10 mM Tris-Cl pH 7.5, 1 mM EDTA, and 1% SDS)
D. 10x Hybridization Buffer (100mM Tris-HCl pH7.5, 1M NaCl, 1mM EDTA)
E. Elution Buffer (10mM Tris-HCl pH8.5)
F. PEX buffer (1X PBS, 2mM EDTA, 0.01% Triton X-100)
G. PEXB buffer (1X PBS, 2mM EDTA, 0.01% Triton X-100 and 0.025% BSA [10mg/ml BSA equal 1% BSA]), add BSA when use PEXB buffer.

Buffers for IP assay

Reaction Buffer

Reagent	Amount	Final concentration
Tris-Cl pH 8.0 1M	1ml	20mM
EDTA 0.5M	200ul	2mM
Triton X-100	500ul	1%
NaCl 5M	1.5ml	150mM
Sodium Deoxycholate 10%	2.5ml	0.5%
SDDW	To 50ml	

Total	50ml	

Filter. Store at Room temp.

Elution buffer

Reagent	Amount	Final concentration
SDS 10%	2ml	1%
NaHCO3 1M	1ml	50mM
SDDW	To 20ml	
Total	20ml	

Filter. Store at Room temp.

2.2.2 Measuring the efficiency of the excision assay

To measure the efficiency of individual steps within the protocol, cells were treated with 25 J/m^2 of UV and underwent a repair incubation of 30 minutes. Samples were processed together up until the designated step and then split in half for the remainder of the protocol. DNA, RNA, and protein concentrations were measured either by DeNovix Inc Spectrophotometer or by ThermoFisher Scientific Fluorometric Quantification.

2.2.3 Cell free extract repair of damaged plasmid

To create a purified, damaged plasmid, a control, undamaged, double stranded DNA plasmid was treated with 100 J/m^2 UV. The damaged plasmid then underwent two sequential immunoprecipitations using antibodies against and 6-4 pyrimidine-pyrimidine dimer (6-4PP) to purify the sample such that on damaged plasmids remained. We chose to IP for 6-4 PP as it is a more easily recognized damage than CPD and was thus more likely to be repaired by cell free extract. The damaged plasmid was incubated with

cell free extract (plus reaction buffer, ATP, BSA, and water) for 1.5 hours at 30°C to allow for nucleotide excision repair to occur. An XPG IP was then conducted using this solution and the remainder of the excision assay protocol was conducted.

2.3 Results

2.3.1 Determining the efficiency of excision assay steps

Testing Experimental Variation of the Excision Assay

In order to identify the amount of variability in excision assay results due to inefficiencies in the protocol itself, we treated a plate of cell with 25 J/m^2. After collecting cells and thoroughly re-suspending them in Buffer A, we split the sample into two equal halves and processed the samples together for the remainder of the protocol. We calculated the percent difference between two technical repeats for five biological repeats. This analysis indicates that there is 30% difference between technical replicates with a range from 6% to 60% (Figure 2.2).

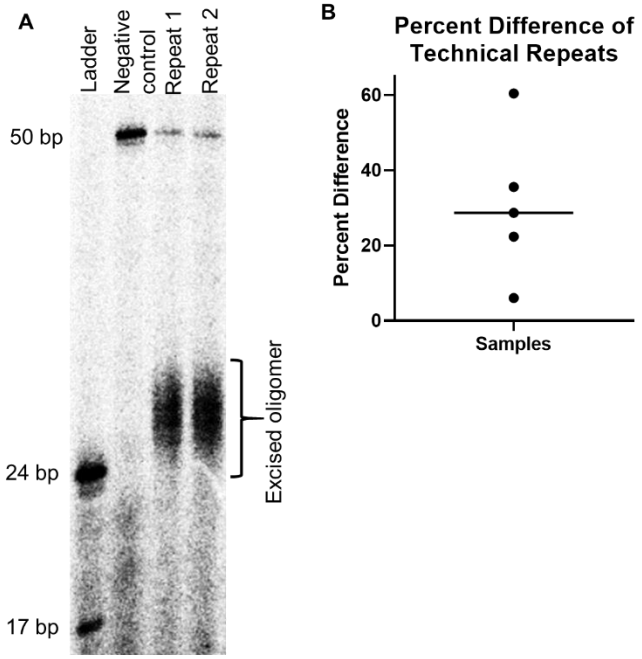

Figure 2.2: Technical variability in the excision assay. One plate of cells per sample was treated, collected, re-suspended in Buffer A, and split into two equal halves. These samples were then processed at the same time for the remainder of the protocol to characterize technical variability. (A) An example excision assay of technical repeats. Lane 1 contains a ladder to indicate where the excised oligomer should be and lane 2 contains an un-treated, negative control sample. Lane 3 and 4 contain the two technical repeats. (B) Percent difference (differences between replicates/average of replicate) between technical replicates for the five samples show that the average difference is 30% (range from approximately 6% - 60%)

This indicates that, not only is there technical variation, this variation is not constant. Thus we aimed to determine the efficiency of the critical steps of the excision assay.

Lysing efficiency

To determine the efficiency of the Buffer A homogenization lysis step, we collected cells and counted the amount of cells per cell line. From each plate, we then created two equal samples of either 500,000 cells or 2,500,000 cells. Cells were then lysed following the specification in the protocol above (steps 4-6). DNA, RNA, and protein concentration were measured to determine the reproducibility of lysis between each sample. Reproducibility between two equal samples of cell lines from the same plates was measured as percent difference. Averaged between DNA concentration, RNA concentration, and protein concentration, there appears to be approximately 12% variability in lysis efficiency between samples.

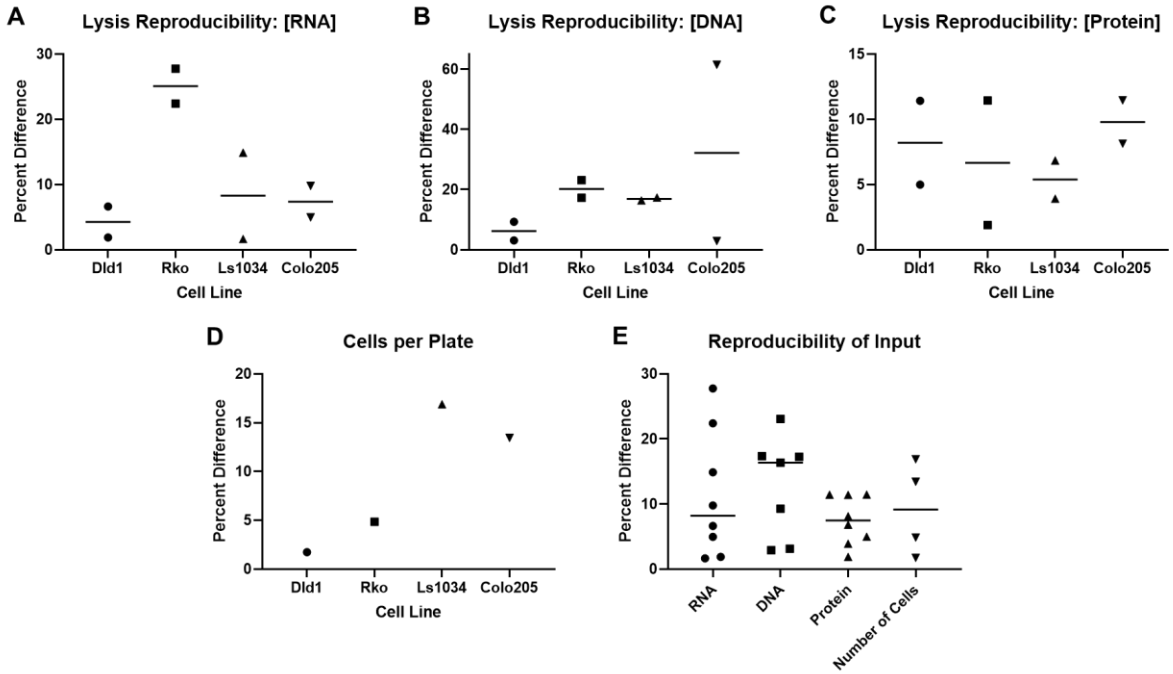

Figure 2.3: Measurements of the reproducibility of lysis efficiency. One plate of cells per sample were collected and cell number was counted. Cells were diluted to two samples of either 500,000 cells or 25,000,000 cells in Buffer A. Samples were then lysed by homogenization. To test reproducibility of lysis efficiency we measured the percent difference between two technical repeats for the concentration of (A) RNA, (B) DNA, or (C) protein. (D) Since input to the excision assay is often counted in plates, we tested the reproducibility of cell number per plate. The percent difference between plates varies between cell lines. Cell lines that grow in a diffuse monolayer (DLD1, RKO) have higher reproducibility than cell lines that grow more in clusters (Ls1034, Colo205). (E) Summary of panels A-D.

Figure 2.3 displays the percent differences between two equal samples for DNA, RNA, and protein concentration broken down by cell line. Interestingly, the reproducibility appears to vary based on cell line as well. We also tested the reproducibility of the number of cells per 100% confluent plate since the input for the excision assay is often quantified by number of plates of cells. Cell lines that grow to confluence as a monolayer had lower levels of variability (<5%) than the cell lines that grow in clusters (>13%). Taken together, this indicates that some of the variability between experiments may be due to variations in lysis efficiency and input however the amount of variation this step accounts for differs between cell lines.

Immunoprecipitation efficiency

To test the efficiency of the TFIIH IP, we ran two a second successive IP using the same antibody on the supernatant from the first IP. This enabled us to test if the first IP retained all excised oligomer or if excised oligomer remained in the IP supernatant due to an inefficient IP. We found that the TFIIH IP was relatively efficient with an

average of ~16% of total signal from both IPs obtained from the second IP (Figure 2.4A, 2.4B).

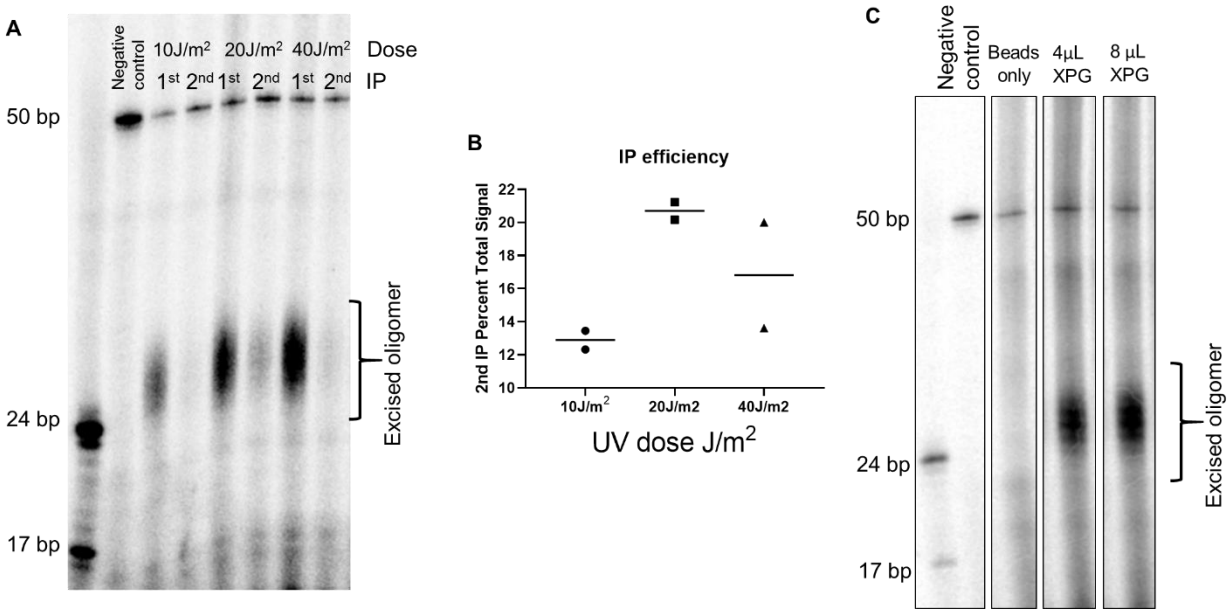

Figure 2.4: Characterization of the TFIIH immunoprecipitation efficiency. (A) A representative excision assay demonstrates the excised oligo signal seen from the initial TFIIH IP and from the subsequent IP on the supernatant from the first IP. Signal from the second IP is weaker than the signal from the first IP indicating a high efficiency of the initial IP. (B) The percent of total signal was calculated for each pair of IPs (1^{st} and 2^{nd}) by dividing the fmols oligomer from the second IP by the total fmols from both the first and second IP. Two replicates were conducted for each of the UV doses. The percent total signal is lowest for 10 J/m^2 UV which indicates that the IP may be more efficient at lower damage levels. (C) Representative excision assay following treatment with 20J/m^2 UV and a 30 minute repair incubation demonstrating the signal seen from using either 4 µL of antibody or 8 µL antibody on technical repeats with equal samples. The fraction of signal from the two repeats was 0.74 and 0.94 indicating that the antibody, at this dose, is not saturated.

To test if the IP antibody was saturated, we processed one sample until the IP at which point we split the sample in equal halves. We tested the fraction of signal from an IP conducted with half the normal amount of antibody (1x=8µL, 0.5x=4µL). If the antibody was saturated, we would expect the signal from 4µL of antibody to be half that of the signal obtained using 8µL of antibody. Two repeats of this experiment showed that the average fraction of 4µL antibody compared to 8µL antibody is 0.84 (repeats are

0.94 and 0.74) indicating that at 8μL of antibody, the antibody is not saturated (Figure 2.4C). Of note, this test was only conducted at 20J/m^2 thus the saturation results may not be generalizable to higher doses of UV.

Overall, while the immunoprecipitation is not saturated and does appear to be relatively inefficient, the incomplete extraction of all excised oligomers may account for some experimental variation.

Labeling, gel running and quantification efficiency

To test the efficiency from labeling samples to the quantification, one sample (from multiple plates) was processed up until the labeling step and subsequently split into 8 subsamples for labeling with ^{32}P-cordycepin. Rather than splitting the samples into 8 equal groups, we diluted the sample into 15μL and split the sample into two repeats of 1x, 2x, 4x, and 8x concentration of the sample (1x= 0.5 μL DNA, 2x=1 μL DNA, 4x= 2 μL DNA, and 8x= 4 μL DNA). We conducted the subsequent steps of the excision assay protocol to obtain the percent difference between the technical repeats. Figure 2.5 shows that the percent difference in signal from the technical repeats is relatively low, averaging at approximately 7%. This is the lowest percent difference found from any step we tested. As an additional measure of the efficiency of these steps, we tested if the signal obtained from the samples matched the appropriate ratio of signal relative to the amount of sample loaded. We would expect that if no signal was lost through these steps, the signal from each sample, normalized to 1x, plotted over the concentration of sample would yield a slope of 1 (Figure 2.5) . Indeed we find that the slope of the best fit line (constrained to a y-intercept of 0) is 0.8195 indicating relatively high efficiency in the final steps of the excision assay protocol. Furthermore,

when fit to a line constrained to a y-intercept of 0 and a slope of 1, our data yields an R^2 value of 0.8265 indicating once again high efficiency of these steps. Overall, labeling samples, running samples on a sequencing gel, imaging, and quantifying the repair signal appears to be highly reproducible between technical replicates.

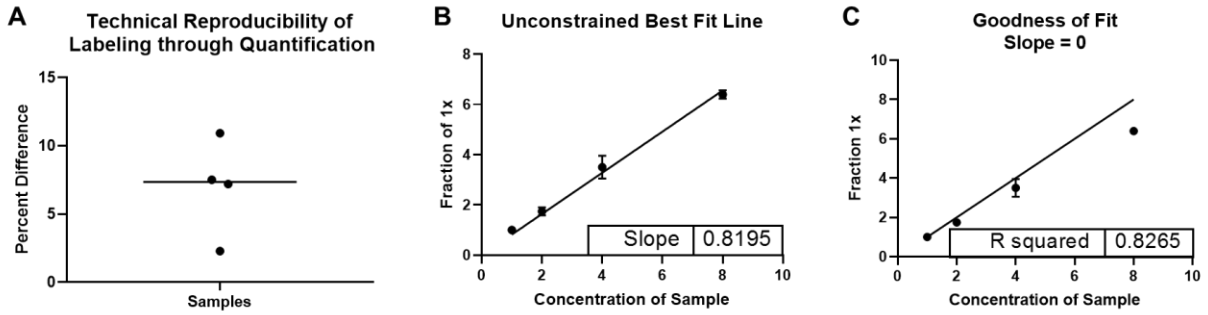

Figure 2.5: Characterization of the efficiency of the final steps of the excision assay (labeling – sequencing gel – imaging – quantification). The reproducibility of results from the labeling step through quantification of signal was measured by processing cells together from UV treatment until labeling step. At the labeling step, the excised oligomer was dissolved into 15µL of molecular grade water with 0.1mg/mL BSA. This was then split into 2 technical replicates of 1x, 2x, 4x, and 8x (0.5 µL, 1 µL, 2 µL, and 4 µL respectively). (A) The percent difference was calculated for the four technical replicates. The average percent difference across all samples is 6.95%. (B & C) The fmols of each sample were normalized to the fmols from the 1x sample for each set of technical replicates. These values were plotted across the concentration level (1, 2, 4, and 8). If the final steps of the excision assay were perfectly efficient, we would expect the slope of the line of best fit to be 1. (B) The line of best fit, constrained to a y-intercept of 0, has a slope of 0.8195. (C) A line constrained to a slope of 1 and a y-intercept of 0 fits the data relatively well with an r^2 value of 0.8265. (B & C) The goodness of fit of these two lines indicates that the final steps are relatively within the linear range.

2.3.2 Cell free extract repair of damaged plasmid

The excision assay was modified and expanded to enable us to sequence the excised oligomers and identify, at single nucleotide resolution, the precise genomic location and relative amounts of nucleotide excision repair. The excision repair sequencing (XR-seq) method uses the same damage, lyse, IP, elution steps as the excision assay however it then moves into a library preparation protocol rather than labeling and imaging. This novel sequencing method has greatly improved our

understanding of nucleotide excision repair, however it is still limited as repair reads are relative to total reads and thus the assay is not quantitative. This limitation is also found in other sequencing methods such as ChIP-seq and RNA-sequencing. Thus identifying a possible spike-in control to use as a normalization factor is essential to convert XR-seq to a quantitative assay.

As mentioned before, adding a spike-in control as early as possible into the protocol allows us to better control for variations between samples through the early steps. Ideally, a spike in control could be added to the cell lysis and processed with the sample starting with the immunoprecipitation step. We therefore needed to identify a reaction where we could control the amount of DNA present as the spike in but where the spike in DNA would still be in complex with repair proteins to enable proper IP. To achieve this, we decided to test repair of a damaged plasmid with cell free extract. After incubating the damaged plasmid with cell free extract to enable repair, the excised oligomers were isolated, labeled and imaged following the standard excision assay protocol. As seen in Figure 2.6 we were able obtain a strong excision signal from our damaged plasmid and cell free extract experiment. Given that plasmids have a known sequence, this reaction can therefore be used as an early spike-in for future XR-seq

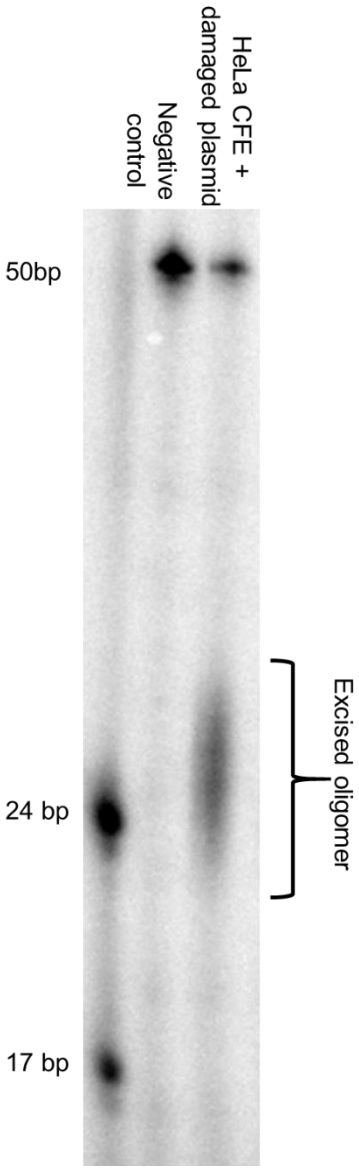

Figure 2.6: Representative excision assay following incubation of cell free extract with damaged DNA plasmid shows repair signal.

experiments whereby equal amounts of the plasmid – cell free extract reaction solution can be added to each sample during the TFIIH IP step and reads specific to the damaged plasmid can be extracted from the sequencing data and used to normalize reads that map to the sample genome.

2.4 Discussion

Overall, we tested the efficiency and reproducibility of the excision assay. We further broke this down to explore the reproducibility of individual steps of the excision assay. Based on these experiments, there appears to be substantial variability (30%) in the technical aspects of this protocol. Specifically, we found that cell lysis accounts for a considerable amount of variation in the samples. We did not specifically test the reproducibility of certain steps, such as phenol chloroform isolations or ethanol precipitations, which may also account for some of the technical dissimilarities. We also didn't test the differences between batches of reagents such as terminal transferase or antibodies which may account for some of the differences between experiments. The results remain highly variable between two biological repeats of the same cell line under the same damaging conditions. Thus further work needs to be done to ensure the experiment can be used effectively as a quantitative assay. One possible avenue for improvement is to identify a mechanism for normalizing the amount of sample added to each IP following cell lysis. This could be done by normalizing for DNA, RNA, or protein concentration of the solution after cell lysis. Preliminary efforts have been made to test if this sort of normalization could bring about more reproducible results between biological repeats. However splitting samples based on DNA, RNA, or protein concentration failed to yield results in a linear range.

This study demonstrated that there is high variability in the excision assay protocol and thus the XR-seq protocol as both methods share the same initial steps. To this end, it is important to have a spike in control for normalizing results and ensuring more quantitative results. Given the variability, it is also important that this control can be added in as early as possible to account for variations between samples at each step. To this end, we incubated cell free extract with a damaged plasmid and demonstrated that we could extract the excised oligomer using the excision assay protocol. This is important as we can now add a spike in control at the start of the IP for XR-seq. Once the sequencing data is back, the plasma-specific oligomers can be used as a normalization factor for the sample reads to determine the actual quantity of repair in each region.

In conclusion, we have characterized technical variability in the excision assay protocol. While additional work is needed to decrease the variability, we have modified the protocol to include the addition of the control 50mer during the elution to account for some of this variation by normalizing our data to the control. We also defined a protocol to enable an early spike in control for XR-seq.

CHAPTER 3: GENOME-WIDE SINGLE-NUCLEOTIDE RESOLUTION OF OXALIPLATIN–DNA ADDUCT REPAIR IN DRUG-SENSITIVE AND -RESISTANT COLORECTAL CANCER CELL LINES[2]

3.1 Introduction

Platinum-based drugs are a mainstay of solid tumor treatment and are used to treat a wide array of tumors. Unfortunately, platinum therapy is very toxic and patients can experience numerous detrimental side effects including severe emesis, nephrotoxicity, ototoxicity, and neurotoxicity (8). Oxaliplatin is a first-line treatment for colorectal cancer, one of the most common forms of cancer and one of the most common causes of cancer related deaths worldwide (136). Despite its common use, approximately half of patients have tumors that are intrinsically resistant to oxaliplatin, and many initially sensitive cancers develop resistance. Patients with resistant tumors of either form endure this toxic treatment with limited or no clinical benefit (137). Thus defining mechanisms that lead to drug resistance is important for providing patients with more effective treatment options.

Platinum-based drugs work by creating intrastrand dinucleotide adducts in DNA with the platinum atom covalently bound to the N7 nitrogen in adjacent guanines (5,7). This damage is solely repaired by nucleotide excision repair (61,63,68). Mammalian nucleotide excision repair initiates when the XPC, RPA, and XPA factors recognize the

[2] This paper was previously published in the *Journal of Biological Chemistry* 135. Vaughn, C. M., Selby, C. P., Yang, Y., Hsu, D. S., and Sancar, A. (2020) Genome-wide single-nucleotide resolution of oxaliplatin-DNA adduct repair in drug-sensitive and -resistant colorectal cancer cell lines. *The Journal of biological chemistry*

damage and recruit the TFIIH complex. Next, XPC dissociates, XPF and XPG bind to the pre-incision complex, and then the damaged strand is cleaved on the 3′ and 5′ side of the damage. The excised damage-containing DNA is then released as a single stranded oligomer approximately 24-30 nucleotides long complexed with TFIIH and XPG. DNA polymerase fills in the resulting single-stranded gap, and ligation of the nick completes repair. Excision repair of damage in the template strand of genes can also be transcription-coupled (79). In this pathway, RNA polymerase II stalls at damage sites and recruits the transcription coupling factors, CSA and CSB, which appear to assist in recruitment of the excision repair factors. Repair then proceeds following the same mechanism as in the global repair pathway. Transcription-coupled repair ensures rapid removal of transcription-blocking damage, especially damage such as platinum adducts, which are relatively slowly repaired by global repair (43).

Given that nucleotide excision repair is the sole repair mechanism for bulky intrastrand adducts, it has been widely speculated that increased repair efficiency would lead to platinum resistance. Many studies have explored how variation of repair at the sequence, expression, or functional level may correlate with response to platinum-based drugs (91,92,95-99,102). However many of the results are not reproducible and are often confounded by the multiple roles of individual proteins. Thus the link between alterations in nucleotide excision repair and response to platinum based drugs remains unclear (113,114). In this study, we use novel methods to provide a comprehensive profile of repair efficiency for a panel of colorectal cancer cell lines that vary in oxaliplatin sensitivity by an order of magnitude. We find no link between sensitivity and repair, rather, resistant cells display diminished oxaliplatin-DNA adduct formation.

3.2 Methods

3.2.1 Cell culture

Dld1, Rko, Ls1034, Ls180, and Colo205 cell lines were purchased from American Type Culture Collection (ATCC). Sw480, Hct116, Ht29, Colo320hsr, and Ls174t cell lines were obtained from the Tissue Culture Facility at the University of North Carolina. All cell lines used are ATCC cell lines and were grown under the conditions specified on their website. Cells were split at a 1:10 ratio when they reached 80% confluence and were never split more than 30 passages. Frozen stocks for each cell line were made on the second and third passages. Cell culture and drug treatments were conducted at 37° C in 5% CO_2.

3.2.2 Oxaliplatin survival

All survival studies were conducted in 96-well Corning Costar plates using the Promega MTT assay. Cells were plated at 5,000 cells per well 24 hours prior to treatment with oxaliplatin. Oxaliplatin from TSZChem was first dissolved as a 6.4M stock in DMSO (made fresh before each biological replicate), and then diluted to a 640μM solution using the culture media appropriate for each cell line. Serial dilutions in the respective culture media were performed to obtain solutions with 160 μM, 40 μM, 10μM, and 2.5μM oxaliplatin. Solutions were then added to the wells at a 1:10 ratio such that cells were ultimately treated with 64 μM, 16 μM, 4 μM, 1 μM, 0.25 μM, or 0 μM. For every cell line, three technical repeats of each dose were conducted for each of the three biological replicates. Four days after the addition of oxaliplatin to the media, MTT dye was added to the media. Three hours after the addition of dye, the media was

replaced with solubilizer solution. Dye intensity was read using a Spectra Max M3 plate reader and SoftMax® Pro 6 microplate reader control and data analysis software. The three technical repeats for each dose were averaged and normalized to the signal from the untreated control. Graph Pad Prism 8 software was used to plot dose response and to determine IC50.

3.2.3 UV survival

Survival following irradiation with principally 254nm UV light was conducted following the same protocol as oxaliplatin survival with the following exceptions. Cells were plated at 50,000 cells/well 24 hours prior to treatment. Immediately before UV irradiation, media was removed and wells were washed with PBS to eliminate any effect of culture media on UV treatment. Fresh media was added to each well following treatment. One 96 well plate was used for each UV dose (0, 5, 10, 20, 40, 80 J/m^2). Irradiations took 80 seconds or less at the dose rate used. Survival was measured one day after UV treatment rather than four days.

3.2.4 Mitomycin C and Hydrogen Peroxide Survival

These survival assays were conducted following the same protocol as the oxaliplatin survival studies with the following exceptions: Mitomycin C was first diluted to a 5M stock in DMSO. This 5M stock was then diluted for each biological replicate using the appropriate culture media to make a 40μM solution and was then serially diluted to make solutions with 20μM, 10μM, 5μM, and 2.5μM concentrations. Hydrogen peroxide came as a 30% solution and was diluted to 640μM concentration in the appropriate culture media. Serial dilutions in media were then made to create solutions with 160 μM,

40 μM, 10μM, and 2.5μM. Both Mitomycin C and hydrogen peroxide solutions were added to wells at a 1:10 ratio yielding final concentrations of 16 μM, 4 μM, 1 μM, and 0.25 μM.

3.2.5 Oxaliplatin slot blot (138,139)

Cells were plated in 100mm round dishes. Cells were treated with 200μM oxaliplatin for two hours once they reached ~100% confluence to eliminate damage level reduction due to cell divisions. After the two hour treatment period, culture media was changed and cells were then either washed with ice cold PBS and collected, or incubated for an additional 4, 10, 22, or 34 hours to allow for repair before collection. DNA was extracted using the QIAamp DNA mini kit. DNA was then treated with RNase A for one hour and purified using a QIAGEN PCR purification kit. DNA was quantified and diluted such that 150 ng of each DNA sample was loaded into each well of a slot blot apparatus for repair kinetics experiments, and 250 ng DNA was loaded into each well for initial damage experiments. DNA was then transferred to a membrane, and blots were blocked in PBS with 0.1% Tween (PBS-T) and 5% milk at 4°C overnight. The next day the blots were washed in PBS-T three times, and incubated in Abcam anti-platinum damage primary antibody (AbCam, 1:10000 in PBS-T) at 4°C overnight. Blots were washed and incubated in GE-Healthcare anti-Rat IgG conjugated to horse radish peroxidase for two hours. BioRad Clarity™ Western ECL Substrates were used to detect signal and signal was quantified using Image Quant. DNA loading was detected with either an antibody against single stranded DNA or with SyberGold. For the repair kinetic study, two technical replicates were done for each of two biological replicates for each cell line. For the initial damage experiments, two technical replicates of three

biological repeats were conducted for each cell line. Graph Pad Prism 8 software was used to plot damage amount and to calculate repair values.

3.2.6 UV slot blot

UV slot blot was conducted following the same protocol as oxaliplatin slot blot with the following exceptions. Immediately before UV irradiation, media was removed and cells were washed with PBS. Cells were treated with 25 J/m^2 and fresh media was added following treatment. Three biological replicates were conducted for each cell line tested.

3.2.7 Excision assay (67,68)

Cells were plated in one 150 mm round dish per dose and allowed to grow to ~100% confluence. Immediately before UV irradiation, media was removed and cells were washed with PBS. Cells were then irradiated with 0, 5, 10, 25, 50, or 100 J/m^2. Fresh media was added following irradiation, and plates were returned to the incubator for a three hour repair incubation. Cells were harvested in cold PBS, suspended in a lysis buffer without SDS, and lysed using a homogenizer. Excised oligomers were isolated from the soluble fraction of homogenates by XPG antibody (Santa Cruz Biotechnology) immunoprecipitation. During the elution of the XPG IP, “spike” control DNA (2 fmol) was added to each sample. The control spike DNA was an undamaged 50-mer oligomer used to monitor subsequent DNA recovery and labeling efficiency. At this point samples containing control and excised DNA were extracted with phenol-chloroform, precipitated with ethanol, labeled with ^{32}P-cordecepin, and run on a sequencing gel. The gels were exposed to a phosphoimager screen and imaged with

the Typhoon detection system. Signal was measured using ImageJ software. Graph Pad Prism 8 software was used to plot excised oligo amount and to calculate repair values. At least four biological replicates were conducted for each cell line tested.

3.2.8 XR-Seq (19,82)

Cells were plated in 150 mm round dishes and allowed to grow to ~100% confluence. The number of plates needed varied by cell line. They were then exposed to 200μM oxaliplatin for two hours and then they were washed with cold PBS and collected. Cells were suspended in a lysis buffer without SDS and lysed using a homogenizer. Excised oligomers were isolated from the soluble fraction of homogenates by XPG antibody (Santa Cruz Biotechnology) immunoprecipitation. The oligomers were then eluted, purified, annealed, and ligated to adaptors. A second IP for platinum damage was then performed to further purify the excised oligomers. The platinum damage was then reversed with sodium cyanide. PCR amplification (15 cycles or fewer) and gel purification were then conducted and samples were sequenced using NextGen sequencing. XR-seq was conducted for two biological replicates for all cell lines except Colo320hsr and Ls174t for a total of 18 libraries. Sequences were aligned to the hg38_UCSC genome and read counts per gene were determined. Each sample had at least 6.8 million unique mapped reads. Repair patterns were visualized using the Integrated Genome Viewer from the Broad Institute. Average repair patterns for a unit gene was determined and plotted as described (139,140). Repair read counts from the transcribed strands of genes were analyzed with the DESeq2 package in R to determine genes with significant differential repair. GSEA software from the Broad

Institute and STRING (SIB, CPR, and EMBL) were used to determine enriched processes for differentially repaired genes.

3.3 Results

3.1.1 Identification of oxaliplatin sensitive and oxaliplatin resistant cell lines.

To study whether nucleotide excision repair efficiency is a determinant of oxaliplatin sensitivity, we used a panel of 10 colorectal cancer cell lines. We first tested their sensitivity to killing by oxaliplatin using the MTT cell viability assay. We treated each cell line with oxaliplatin concentrations varying from 0μM to 64μM and tested survival four days later. Dose response curves clearly identified three resistant cell lines and seven sensitive cell lines (Figure 3.1A). IC50 values for each cell line are shown in Figure 3.1B. Cell line characteristics, including key driver mutations and source information are summarized in Appendix 1 (141,142).

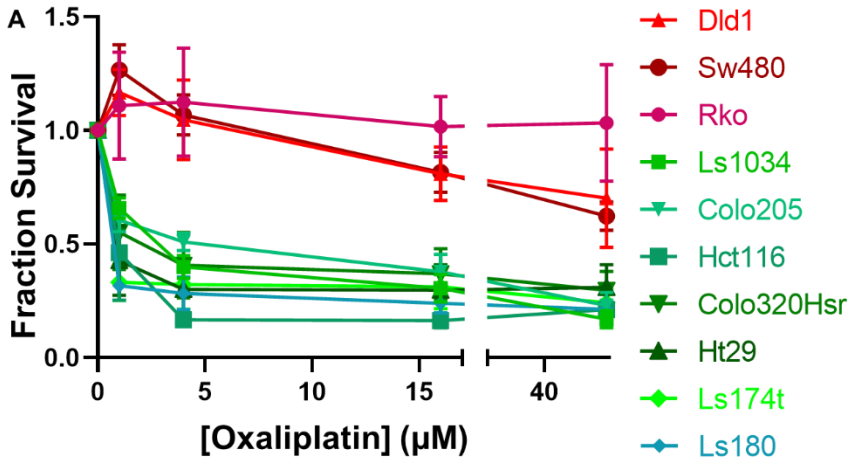

B

Cell Line	IC50 (μM)
Dld1	10.920
Sw480	7.934
Rko	7.037
Ls1034	1.592
Colo205	0.910
Hct116	0.843
Colo320hsr	0.507
Ht29	0.292
Ls174t	0.183
Ls180	0.176

Figure 3.1: Defining a panel of oxaliplatin-sensitive and oxaliplatin-resistant colorectal cancer cell lines. Ten colorectal cancer cell lines were tested using an MTT assay. Oxaliplatin was added to media at concentrations ranging from 0.25μM to 64μM. Four days following addition of oxaliplatin, survival was measured and normalized to an untreated control. (A) Oxaliplatin dose response curves identified seven oxaliplatin-sensitive cell lines (green) and three oxaliplatin-resistant cell lines (red). (B) The IC50 for each cell line was calculated using PRISM.

3.3.2 Oxaliplatin repair kinetics are similar between oxaliplatin-sensitive and -resistant cell lines

To evaluate repair efficiency in the sensitive and resistant cell lines, we first examined rates of oxaliplatin removal from the genome using slot blot assays. Each cell line was incubated with 200 uM oxaliplatin for two hours, an early damage formation time point, while still allowing for measurable damage levels (143). Then, fresh media was added and cells were incubated for an additional 0 to 34 hours. The results in Figure 3.2A show loss of oxaliplatin from the genome with time in a representative sensitive (Colo205) and resistant (Dld1) cell line. Damage levels were quantified by first normalizing the signal intensity of each damage band to its respective total amount of DNA (detected by SyberGold staining), and then calculating the fraction of damage remaining at each time point compared to 2 hours. Average values for all sensitive and all resistant cell lines are plotted in Figure 3.2B. The time for 50% of the peak initial damage to be repaired (Repair50) is listed for each cell line in Appendix 2. Sensitive and resistant lines show very similar repair rates, indicating that faster DNA damage repair is not a necessary component of oxaliplatin resistance.

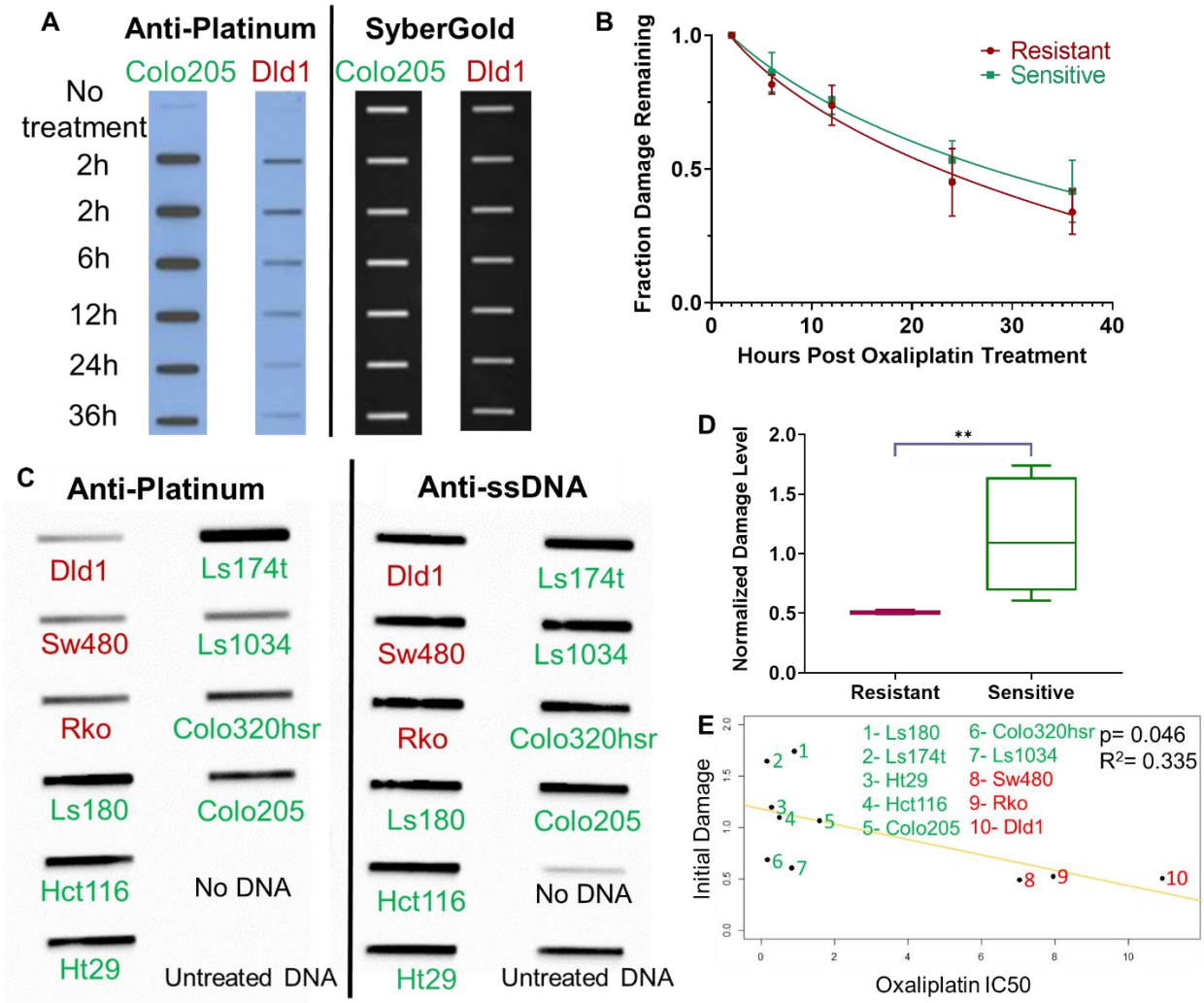

Figure 3.2: Oxaliplatin repair and damage formation. (A) Repair kinetics in oxaliplatin-sensitive and -resistant cell lines. Representative slot blot shows loss of damage from the genome with time following 2 hours of treatment of a sensitive cell line (Colo205) and a resistant cell line (Dld1) with 200μM oxaliplatin. Probing with anti-platinum-DNA adduct antibody (left) reveals the genomic DNA damage levels, and subsequent SyberGold staining of the same blot (right) shows the total amount of DNA blotted onto the membrane through each slot. (B) Average values for repair in the three sensitive and two resistant cell lines assayed are plotted and show no significant difference in repair rate. Two technical replicates of two biological replicates were done for each cell line. (C) Representative slot blot showing damage level following 2 hours exposure of the oxaliplatin-resistant (red) and -sensitive (green) cell lines to oxaliplatin. Probing with anti-ssDNA reveals the total amount of DNA on the membrane. (D) A plot of average initial damage levels for three resistant cell lines (red) and seven sensitive cell lines (green) shows a significant difference (p=0.008, Welch's t-test) between the two groups, indicating that a lower initial damage level correlates with resistance. (E) A trend line fitting the IC50 values (x-axis) and normalized initial damage levels (y-axis) is plotted. A significant (Pearson's correlation, p=0.046), inverse correlation again indicates that lower initial damage levels correlate with resistance.

3.3.3 Initial damage differs significantly between sensitive and resistant cell lines

Inspection of the oxaliplatin repair slot blots such as in Figure 2A suggested uneven levels of initial damage among the cell lines. Oxaliplatin treatment is known to be influenced by factors such as drug influx, efflux, and neutralization (144-146). We therefore systematically compared the amount of initial damage incurred following treatment of each cell line with 200 uM oxaliplatin for 2 hours. The results in Figure 3.2C and Table S2 reveal substantial variations in initial damage levels. The average initial damage level was lower in resistant cells, as shown in Figure 3.2D, furthermore, a significant, inverse correlation was found between oxaliplatin IC50 and initial damage level using a Pearson's correlation test (Figure 3.2E). This association, while not perfect, indicates that initial damage levels contribute to cellular sensitivity. Damage levels were consistently low in the resistant lines. However, variability was seen among the sensitive lines. Several possible scenarios could explain the sensitive lines with relatively low initial damage, notably, it is possible that these two lines (Colo320hsr and Ls1034) have repair deficiencies not detected by the slot blot assay or other alterations in DNA metabolism.

3.3.4 Oxaliplatin-sensitive and -resistant cell lines have similar repair responses to UV irradiation.

We next evaluated the role of repair on oxaliplatin sensitivity employing means to avoid the confounding factors of drug treatment mentioned above. Unlike platinum-based drugs, UV irradiation rapidly and uniformly induces the intrastrand DNA diadducts cyclobutane pyrimidine dimers (CPDs) and 6-4 pyrimidine-pyrimidone photoproducts (6-4 PPs) that, like platinum-induced bulky adducts, are solely repaired by nucleotide

excision repair. CPDs, the predominant photoproduct, are similar to platinum adducts in that they are relatively poorly recognized and slowly repaired by the global excision repair pathway, while 6-4 PPs are more rapidly repaired (61). We measured the repair of UV photoproducts in our cell lines to provide a more well-controlled assessment of repair efficiency.

We first measured survival in response to UV treatment. The results in Figure 3.3A and UV IC50 values in Table S2 show that while there is some variation in UV survival among cell lines, overall UV sensitivity is similar among cell lines, in contrast to the order of magnitude differences in sensitivity to oxaliplatin (Figure 3.1A). Thus oxaliplatin resistance is not associated with a more resilient response to intrastrand adducts either by increased repair or decreased apoptotic signaling in response to similar initial damage levels.

We then characterized UV repair using slot blot assays to measure removal of CPD adducts from the genome. Results obtained with representative oxaliplatin -sensitive (Ls1034) and -resistant (Rko) cell lines are shown in Figure 3.3B, and average values for the three sensitive and two resistant lines tested are shown in Figure 3.3C (individual cell line UV Repair50 values are listed in Table S2). CPDs were removed from the genome at the same rate in sensitive and resistant cell lines.

We next used excision assays to measure the amount of excised oligomer present in cells three hours following varying doses of UV irradiation. The excision assay uses an XPG immunoprecipitation to capture the excised, damage-containing oligomers. The oligomers are isolated, purified, labeled, and resolved on a gel. The intensity of the oligomer bands can be quantified by normalizing to a known

concentration of spiked in control DNA (50mer, Figure 3.3D). The amount of excision product present at any given time reflects both the rate of oligomer release and concurrent degradation. Excision in representative sensitive (Hct116) and resistant (Sw480) cell lines are shown in Figure 3D, and the UV dose required to obtain 50% maximum repair for each cell line is listed in Table S2. Average values for the three oxaliplatin -resistant cell lines and four -sensitive cell lines tested show no difference in UV photoproduct excision as a function of dose (Figure 3.3E). These experiments further support the finding that improved nucleotide excision repair is not a necessary component of oxaliplatin resistance.

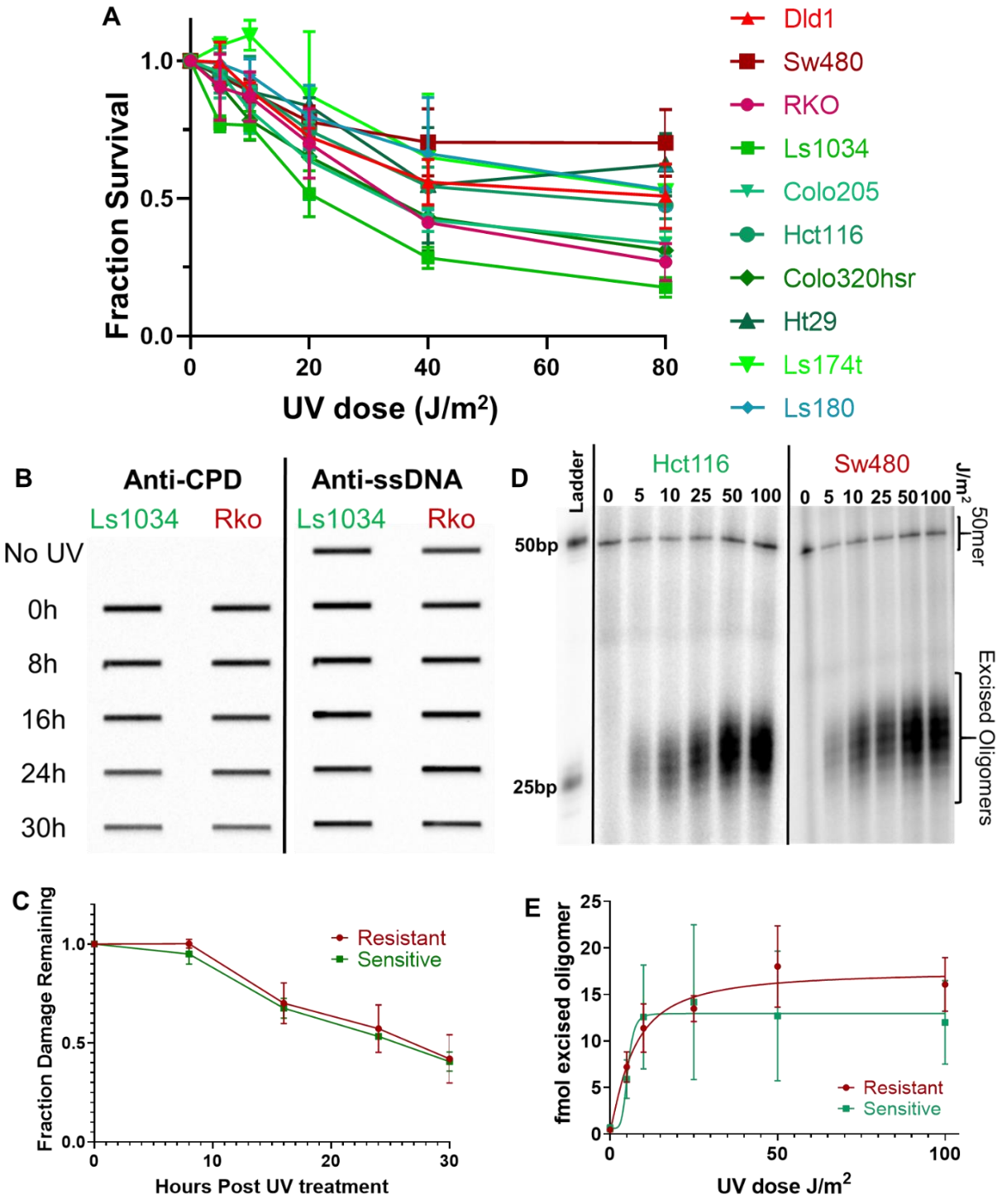
A
Fraction Survival
1.0
0.5
0.0
0
20
40
60
80
UV dose (J/m²)
Dld1
Sw480
RKO
Ls1034
Colo205
Hct116
Colo320hsr
Ht29
Ls174t
Ls180
B
Anti-CPD
Anti-ssDNA
Ls1034
Rko
Ls1034
Rko
No UV
0h
8h
16h
24h
30h
D
Ladder
Hct116
Sw480
0 5 10 25 50 100
0 5 10 25 50 100
J/m²
50bp
25bp
50mer
Excised Oligomers
C
Fraction Damage Remaining
1.0
0.5
0.0
0
10
20
30
Hours Post UV treatment
Resistant
Sensitive
E
fmol excised oligomer
25
20
15
10
5
0
0
50
100
UV dose J/m²
Resistant
Sensitive

Figure 3.3: Repair of UV damage in oxaliplatin-sensitive and -resistant cell lines. UV creates intrastrand adducts that, like platinum intrastrand adducts, are solely removed by nucleotide excision repair. UV damage, however, is not influenced by drug influx, efflux, or neutralizing mechanisms which influence response to platinum drugs. (A) UV survival dose response curves for all cell lines fail to recapitulate the sensitive and resistant grouping seen with oxaliplatin survival curves. This indicates that the sensitive/resistant status of each cell line is not based on repair of intrastrand diadducts. (B) Representative slot blots (n=3 blots per cell line) measuring UV-induced CPD damage levels over time are shown for a representative oxaliplatin-sensitive cell line (Ls1034) and a representative oxaliplatin resistant cell line (RKO). Blots were probed first with anti-CPD antibody to measure damage (left), stripped, then probed with anti-ssDNA antibody (right) to measure the amount of DNA on the membrane. (C) Average damage levels, normalized to initial damage, of two oxaliplatin-resistant cell lines (red) and three oxaliplatin-sensitive cell lines (green) are plotted as a function of repair time. No difference in UV repair rate is seen between the oxaliplatin-sensitive and oxaliplatin-resistant cell lines. (D) A representative excision assay shows similar amounts of excision product following varying doses of UV in both a representative oxaliplatin-sensitive cell line (Hct116) and a representative resistant cell line (Sw480). (E) The average amount of excision product, measured as femto-mol of excised oligo, in oxaliplatin-sensitive cell lines (green, n=4 repeats) and oxaliplatin-resistant cell lines (red, n=3 repeats) are plotted as a function of UV dose. No significant difference in amount of repair is seen between sensitive and resistant cell lines.

3.3.5 Oxaliplatin-sensitive and oxaliplatin-resistant cell lines have similar genome-wide repair patterns.

While overall repair rates, measured by slot blot and excision assays do not differ between oxaliplatin sensitive and oxaliplatin resistant cell lines, we hypothesized that resistant cell lines may, to their benefit, prioritize repair of certain genomic regions differently from sensitive cell lines. To test this hypothesis we used XR-seq after treating the cells with 200μM oxaliplatin for two hours (19,82). In XR-seq, the damage-containing oligomers excised during repair are isolated and purified by sequential immunoprecipitations, first using repair protein antibodies, and then using platinum damage antibodies. The damage is then reversed and the oligomers are amplified by PCR, and sequenced. The oligomer sequences are then aligned to the genome. The result is a nucleotide level map of repair throughout the genome. The screenshot in Figure 3.4A shows XR-seq results for a representative 250,000 Kbp section of the

genome. This section contains the *Dhfr* and *Msh3* genes, which are transcribed in opposite directions. Repair in each strand (plus and minus) of a representative resistant (Dld1, red) and sensitive (Ls180, green) cell line is shown. Excised oligo reads per kilobase per million total reads (RPKM, y-axis) are represented as peaks across the gene and indicate the number of excision products found at a given location. Clearly evident in the screenshot is preferential, transcription-coupled repair of the transcribed strand (TS) of the *Dhfr* and *Msh3* genes in both cell lines. We quantified the RPKM for both strands of each gene, then averaged the repair values for all sensitive and all resistant cell lines, and found no difference in strand-specific repair levels at any significance threshold (Figure 3.4B).

To compare transcription coupled repair in all genes and cell lines, we first constructed a “unit gene” for all ten cell lines (n=2 for all cell lines except n=1 for Ls174t and Colo320hsr). The unit gene illustrates the average repair of each gene in a cell line. To do this, for each cell line, results for all non-overlapping genes over 1kbp were divided into 100 bins, and the repair level for each bin was averaged from the first bin at the transcription start site (TSS) to the last bin at the transcription end site (TES). Average repair 2 Kbp upstream and downstream was also determined for each unit gene. Next, repair across the sensitive and resistant cell lines were averaged. The average unit gene repair profiles in Figure 3.4C are similar to profiles seen in other human cell types, and in cells of other species, which show elevated TS repair which peaks near the TSS, and largely depressed non-transcribed strand (NTS) repair which peaks immediately upstream of the TSS and results from antisense transcription at the promoter (19,139,140,147,148). Figure 3.4C shows that overall, there is no difference in

amount or pattern of gene-specific repair between oxaliplatin-sensitive and oxaliplatin-resistant cell lines. This indicates that the levels of transcription coupled repair are similar in both groups. These analyses extend our observation that repair efficiency is not an essential component of oxaliplatin resistance.

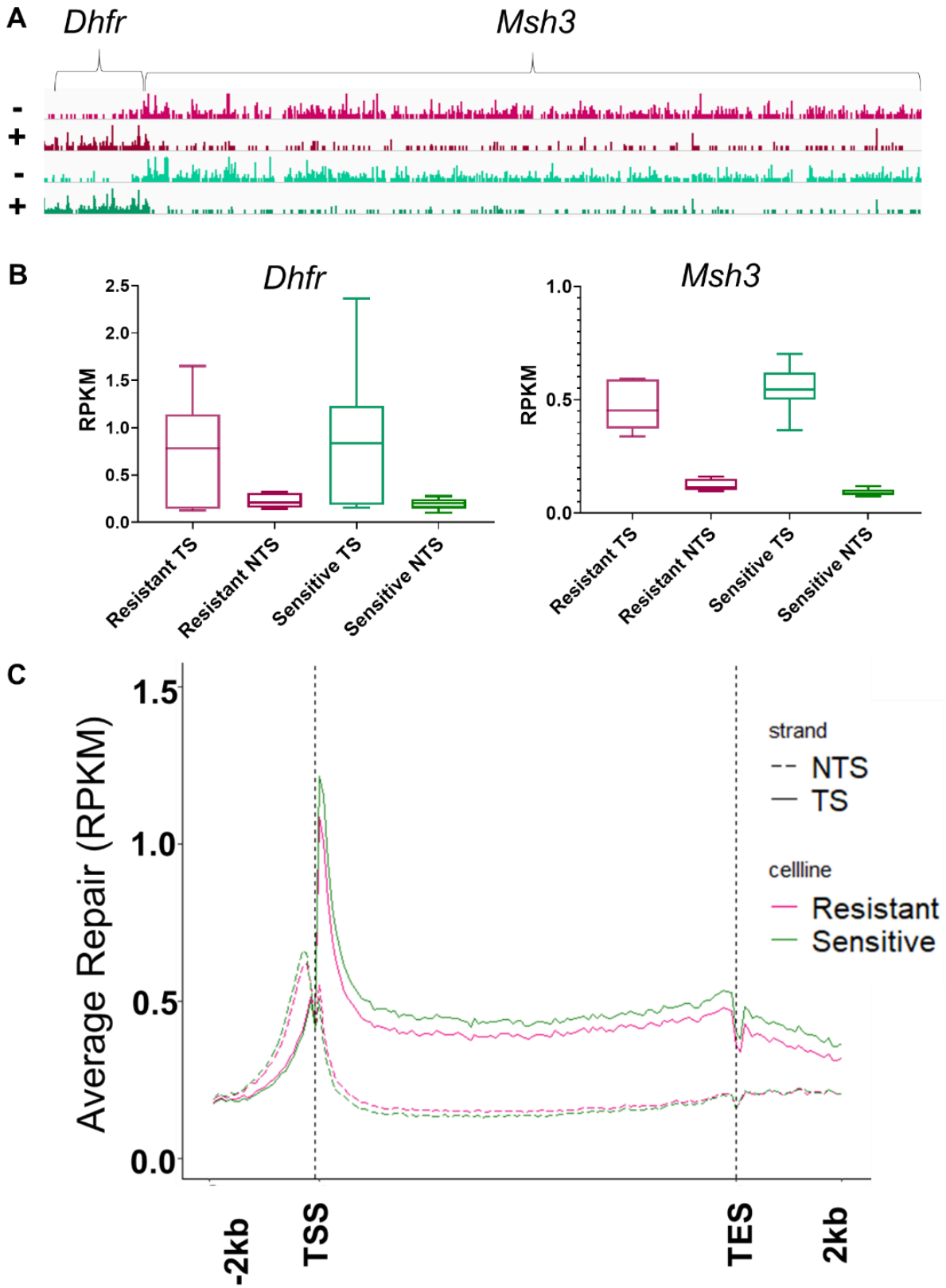
A
Dhfr
Msh3
-
+
-
+
B
Dhfr
Msh3
RPKM
2.5
2.0
1.5
1.0
0.5
0.0
Resistant TS
Resistant NTS
Sensitive TS
Sensitive NTS
C
Average Repair (RPKM)
1.5
1.0
0.5
0.0
-2kb
TSS
TES
2kb
strand
NTS
TS
cellline
Resistant
Sensitive

Figure 3.4: Oxaliplatin-sensitive and -resistant cell lines show similar genome wide repair patterns. Repair maps were created for all cell lines using XR-seq after two hours of treatment with 200μM oxaliplatin (2 biological replicates for all cell lines except Ls174t and Colo320hsr). (A) Representative genes, DHFR and MSH3, show similar repair levels and patterns in sensitive (green, Ls180) and resistant (red, DLD1) cell lines. Both genes have strong transcription coupled repair as indicated by the stronger repair signal seen in the transcribed strand (TS) compared to the non-transcribed strand (NTS). The minus strand is the TS in *Msh3* and the plus strand is the TS in *Dhfr*. (B) Average RPKM for the TS and NTS of DHFR and MSH3 from all XR-seq experiments show similar repair levels between all sensitive (green) and all resistant (red) cell lines. (C) Average RPKM of all resistant cell lines (red) and all sensitive cell lines (green) for all genes over 1kbp with ≥5kbp between genes are plotted for the TS and NTS, scaled to a 'unit gene'. Each gene is split into 100 bins to create the X- axis, and the average bin values for all genes are plotted as RPKM. TSS-transcription start site, TES-transcription end site. No significant difference is seen in repair pattern or in level of transcription coupled repair.

3.3.6 Differences in gene expression in oxaliplatin-sensitive and oxaliplatin-resistant cell lines indicate a role for membrane transport in oxaliplatin-resistance.

While overall, average transcription-coupled repair of all genes showed no difference in sensitive versus resistant cell lines (Figure 3.4), we extended our analysis to detect possible differences in transcription coupled repair within individual genes. To do this, we used the RPKM values for the TS of each gene, which reflects each gene's transcription-coupled repair level and thus gene expression level. Focusing first on individual repair genes, as shown in Figure 3.5A, we found comparable levels of expression in sensitive and resistant cell lines, with the exception of *XPF* which, despite claims that *XPF* upregulation correlates with platinum resistance (149), displayed higher expression in sensitive cell lines than in resistant lines. We next tested the copper efflux (*ATP7A*, *ATP7B*) and influx channels (*SLC31A1*, *SLC31A2*) that have been strongly implicated in platinum resistance (150-152). No difference in expression of these transporter genes was detected with the possible exception of *SLC31A1*. Repair of the TS of *SLC31A1* was lower in resistant lines at a p value of 0.015 (Welch's t-test, Figure

3.5B), although the association between *SLC31A1* and DNA damage in the ten cell lines was not significant (Pearson's correlation test, Figure 3.5C).

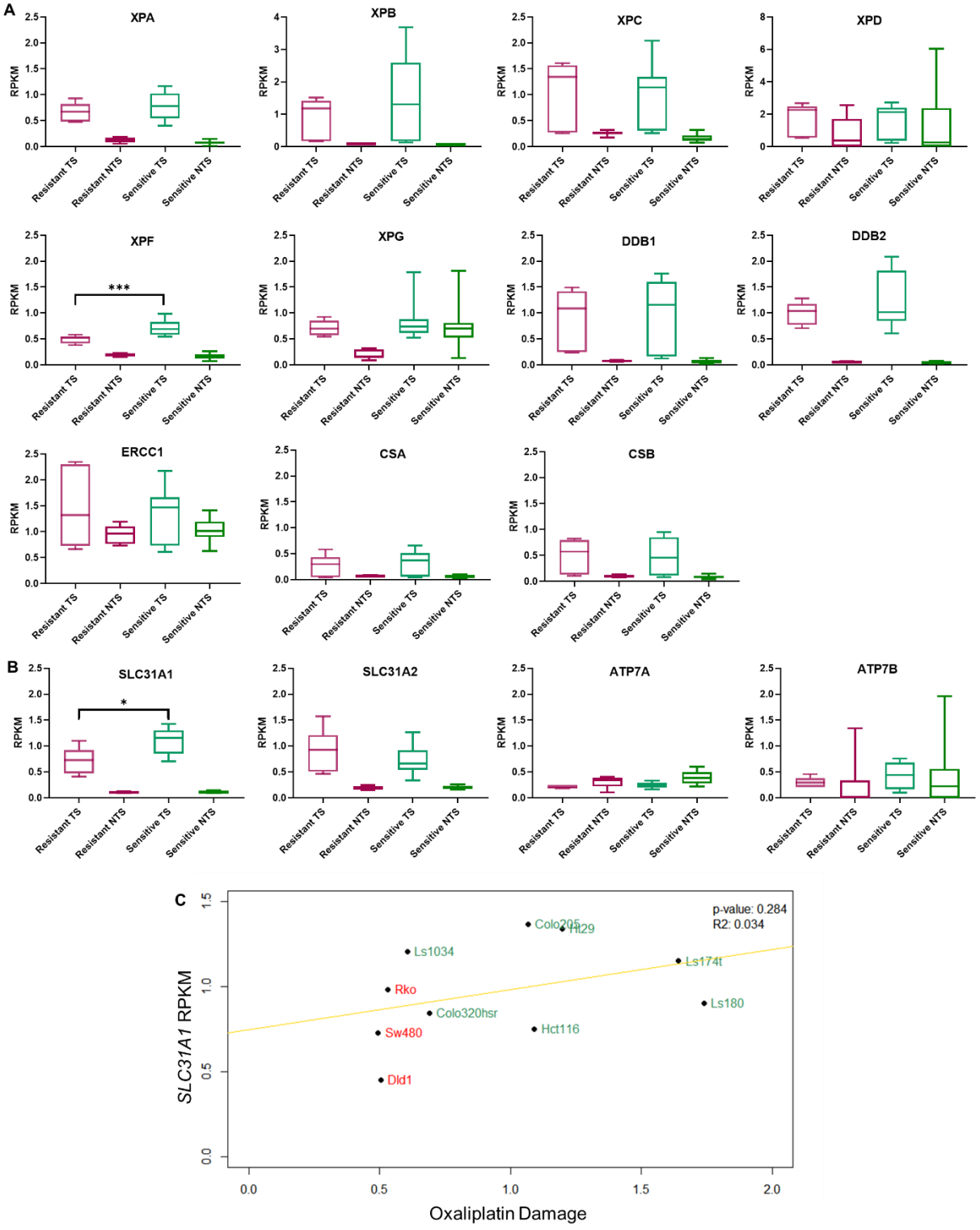

Figure 3.5: Transcription-coupled repair in select repair genes and transporter genes. Average RPKM for transcribed and non-transcribed strands for all sensitive and all resistant cell lines for (A) genes encoding repair proteins and (B) genes encoding copper transporters implicated in platinum influx (*SLC31A1, SLC31A2*) and efflux (*ATP7A, ATP7B)*. In most genes, active transcription is evident from higher repair in the TS versus the NTS, except in some cases where high error in the NTS may obscure the signal (XPD, ATP7B). With the exceptions of *XPF* (Welch's t-test, p=0.0005) and *SLC31A1* (Welch's t-test, p=.015), there are no significant differences between sensitive and resistant cell lines. Results for *ERCC1* are confounded by overlapping genes (not shown). (C) Comparison of initial oxaliplatin damage (x-axis) and TS repair in *SLC31A1* (y-axis) shows an apparently weak but not significant correlation (Pearson's correlation, p= 0.284).

The above comparisons of TS repair, done on a gene-by-gene basis, were extended to compare expression of all genes in sensitive versus resistant cell lines using the DESeq2 analysis package (153). Among the approximately 30,000 genes analyzed, we identified 1122 differentially repaired genes with an adjusted p-value less than 0.05 (Figure 3.6A). 417 of these genes had higher repair levels in resistant cell lines compared to sensitive cell lines and 705 of the genes had higher repair levels in sensitive cell lines compared to resistant cell lines (Figure 3.6B). One or more of these genes, listed in Appendix 3, could be involved in processes such as oxaliplatin transport, stability, or processing.

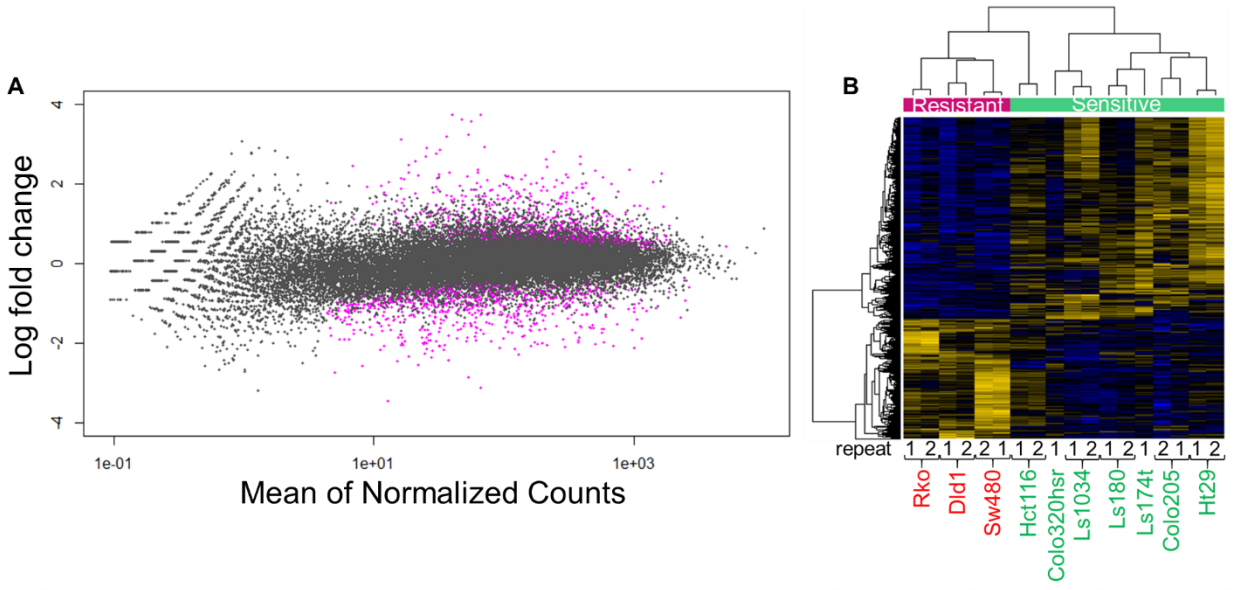

C

Top 10 Pathways Enriched in Resistant Cell Lines	SIZE	NES	FDR q-val
GO_REGULATION_OF_POTASSIUM_ION_TRANSPORT	40	2.201	0.011
GO_POSITIVE_REGULATION_OF_POTASSIUM_ION_TRANSPORT	17	2.071	0.055
GO_NEGATIVE_REGULATION_OF_ION_TRANSPORT	66	1.977	0.056
GO_ION_CHANNEL_REGULATOR_ACTIVITY	61	1.981	0.063
GO_ENDOCRINE_HORMONE_SECRETION	24	1.953	0.069
GO_REGULATION_OF_METAL_ION_TRANSPORT	172	1.935	0.069
GO_NEGATIVE_REGULATION_OF_SYNAPTIC_TRANSMISSION	29	1.987	0.069
GO_SARCOPLASMIC_RETICULUM_MEMBRANE	15	1.941	0.071
GO_CALCIUM_ION_IMPORT	35	1.913	0.071
GO_POSITIVE_REGULATION_OF_ERBB_SIGNALING_PATHWAY	18	1.920	0.071

Figure 3.6: Genes differentially expressed in sensitive versus resistant cells. Oxaliplatin-resistant cells show enrichment for membrane components and transport in resistant cells, and sensitive cells exhibit enrichment for metabolic processes. (A) MAplot of genes shows that a small fraction of genes are significantly differentially repaired (expressed) between sensitive and resistant cell lines. For each gene (plotted as a dot), the difference between sensitive and resistant cell lines (log fold change) is plotted over the average counts across all samples (mean of normalized counts). Genes exhibiting significantly different repair (expression) are plotted in purple (padj<0.05) (B) Heatmap of the genes repaired differentially in sensitive (green band) versus resistant (red band) cell lines. Yellow lines indicate higher expression while blue lines indicate lower expression. 417 genes were found to have significantly higher repair in resistant cell lines while 705 genes were found to have significantly higher repair in sensitive cell lines. R1 and R2 denote repeats for each cell line. (C). Gene set enrichment analysis of the differentially repaired genes showed enrichment of membrane transport pathways in resistant cell lines (FDR q-value <25%). The top 10 most significantly enriched pathways are shown, additional pathways are in Table S1. No significantly enriched pathways (FDR q-value <25%) were identified from the genes upregulated in sensitive cell lines (Table S2). Size= number of genes from our input in the pathway, NES = Normalized enrichment score, the quantification of the overrepresentation of a gene set in the top or bottom of a ranked list of genes normalized for all dataset permutations; FDR= False discovery rate, the probability a NES score is a false positive finding(3)

It is possible that resistance is determined by the outcome of several of the 1122 differentially expressed genes acting in a related manner, for example having related functions, cellular locations, or regulation. We tested this supposition by applying gene set enrichment analysis (GSEA) of the 1122 genes. In agreement with other studies (144,154), our analysis found that oxaliplatin-resistant cells were enriched in gene sets including membrane transporters and channels, and their regulators, at a false discovery rate q-value of under 25% indicative of a low chance that these findings are false positives (Appendix 4)(3). Transport processes and plasma membrane components were also identified as significantly upregulated in resistant cells using the publically available STRING database pathway analysis software (155). Among oxaliplatin-sensitive cell lines, enrichment of the cell cycle and metabolism gene sets was the strongest; however, none of these were below a 25% false discovery rate (Appendix 5).

We were particularly interested in understanding why the Ls1034 and Colo320hsr cell lines were sensitive even though they displayed relatively low initial damage. To this end, we first compared gene expression (as transcribed strand repair level) in these two lines with expression in the other sensitive lines (that exhibited high levels of oxaliplatin damage) by analyzing with DESeq2. 4117 differentially expressed genes were identified. Comparison of gene expression in Ls1034 and Colo320hsr with the resistant cells lines revealed 3603 differentially expressed genes. It is possible that one or more genes in these two sets contribute to relatively high toxicity of low levels of oxaliplatin-DNA damage. Inspection of these two data sets, focusing on the most differentially expressed genes yielded some provocative candidates. For example,

compared to resistant cell lines, low-damage sensitive lines have 5.5x higher expression of Colon Cancer Associated Transcript 2 (CCAT2). CCAT2 is expressed at higher levels in colorectal tumor tissue compared to adjacent healthy tissue, and promotes cancer cell proliferation by downregulating expression of the micro RNA-145 tumor suppressor. It is linked to clinical outcome, (156-159) and a functional SNP in CCAT2 has been shown to correlate with improved response to oxaliplatin (160). Thus CCAT2 may be an important factor in activating cell death in response to low initial oxaliplatin damage levels. We found other cancer associated non-coding RNAs among the top upregulated genes in low damage sensitive cell lines compared to resistant cell lines (CCAT2 and CASC8) and compared to high-damage sensitive lines (CASC11, CASC8, and PCAT1), supporting a possible role for regulatory RNAs in oxaliplatin response (Figure 3.7) as previously described (161). GSEA and STRING analysis of the two differentially expressed gene data sets did not yield any sets of genes associated with resistance.

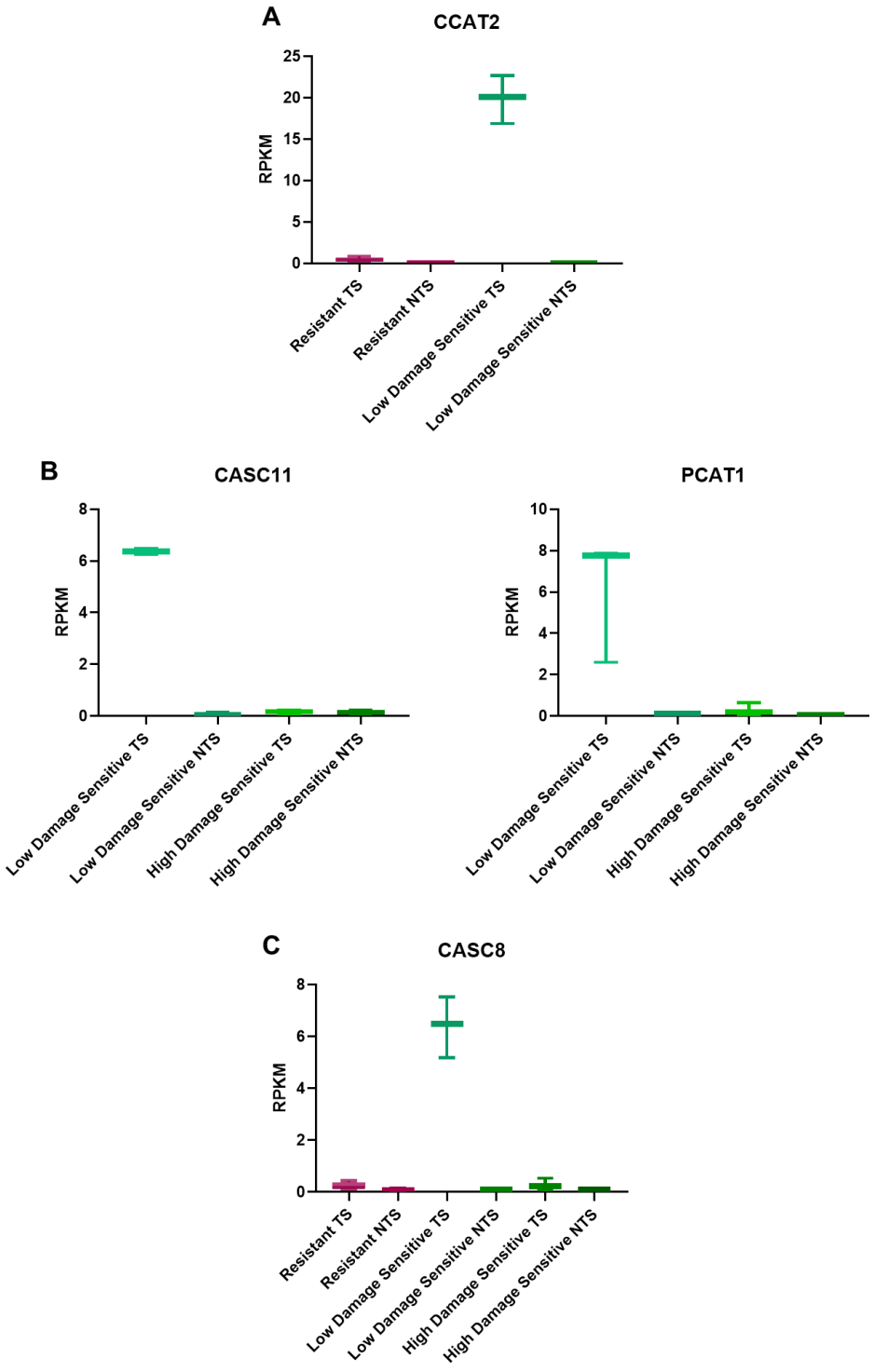

Figure 3.7: Average repair (y-axis) in TS and NTS of non-coding RNAs that are upregulated in low damage sensitive cell lines compared to (A) resistant cell lines, (B) high damage sensitive cell lines, or (C) both resistant and high damage sensitive cell lines.

3.3.7 Oxaliplatin-sensitive and –resistant cell lines have similar responses to mitomycin C and hydrogen peroxide.

In addition to forming intrastrand diadducts, platinum-based drugs induce very low levels of interstrand crosslinks, and it has been proposed that these crosslinks contribute to sensitivity (162). To examine the sensitivity of our cell lines to this type of DNA damage, we treated them with mitomycin C, an interstrand crosslinker, and measured cell viability four days later (Figure 3.8A, Table S2). No significant correlation was found between oxaliplatin IC50 and mitomycin C IC50, suggesting that enhanced repair of interstrand crosslinks is not a common pathway in oxaliplatin resistance. Results also show that the two oxaliplatin-sensitive lines (Colo320hsr and Ls1034) that exhibited relatively low levels of oxaliplatin damage are not hypersensitive to mitomycin C, therefore, their sensitivity is unlikely due to deficient crosslink repair.

Platinating drugs may also induce reactive oxygen species that damage DNA (163). To test if oxaliplatin response correlates with response to this damage type, we treated our cell lines with hydrogen peroxide and measured viability four days later (Figure 3.8B, Table S2). While two of the three oxaliplatin-resistant cell lines were more resistant to reactive oxygen damage, the third was quite sensitive and thus there was no significant correlation between oxaliplatin IC50 and hydrogen peroxide IC50, suggesting that enhanced repair of reactive oxygen-mediated oxaliplatin damage is not a common pathway for resistance. Again, the Colo320hsr and Ls1034 lines were not hypersensitive to hydrogen peroxide and therefore their apparent high sensitivity to oxaliplatin is probably not due to inadequate repair of oxidative damage produced by oxaliplatin.

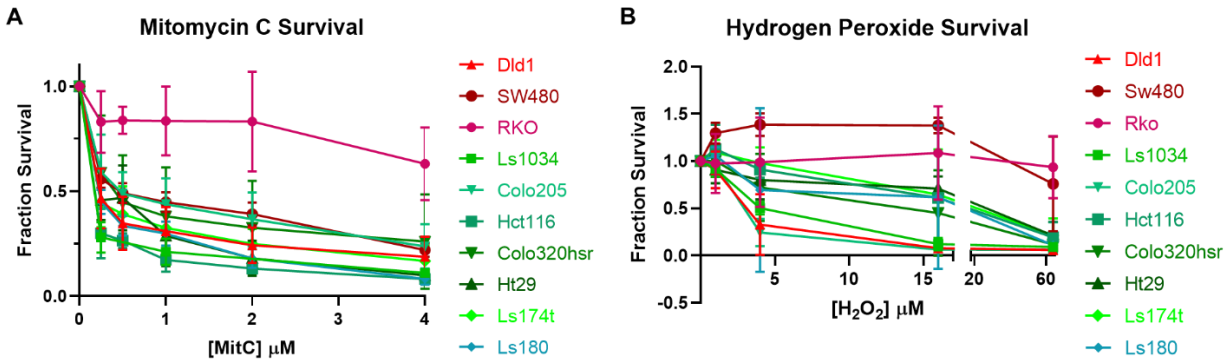

Figure 3.8: Oxaliplatin sensitivity does not correlate with response to interstrand crosslinks or reactive oxygen species. (A) To test if cell line sensitivity is associated with repair of the low level of interstrand crosslinks produced by oxaliplatin, cells were exposed to the interstrand cross-linker Mitomycin C. Mitomycin C dose response curves fail to recapitulate the sensitive and resistant groups seen with oxaliplatin dose response curves (Figure 1A). (B) Oxaliplatin also induces reactive oxygen species. To test if oxaliplatin response may be due to reactive oxygen damage, cells were treated with hydrogen peroxide. Dose response curves fail to recapitulate the sensitive and resistant groups shown in the oxaliplatin dose response curves.

3.4 Discussion

Enhanced excision repair capacity has been proposed as a contributing factor in cellular resistance to platinating anticancer drugs; however the current data to support this notion are inconsistent and fail to address confounding factors (91,92,95-99,102,113,114). To our knowledge, ours is the most comprehensive study to address this issue, compounding multiple novel methods to create the most complete characterization of nucleotide excision repair in cancer cell lines. Notably, this is the first time excision repair maps have been generated to study drug response. This is also one of the first studies to measure the repair response to UV in the context of platinum resistance allowing us to control for confounding factors such as drug transport and additional damage types. We analyzed the excision repair capacity of seven oxaliplatin-sensitive and three oxaliplatin-resistant colorectal cancer cell lines. IC50 values for these lines varied by an order of magnitude, yet the measures of repair that we

employed revealed no consistent association between resistance and repair. Repair measurements included slot blot assays to detect removal of both oxaliplatin and UV photoproducts from the genomes of each line. UV photoproduct repair was also measured among cell lines by excision assay, which detects the relative repair rate at the time sampled, as opposed to the slot blot assay, which detects cumulative repair at each time sampled. Oxaliplatin is known to produce interstrand crosslinks at a low level, and also may damage cells by producing reactive oxygen species (162,163). We tested response to UV, the interstrand crosslinking agent mitomycin C, and hydrogen peroxide and found that oxaliplatin response does not significantly correlate with response to any individual damage type. Finally, we assayed repair by XR-seq to detect how the different cell lines prioritize repair across the genome. Overall, repair patterns were the same in all cell lines. Interestingly, transcription-coupled repair in a small set of genes varied consistently between sensitive and resistant lines. However, these differences reflect differences in transcription, not repair per se. Our consistent finding that repair differences cannot account for differences in oxaliplatin response in our cell lines is further supported by our XR-seq analysis which showed no increased expression of repair genes in resistant cell lines.

Platinating anticancer drugs kill cells by binding to DNA. In light of our results showing that differences in DNA repair do not account for the cellular resistance we observed, it makes sense that this resistance is related to lower net influx of drug, as has been found in other studies and now is strongly supported by this study (143,164-166). Low initial platinum levels in resistant cells are thought to arise from reduced influx and/or increased efflux of drug, and several membrane proteins have been implicated in

transmembrane transport of platinum drugs (150-152). Analysis of gene expression based upon our XR-seq data support a role for one of these proteins, CTR1 (encoded by *SLC31A1*), which transports copper into the cell and was downregulated in our resistant cells. Interestingly, our data did not support a role for the other three candidate transport proteins, rather, our data identified a novel set of membrane proteins as candidates for future study. Identifying whether any of these factors contribute to oxaliplatin resistance could improve treatment options for patients. For example, co-treatment of oxaliplatin with an inhibitor to an upregulated oxaliplatin efflux pump could in theory render resistant cells sensitive again.

While the initial level of DNA damage is a major determinant of oxaliplatin sensitivity, however, other factors may also contribute. Notably, sensitive lines demonstrated a relatively wide range of initial damage and two of these lines demonstrated relatively low levels of initial damage. Analysis of our XR-seq data identified several factors including cancer-associated non-coding RNAs that may contribute to the high sensitivity of these two cell lines to relatively low levels of damage.

Our data showed a wide range in response of cell lines to mitomycin C and peroxide, and it is possible that enhanced repair of interstrand crosslinks and oxygen-mediated damage have a modest role in resistance to oxaliplatin in some cell lines. If enhanced repair of DNA crosslinks or oxygen-mediated damage by oxaliplatin were to substantially increase resistance, then we would have observed resistant cells that demonstrate high levels of oxaliplatin damage. This was not observed. None of our cell lines showed both high resistance and high damage. Conversely, the two sensitive cell lines that exhibited relatively low levels of oxaliplatin were not hypersensitive to

mitomycin C or hydrogen peroxide suggesting no substantial role of crosslink or oxidative damage repair in the sensitivity of these cells.

Overall, we characterized a panel of colorectal cancer cell lines to provide the most holistic view of the role of nucleotide excision repair in oxaliplatin resistance possible with current methods. All of our results support the conclusion that repair is not a necessary determinant of oxaliplatin resistance. We also show that damage levels play a major role in determining oxaliplatin treatment outcome in our cell lines; however, damage levels do not completely predict sensitivity. Additional studies are needed to determine the factors that both lead to and mitigate initial damage formation and their roles in oxaliplatin response. Our repair sequencing datasets provide a starting point to identify these factors.

CHAPTER 4: AMPLIFIED REGION OF CHROMOSOME 8Q24.21 FOUND IN OXALIPLATIN SENSITIVE CELL LINES WITH LOW INITIAL DAMAGE LEVELS

4.1 Introduction

Colorectal cancer is a leading cause of cancer incidence and cancer-related deaths worldwide (136). Oxaliplatin, a third generation platinum-based chemotherapy, is a first line treatment for colorectal cancer and works by inducing guanine-guanine dinucleotide DNA adducts (5,7,8). Unfortunately, approximately half of all patients receiving this treatment will have tumors that are either intrinsically resistant or that develop resistance over the course of treatment (137). There are many proposed mechanisms of resistance to oxaliplatin; notable mechanisms include decreased drug influx, increased drug efflux, impaired drug activation, repair of oxaliplatin-induced DNA damage, and variations in pathway activation in response to this damage (92,144-146). Determining ways to re-sensitize resistant tumors could provide more treatment options and, theoretically, better patient outcomes.

We previously characterized response to oxaliplatin in ten colorectal cancer cell lines and identified three resistant cell lines and seven sensitive cell lines (134). Given that oxaliplatin induced guanine-guanine dinucleotide adducts are solely repaired by nucleotide excision repair (61,63), we tested nucleotide excision repair efficiency in these cell lines. For nucleotide excision repair to occur, bulky DNA adducts are recognized, then repair factors are recruited, next single stranded incisions are made on both the 5′ and 3′ end of the damage, the single stranded DNA fragment containing the

damage (excised oligomer) is then released in complex with repair factors, and the remaining gap in the DNA is re-synthesized and ligated (61,63,68). This process can occur in a transcription-coupled manner, where stalled RNA polymerase recruits repair factors, or in a global repair manner where damage is recognized independent of transcription (79). To characterize nucleotide excision repair in the colorectal cancer cell lines, we measured repair rate via slot blot (138,139), repair amount via excision assay (67,68), a method that involves capturing, labeling, and imaging the excised oligomer, and by excision repair sequencing (XR-seq) (19,81,82), a method by which the excised oligomer is captured, purified, sequenced, and aligned back to the genome to provide single nucleotide resolution of repair throughout the genome. We determined that there was no measurable difference in repair efficiency, by rate, amount, or pattern, between sensitive and resistant cell lines (134).

Damage recognition is the rate limiting step of nucleotide excision repair as most adducts only lead to minor changes in DNA structure (43,167-169). Thus repair of platinum damage occurs primarily through transcription coupled repair as the damage is not as well recognized without stalled RNA polymerase. Because of this, our previous analysis focused mainly on transcribed regions of the genome. However this approach leaves a significant portion of the genome unstudied. Furthermore, these unstudied regions contain regulatory elements that influence the transcriptional profile of each cell line thus unrepaired damage could lead to dramatic changes in the cell (170). To address this gap in our analysis, we created a novel analysis pipeline to identify differential repair in intergenic regions between cell lines.

While we saw no difference in nucleotide excision repair efficiency between the cell lines, we did see a significant difference in initial damage. Oxaliplatin resistant colorectal cancer cell lines exhibited significantly lower levels of oxaliplatin induced DNA damage two hours following addition of oxaliplatin to the media when compared to oxaliplatin sensitive cell lines. Interestingly, oxaliplatin sensitive cell lines exhibited more variable initial damage levels. Most notably, two of the sensitive cell lines exhibited similar initial damage levels to the oxaliplatin resistant cell lines indicating that low initial damage levels are not sufficient to confer resistance (134). In this report, we aimed to determine possible factors that contribute to cell death in oxaliplatin sensitive cell lines with lower initial damage levels using our novel pipeline.

4.2 Methods

4.2.1 Oxaliplatin slot blot (138,139):

Cells were plated in 100mm round dishes. Cells were treated with 200μM oxaliplatin once they reached ~100% confluence to eliminate damage level reduction due to cell divisions. Cells were collected at 2, 6, 12, 24, or 36 hours post addition of oxaliplatin to each plate. After collection, cells were washed with ice cold PBS and collected. DNA was extracted using the QIAamp DNA mini kit. DNA was then treated with RNase A for one hour and purified using a QIAGEN PCR purification kit. DNA was quantified and diluted such that 150 ng of each DNA sample was loaded into each well of a slot blot apparatus. DNA was then transferred to a membrane, and blots were blocked in PBS with 0.1% Tween (PBS-T) and 5% milk at 4°C overnight. The next day the blots were washed in PBS-T three times, and incubated in Abcam anti-platinum damage primary antibody (AbCam, 1:10000 in PBS-T) at 4°C overnight. Blots were

washed and incubated in GE-Healthcare anti-Rat IgG conjugated to horse radish peroxidase for two hours. BioRad Clarity™ Western ECL Substrates were used to detect signal and signal was quantified using Image Quant. Graph Pad Prism 8 software was used to plot damage amount and to calculate repair values.

4.2.2 Binned genome analysis

To test repair in intergenic regions, we used our previously published XR-seq datasets (134). To compare repair in intergenic regions, the hg38 genome was binned into 10kbp windows using the makewindows function in bedtools. This was stored as a .bed file and transcribed regions (also stored as a .bed file) were removed from these windows using the subtract function in bedtools. Next, counts per window for each sample were determined using the multicov function in bedtools with the bam files for each XR-seq datasets as the input files.

```
bedtools makewindows -g hg38.chrom.sizes -w 10000 > hg38.10K.windows.bed

bedtools subtract -a hg38.10K.windows.bed -b
plusStrandTranscribedRegion.bed > BinsNoPlusTS.bed

bedtools subtract -a BinsNoPlusTS.bed -b minusStrandTranscribedRegion.bed >
BinsNoTS.bed

bedtools multicov -bams <input1.bam, input2.bam …> -bed BinsNoTS.bed >
BinCounts.txt
```

This analysis produces a matrix with columns for the chromosome, the bin start site, and the bin end site followed by columns with the number of repair reads in that

window for each sample. This data was then used as input for the DESeq2 package in R which determines which bins have significantly different repair levels between two groups defined by the user.

4.2.3 Quantitative polymerase chain reaction (qPCR)

Primers were designed on the Primer3 website (http://bioinfo.ut.ee/primer3-0.4.0/) and confirmed with serial cloner software for two control DNA segments on either side of our region of interest and three DNA segments within the region of interest. DNA was extracted for three biological replicates for each cell line using the QIAamp DNA mini kit. DNA was then treated for one hour with RNase A and purified using a QIAGEN PCR purification kit. 875 picograms of DNA were used for each RT-qPCR reaction. Reactions were conducted on a QuantStudio™ 6 Flex Real-Time PCR System using iTaq™ Universal SYBR® Green Supermix from Bio-Rad. The $2^{-\Delta\Delta CT}$ values were calculated for each biological replicate of each cell line. To start the two technical replicates for each condition were averaged together. Next the CT values for the three sections within the region of interest were averaged together and the CT values for the two control regions were averaged together for each biological replicate of each cell line. The difference between the amplified region and the control segments were then determined and this value was compared to the difference found for Hct116 (set as the control cell line as it had the median CT value for the amplified region in the non-low damage sensitive cell lines). Finally 2 was raised to the negative of this value. Graph Pad Prism 8 software was used to visualize the data.

4.2.4 Polymerase chain reaction

To confirm the results from the qPCR, PCR and gel electrophoresis were run to visualize the difference in DNA amount of the region of interest. Template DNA was the same as in the qPCR reactions. The PCR reaction was conducted using the Thermo Scientific Maxima Hot Start Green PCR reagent and protocol. Following PCR amplification, samples were run on an agarose gel containing ethidium bromide. The gel was imaged using a BioRad ChemiDoc XRS+ Imaging System and band intensity was quantified using Image Quant software. Graph Pad Prism 8 software was used to visualize the data.

4.3 Results

4.3.1 Determination of three cell line groups based on oxaliplatin response and initial damage levels.

We previously determined and reported the oxaliplatin IC50s of ten colorectal cancer cell lines. Briefly Dld1, Sw480, and Rko are resistant to oxaliplatin while Ls1034, Colo205, Hct116, Colo320hsr, Ht29, Ls174t, and Ls180 are sensitive to oxaliplatin (cell lines listed from highest IC50 to lowest IC50). We also reported the initial oxaliplatin damage levels of these cell lines. Using this data, we created three groups of cell lines: oxaliplatin resistant (low damage), low damage oxaliplatin sensitive, and high damage oxaliplatin sensitive. Figure 4.1A shows the average initial damage levels for each cell line in the three groups. Initial damage levels are significantly higher in the high damage sensitive cell lines compared to either low damage sensitive or resistant cell lines. However, initial damage levels are not significantly different between low damage

sensitive and resistant cell lines. This indicates that while low initial damage levels- likely due to decreased drug influx, increased drug efflux, and/or impaired drug activation- play an important role in determining cellular response to oxaliplatin, they cannot account for the entire response.

Figure 4.1: Damage formation in resistant, low initial damage sensitive, and high initial damage sensitive cell lines. (A) Two hour oxaliplatin damage levels (data from ##). Slot blot assays were conducted on all cell lines (n≥3) following 2 hours exposure to oxaliplatin to determine initial damage levels. Cell lines were split into three groups: oxaliplatin resistant (red), low initial damage oxaliplatin sensitive (blue), and high initial damage oxaliplatin sensitive (green) cell lines. A plot of average initial damage levels for these three groups demonstrates a significant difference between resistant and high damage sensitive (p=0.0041, Welch's t-test) and between low damage sensitive and high damage sensitive (p=0.0066, Welch's t-test), but not between resistant and low damage sensitive (p=0.1701, Welch's t-test). (B) Slot blot of oxaliplatin damage formation over time in a representative resistant and high damage sensitive cell lines and the two low damage sensitive cell lines demonstrates that, over 36 hours, the low damage sensitive cell lines continue to have lower damage than the high damage cell lines. (C) Quantification of the damage formation slot blot shows that the peak time for damage is earliest (11.33 hours post addition of oxaliplatin to the media) for resistant cell lines and latest (24 hours) for high damage sensitive cell lines (p=0.0604 between the two). The low damage sensitive cell lines peak damage occurs at 18 hours which falls between the resistant and high damage sensitive cell lines (p>0.05 compared to either group). This indicates that resistant cell lines may deactivate oxaliplatin more rapidly than the high damage sensitive cell lines.

To test if damage levels remained low over time or if damage formation takes longer in the low damage sensitive cell lines, we conducted slot blot at time points between 2 and 36 hours after the addition of oxaliplatin to the cell lines. Figure 4.1B demonstrates that the damage signal remains low in the low damage sensitive cell lines compared to sensitive cell lines over the course of 36 hours. We calculated the time of

peak damage as a measure of the ability of each cell line to deactivate and/or eliminate the drug over time (Figure 4.1C). As expected, resistant cell lines have the earliest peak damage time and high damage sensitive cell lines have the latest peak damage. Low damage sensitive cell lines peak damage occurs between resistant cell lines and high damage sensitive cell lines. However none of these differences are statistically significant and thus cannot explain differences in cell response to oxaliplatin. We next aimed to determine factors that lead to cell death in the sensitive cell lines with low damage levels.

4.3.2 Creation and validation of a bioinformatics pipeline to identify differentially repaired intergenic bins.

In order to better examine oxaliplatin repair in intergenic regions and, more specifically, to compare repair in these regions between cell lines, we needed to create a new data analysis pipeline. We previously published excision repair sequencing (XR-seq) data on all ten cell lines used in this study (n=2 for all cell lines except n=1 for Ls174t and Colo320hsr) (134). These data allow us to visualize the location and relative amount of repair throughout the genome at single nucleotide resolution. However, our previous work with this data largely focused on repair in transcribed regions using repair of the non-transcribed strand (NTS) to measure global repair. For this new analysis, we aimed to study repair solely in non-transcribed regions. Briefly, we created 10kbp windows and removed transcribed regions from these windows. We then counted the number of repair reads in each window for each dataset. Next, we used this counts data as input for the DESeq2 package in R which determines significantly differentially repaired bins between two user-defined groups.

We first tested the percent of differentially repaired bins that would be identified from random groupings of our datasets to determine the results we could see due to random differences between cell lines. To do this we grouped our 10 cell lines in five different random groupings (Figure 4.2A, 4.2B). In our random groupings, we kept replicates of the same cell line together to ensure that we were seeing random results due to cell line differences. We found that on average, 0.539% of bins were identified as significantly differentially repaired between random groupings of our cell lines with a range from 0.001% to 1.721%.

A

Group 1	Group 2	Significant Bins	Total Bins	Percent Bins
Random A (9)	Random B (9)	2	185246	0
Random2 A (9)	Random2 B (9)	3188	185246	1.72
Random3 A (12)	Random3 B (6)	639	185246	0.34
Random4 A (9)	Random4 B (9)	672	185246	0.36
Random5 A (7)	Random5 B (11)	490	185246	0.26
NHF1 (4)	XPC (2)	65401	161488	40.5
XPC (2)	CSB (2)	65400	162129	40.34
Male (10)	Female (6)	1522	185221	0.82
Human Lymphocytes Cisplatin (2)	Human Lymphocytes Oxaliplatin (2)	12380	163140	7.59

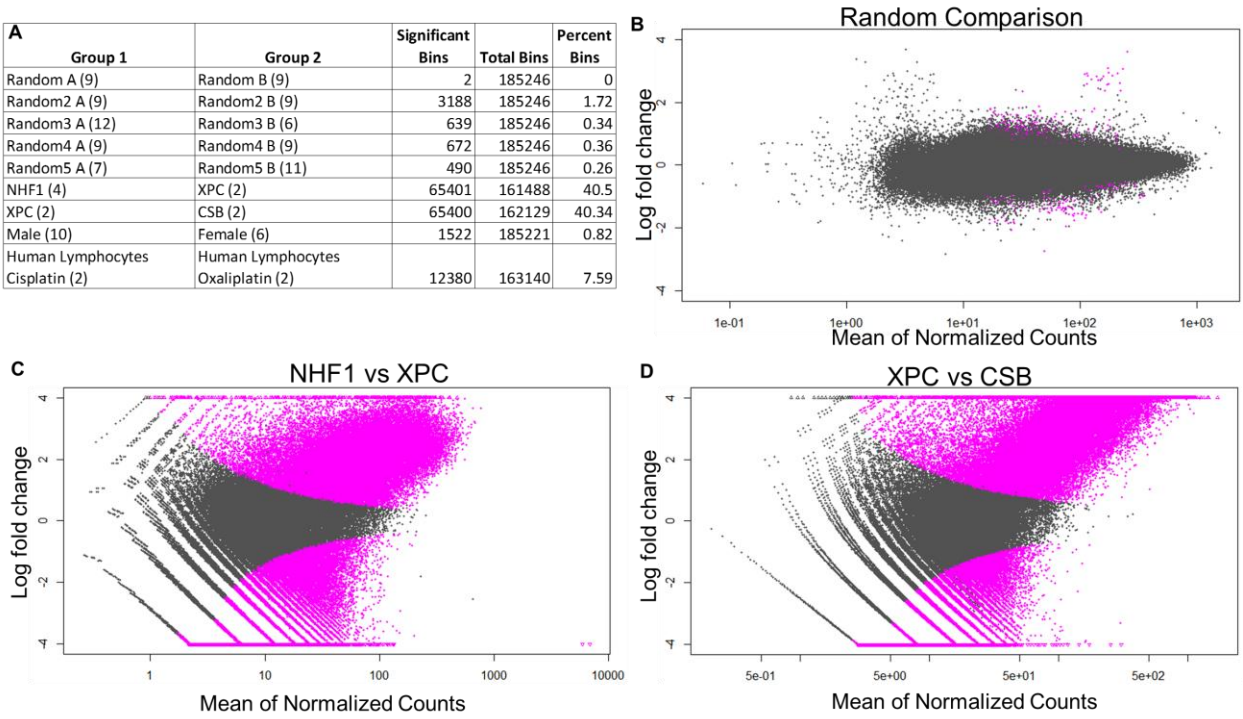

Figure 4.2: Control comparisons of differential repair in intergenic bins. (A) Table of the differentially repaired bins for each control comparison. “Group 1” and “Group 2” indicate the comparison groupings, the number in parentheses indicates the number of XR-seq datasets in each group. “Significant bins” are the number of differentially repaired bins identified by our analysis. “Total bins” is the number of bins used in the differential repair analysis. The number of total bins varies between comparison groups since bins with no or extremely low total counts across all samples are filtered out. “Percent bins” indicates the percent of total bins that are significantly differentially repaired. (B) MA plot of repair in intergenic bins compared between two random groupings of cell lines shows low levels of significantly differentially repaired bins. For each bin (plotted as a dot), the difference between the two groups of cell lines (log fold change) is plotted over the average counts across all samples (mean of normalized counts). Bins exhibiting significantly different repair (expression) are plotted in purple (padj<0.05). (C & D) Same as B but for the positive control comparisons between (C) NHF1 vs XPC mutant cell lines or (D) XPC mutants and CSB mutants. A larger portion of bins exhibit significantly different repair in these positive control groups.

As a positive control to see how many significantly differentially repaired bins we could identify using this method, we compared a wildtype normal human fibroblast cell line (NHF1) with normal nucleotide excision repair function with XPC mutant cell lines which lack global repair and thus can only conduct transcription coupled repair (Figure 4.2A, 4.2C). The data for these cell lines came from XR-seq studies on the repair of cyclobutane pyrimidine dimers. Since we removed the known transcribed regions, we

expected to see a high percentage of significantly repaired bins given that only wildtype NHF1 cell lines can repair these regions. We found that approximately 40% of bins tested are significantly differentially repaired between wildtype and XPC cell lines. This percentage was also achieved by comparing XPC mutant cell lines with CSB mutant cell lines, which lack transcription coupled repair, indicating that 40% of bins is likely the maximum amount of difference our method can detect (Figure 4.2A, 4.2D). While this is less than we initially expected, this maximum level is not surprising given the low overall read depth of XR-seq combined with the low levels of repair in heterochromatic regions. These two factor combined could mean that our XR-seq data may not detect enough reads from these regions to ascertain a difference between cell lines.

Surprisingly, we found that a number of intergenic bins were upregulated in the XPC mutant cell lines which should only exhibit transcription coupled repair. Since XR-seq is not completely quantitative and calculates repair relative to other regions, a sample with repair in fewer locations throughout the genome will exhibit stronger relative reads than a sample in which repair occurs more frequently throughout the genome. Repair in XPC mutants may provide a dataset to study low levels of transcription in intergenic regions (171,172). This possibility is supported by the finding that regions with significantly enriched repair in XPC mutant cell lines show preferential repair of one strand over another (Figure 4.3). Interestingly, repair in these regions appears to be equal between strands in wildtype and CSB mutant cell lines.

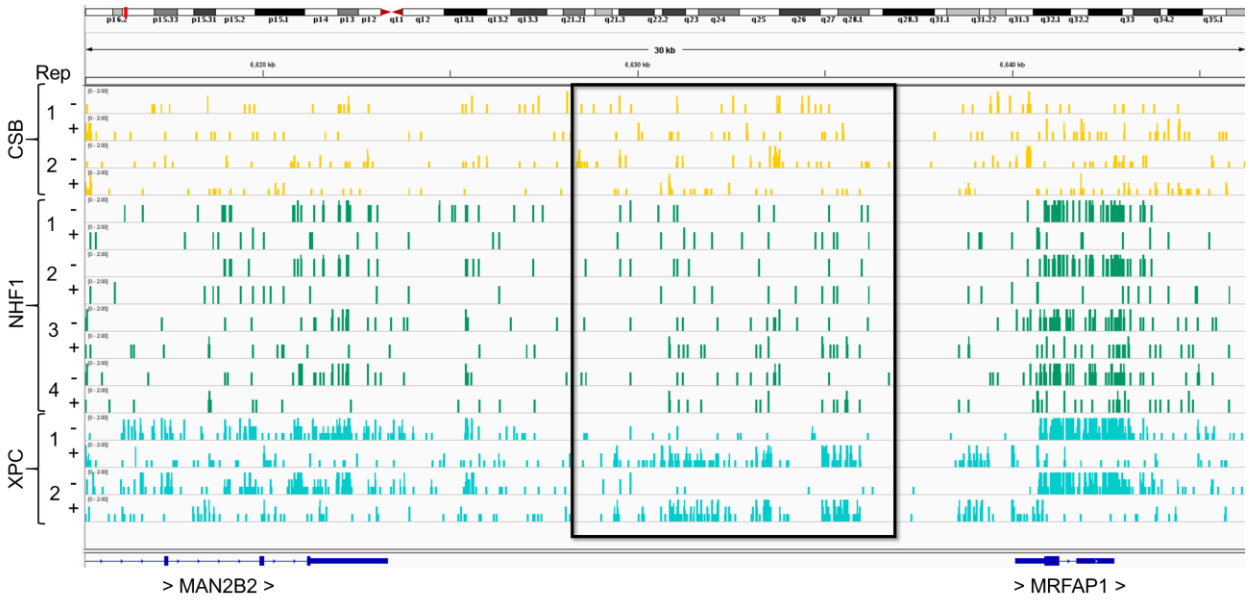

Figure 4.3: XPC mutant cell lines sensitively identify transcription. An example of this is shown in this 30 Kb window of Chromosome 4 (6,615,256 – 6,646,369). XPC mutant cell lines (blue) show strong preferential repair for the plus strand in a non-transcribed region (outlined by the black box) of the hg38 human genome, mimicking the transcription coupled repair patterns seen at known genes, such as MRFAP1. Interestingly, wildtype NHF1 cell line (green), which exhibit transcription coupled repair, do not show strong strand preference in this region. CSB mutant cell lines (yellow), which lack transcription coupled repair, do not show preferential repair of one strand over the other in this region.

4.3.3 Determination of differentially repaired intergenic bins in colorectal cancer cell lines with different oxaliplatin sensitivities and initial damage level.

We next compared reads per bin between our oxaliplatin sensitive and oxaliplatin resistant cell lines and found that 2.939% of bins were significantly differentially repaired (63% of these bins were upregulated in the sensitive cell lines and 37% were upregulated in the resistant cell lines). While this is a low percentage, it is over 5 fold higher than the average of our random trials indicating that there is probably some significance to this finding. When we repeated this study by grouping the cell lines into those that exhibit low initial damage in response to oxaliplatin treatment and those that exhibit higher levels of damage in response to the same dose of oxaliplatin, the percent

of significantly differentially repaired bins increases to 7.033%, indicating that the difference between sensitive and resistant cell lines may be due to the initial damage level (Figure 4.4).

Since we are interested in determining what causes the low damage sensitive cell lines to induce cell death in response to lower levels of damage, we tested the percent of significantly differentially repaired bins between these cell lines and the resistant cell lines and between these cell lines and the high damage sensitive cell lines. We found a 5.510% and a 9.530% difference respectively (Figure 4.4A).

While comparing the percentage of significantly differentially repaired bins can give us some insight into the repair properties of these cell lines, we can better understand the cell biology that may drive the differences in drug response by connecting these differentially repaired bins with genomic features.

A Group 1	Group 2	Significant Bins	Total Bins	Percent Bins
Sensitive (12)	Resistant (6)	5444	185246	2.94
Low Damage (9)	High Damage (9)	13029	185246	7.03
Resistant (6)	Low Damage Sensitive (3)	10195	185034	5.51
Low Damage Sensitive (3)	High Damage Sensitive (9)	17641	185108	9.53

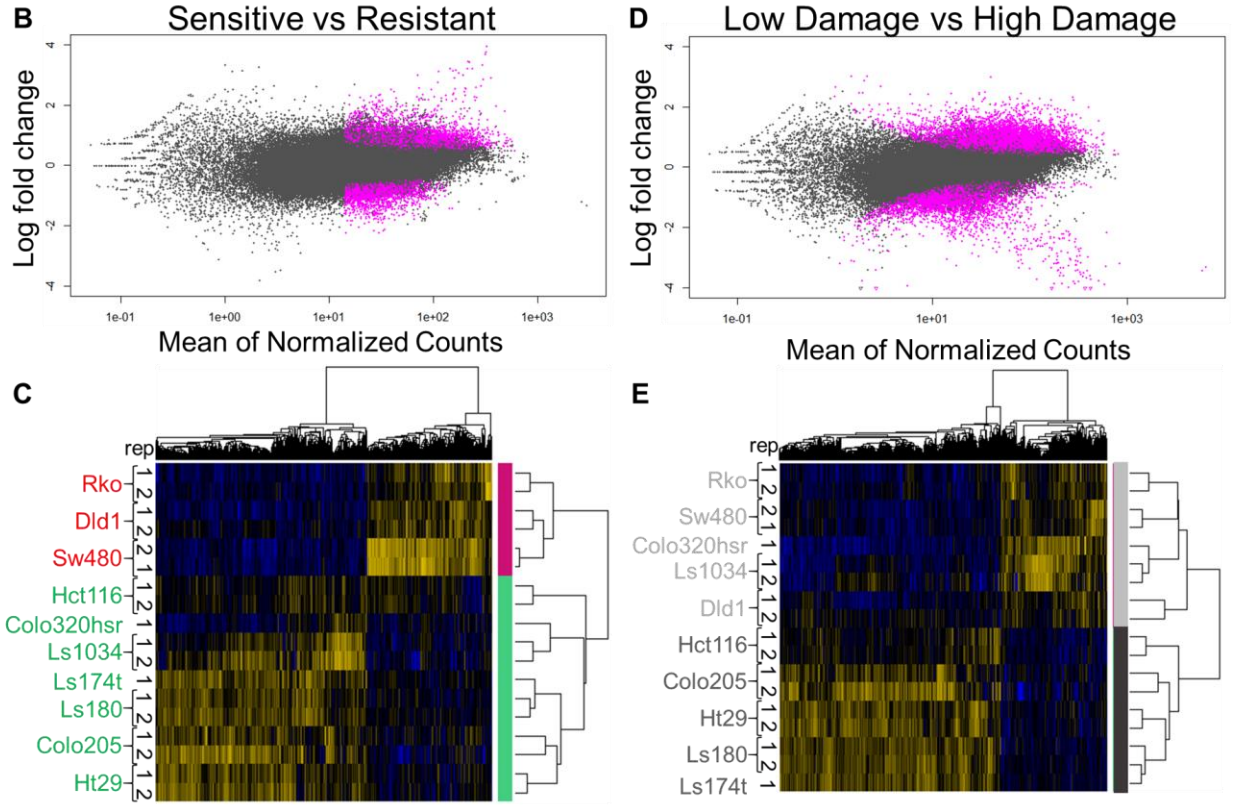

Figure 4.4: Differentially repaired, intergenic bins between oxaliplatin –sensitive and –resistant cell lines and between high damage and low damage cell lines. (A) Table of the differentially repaired bins for each test comparison. Group 1 and Group 2 indicate the comparison groupings, the number in parentheses indicates the number of XR-seq datasets in each group. The significant bins are the number of differentially repaired bins identified by our analysis, the total bins is the number of bins used in the differential repair analysis. The number of total bins varies between comparison groups since bins with no or extremely low total counts across all samples are filtered out. Percent bins indicates the percent of total bins that are significantly differentially repaired. (B) MA plot of repair in intergenic bins compared between sensitive and resistant cell lines. For bin (plotted as a dot), the difference between sensitive and resistant cell lines (log fold change) is plotted over the average counts across all samples (mean of normalized counts). Bins exhibiting significantly different repair (expression) are plotted in purple (padj<0.05). (C) Heatmap of the differentially repaired bins between sensitive (green band) and resistant (red band) cell lines. Yellow lines indicate higher repair while blue lines indicate lower repair. (D & E) Same as B and C except compared between the low initial oxaliplatin damage (light gray) and high initial oxaliplatin damage (dark gray) cell lines.

4.3.4 Identification of a large region of chromosome 8q24.21 with amplified repair in low damage sensitive cell lines

Using our novel analysis pipeline, we identified an approximately 1.6 mega-base pair long region in chromosome 8 that has significantly higher repair in low damage sensitive cell lines compared to resistant or high damage sensitive cell lines. Figure 4.5A shows repair reads in this region. By calculating the RPKM of the amplified region and control regions of the same length flanking the amplified region (Fig 4.5B, 4.5C, 4.5D), we can quantify the difference in repair. While the flanking control regions show no significant difference in repair levels between the three groups, there is significantly higher repair of the region of interest in low damage sensitive cell lines compared to resistant cell lines ($p=0.0004$) and compared to high damage sensitive cell lines ($p<0.0001$). Indeed, on average there is 18.43 times higher repair in the low damage sensitive cell lines compared to all other cell lines. Importantly, no significant difference in repair level is seen between resistant cell lines and high damage sensitive cell lines.

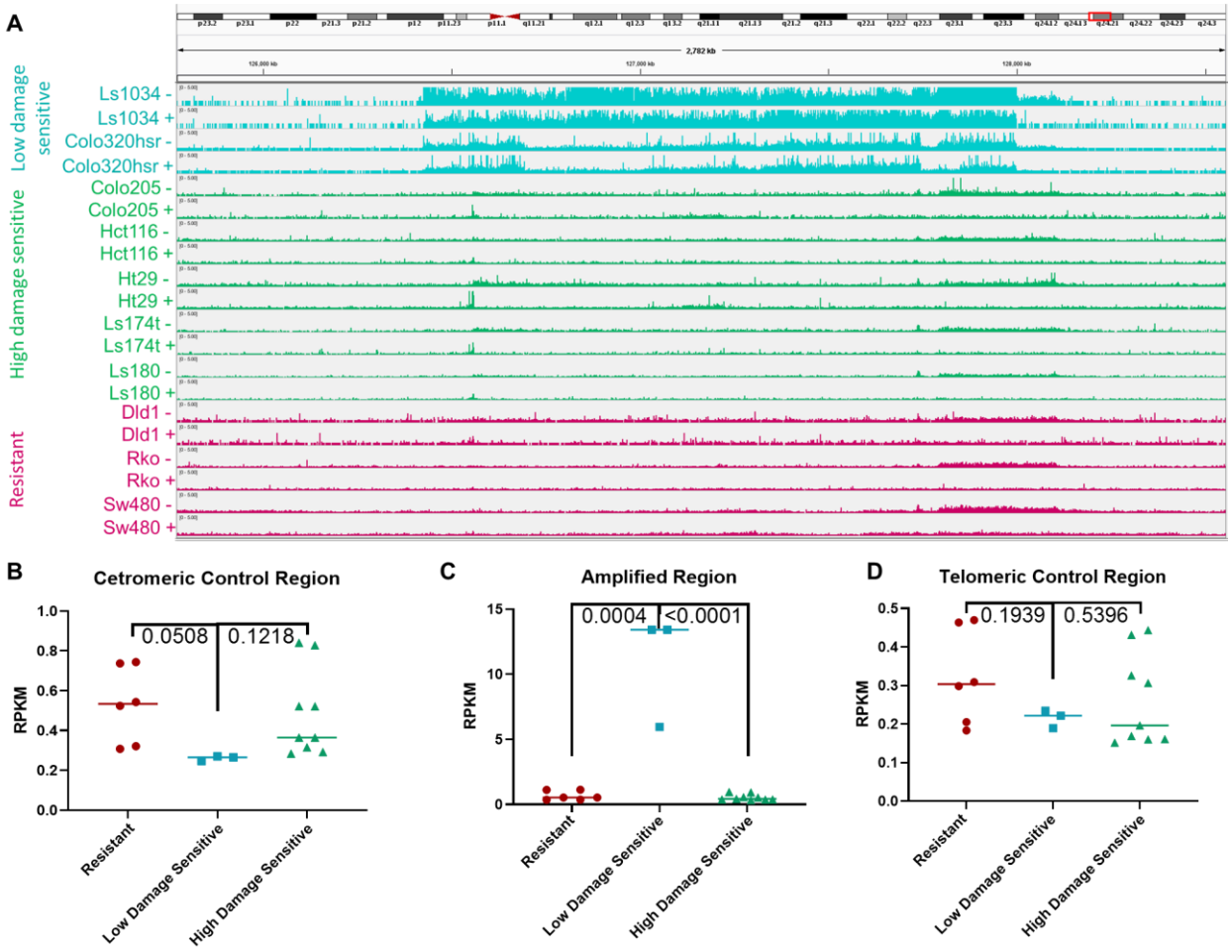

Figure 4.5: Amplified oxaliplatin repair in a 1.6 mega-base pair region of chromosome 8 q24.21 in oxaliplatin sensitive colorectal cancer cell lines with low levels of oxaliplatin damage. XR-seq was conducted on ten colorectal cancer cell lines (2 low damage oxaliplatin sensitive=blue, 5 high damage oxaliplatin sensitive= green, 3 oxaliplatin resistant= red) two hours following treatment with oxaliplatin. (A) Repair reads plotted over a 2.782 mega base pair region, highlighted by a red box over a diagram of chromosome 8. While oxaliplatin resistant and high damage sensitive cell lines show similar repair levels across the entire region, low damage sensitive cell lines show highly amplified repair over a 1.6 mega base pair region. (B-D) Reads per kilobase million for the resistant cell lines (red), low damage sensitive (blue), and high damage sensitive (green) over 1,592,775 base pairs (B) immediately adjacent on the centromeric side of the amplified region, (C) over the amplified region, (D) immediately adjacent on the telomeric side of the amplified region shows no significant difference in repair on either side of the amplified region but a significant increase in repair in the amplified region in the low damage sensitive cell lines compared to resistant cell lines ($p=0.0004$) and compared to high damage sensitive cell lines ($p<0.0001$).

4.3.5 Determination of DNA amplification in the chromosome 8q24.21 amplified repair region

To determine if this amplification in repair is due to amplification of the DNA in this region or due to some alternative mechanism (ie enhanced repair due to altered chromatin architecture), we conducted quantitative PCR (qPCR) on the region of interest and adjacent control regions. We designed primers for three DNA segments within the amplified region and two control segments flanking the amplified region.

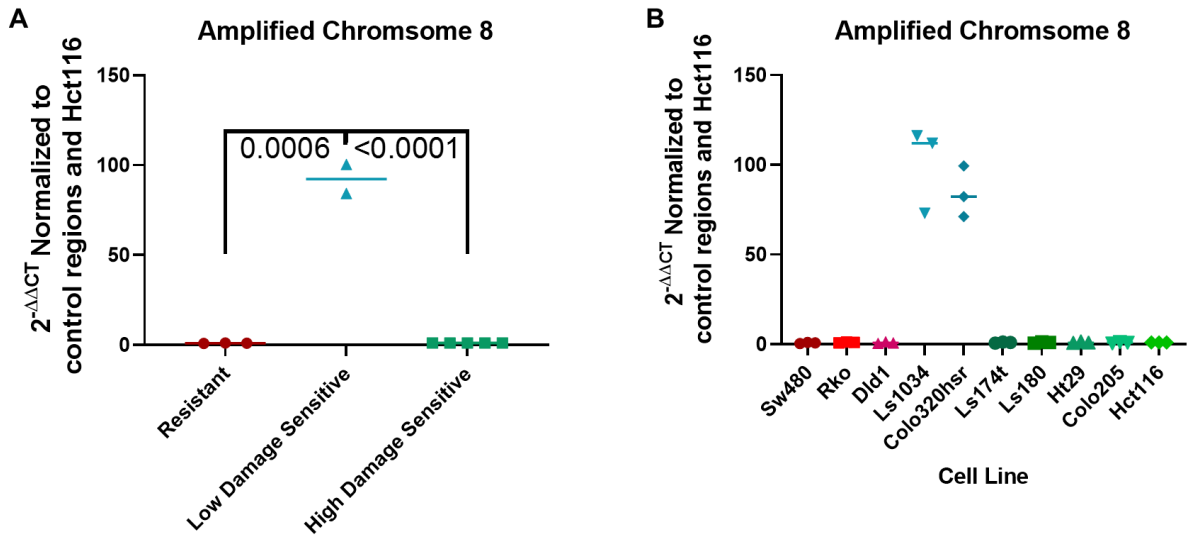

Figure 4.6: DNA levels in the region of interest are significantly higher in low damage sensitive cell lines compared to resistant and high damage sensitive cell lines. qPCR was conducted on three DNA segments within the amplified region and two control segments flanking the amplified region. The CT value was determined for two technical replicates of each of three biological replicates for each cell line. The control CT values and the amplified region CT values were averaged for each biological replicate and the difference between the amplified region and the control region was determined. The high damage sensitive cell line, Hct116, was used as the control cell line as it had the median CT value for the amplified region (excluding the low damage sensitive). (A) qPCR shows significantly higher DNA levels , approximately 100 fold higher, were found in the low damage sensitive cell lines (blue) compared to the resistant cell lines (red; p=0.0006) and the high damage sensitive cell lines (green; p<0.0001). (B) qPCR shows consistent DNA amplification in the low damage sensitive cell lines (blue; Ls1034 and Colo320hsr) between both cell lines and biological replicates compared to resistant cell lines (red; Sw480, Rko, and Dld1) and high damage cell lines (green; Ls174t, Ls180, Ht29, Colo205, and Hct116).

As seen in Figure 4.6, there is a significantly higher amount of DNA from this region in the low damage sensitive cell lines compared to either the resistant ($p=0.0006$) or high damage sensitive cell lines ($p<0.0001$). PCR and gel electrophoresis on a representative DNA segment from the control region and from the region of interest on the low damage sensitive cell lines and Hct116 as a control cell line confirm these results (Figure 4.7). No significant difference was seen in DNA amount between the resistant cell lines and high damage sensitive cell lines. This indicates that the amplified repair seen in our initial analysis is likely due to an increase in DNA amount.

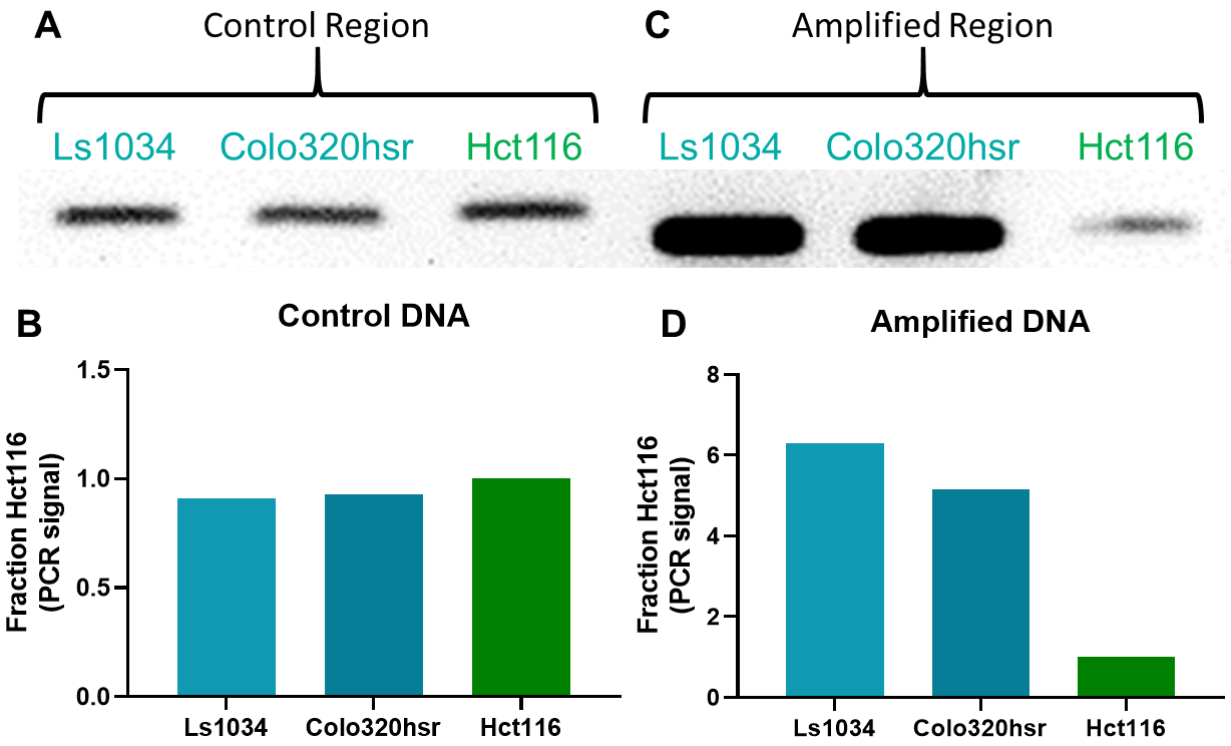

Figure 4.7: Validation of the DNA amplification found in the low damage sensitive cell lines. PCR and gel electrophoresis was conducted on a control region and on a region within the amplified section of the low damage sensitive for the two low damage sensitive cell lines (blue; Ls1034 and Colo320hsr) and one control cell line (green; Hct116). (A) Equal DNA levels are seen across all three cell lines. (B) Quantification of the PCR signal using Image Quant and Prism software shows similar DNA amounts. (C) DNA amplification is seen in the region of interest in the two low damage sensitive cell lines while the signal is much lower in the control cell line. (D) Quantification of the region of interest bands confirms DNA amplification in the low damage sensitive cell lines.

4.3.6 Characterization of transcription in the amplified region

We next aimed to determine if the amplified region may be involved in response to oxaliplatin. The relationship between DNA amplification and expression levels of genes in the amplified region is not necessarily direct (173,174). Therefore we next identified the genes encoded in the amplified region and tested to see if they exhibited higher levels of transcription in low damage sensitive cell lines compared to resistant cell lines and high damage sensitive cell lines. There are 17 coding and non-coding genes in the amplified region. Table 4.1 list these genes, their functions, and any connection with oxaliplatin resistance that has previously been described (160,175-180). Many of the genes in this region have been associated with carcinogenesis and tumor progression, most notably the oncogene *MYC* is found in this region.

Genes	Full Name	Function	Cancer associations	Association with Oxaliplatin resistance
PCAT1	Prostate Cancer-Associated Transcript 1	Long non-coding RNA promotes cell proliferation; negatively regulates BRCA2 and positively regulates Myc; may act as a microRNA sponge	Significantly upregulated in prostate and colorectal cancer; expression correlates with distant metastasis	N/A
PRNCR1	Prostate Cancer Associated Non-Coding RNA 1	Long non-coding RNA; binds androgen receptor; suggested enhancer activity (CARLO2) for MYC	Prostate cancer, colorectal cancer (?)	N/A
CASC21	Cancer Susceptibility Candidate 21	Long non-coding RNA; enhancer activity (CARLO2)	Colorectal cancer (?)	N/A
CCAT2	Colon Cancer Associated Transcript 2	Long non-coding RNA; promotes cell proliferation; suppresses apotosis; negatively regulates biogenesis of MIR145	Upregulated in colorectal cancer	SNP associated with response;
POU5F1B	POU Class 5 Homeobox 1B	Encodes a functional protein; weak transcriptional activator; may play a role in carcinogenesis; may play a role in eye development	Prostate cancer (maybe others)	N/A
MYC	MYC Proto-oncogene, BHLH Transcription Factor	Encodes nuclear phosphoprotein; involved in cell cycle progression and cellular transformation and inhibits apoptosis; binds E box and regulates transcription	many (including colorectal cancer)	myc overexpression correlates with cisplatin resistance and myc expression increases following cisplatin treatment; overexpression of c-myc in pancreatic cancer cells sensitized cells to cisplatin (through cyclin D); c-myc overexpression in colorectal cancer cell lines increases resistance to oxaliplatin
MIR1204	MicroRNA 1204	micro RNA	ovarian squamous cell carcinoma, plasma cell neoplasm	N/A
MIR1205	MicroRNA 1205	micro RNA	N/A	N/A
MIR1206	MicroRNA 1206	micro RNA	Plasma cell neoplasm	N/A
PVT1	Pvt1 Oncogene	long non-coding RNA; candidate oncogene; regulated by p53; implicated in regulating MYC levels (promoting tumorigenesis); MYC does not advance cancer without overexpression of PVT1 as well	overexpression associated with breast cancer, ovarian cancer, acute myeloid leukemia, and hodgkin lymphoma	N/A
FAM84B	Family with sequence similarity 84, Member B	Interacts with alpha-1 catenin; maybe tumor suppressor	upregulated in breast cancer	FAM84B-AS expression increases sensitivity to platinum in gastric cancer cells
PCAT2	Prostate Cancer Associated Transcript 2	Long non-coding RNA; part of CARLO4 enhancer activity	Prostate cancer	N/A
CASC19	Cancer Susceptibility Candidate 19	Long non-coding RNA; part of CARLO6 enhancer activity	colorectal cancer	N/A
CCAT1	Colon Cancer Associated Transcript 1	long non-coding RNA; promotes tumor formation; may regulate long range chormosomal interations; may be a molecular sponge for miRNA; part of CARLO5 enhancer activity	upregulated in colorectal cancer (and other cancers)	N/A
CASC8	Cancer Susceptibility Candidate 8	Long non-coding RNA; CARLO1 enhancer activity	Childhood Acute Lymphocytic Leukemia; Bladder Cancer	N/A
CASC11	Cancer Susceptibility Candidate 11	Long non-coding RNA; CARLO7 enhancer activity	Colorectal cancer, Astrocytoma	CASC11 expression increases with platinum (ox, cis, and carbo) and this increase in turn leads to platinum resistance (siRNA knockdown of CASC11 re-sensitizes cells)
TMEM75	Transmembrane Protein 75	Long non-coding RNA	N/A	N/A

Table 4.1: Genes in amplified region and their functions and cancer associations

We measured transcription levels, relative to the amount of DNA, of 16 of the 17 genes in the region (we eliminated *MIR1206* as it has extremely low RPKM values, often 0, for both strands across all cell lines). For this analysis, we calculated the ratio of

the reads from the transcribed strand (TS) of each gene over the total reads, transcribed strand plus non-transcribed strand (NTS). This enables us to test if the genes are transcribed at similar rates in all cell lines. Given that platinum damage is more readily recognized through transcription coupled repair, we expect ratios greater than 0.5 for transcribed genes. If similar TS/ (NTS+TS) ratios between all cell lines indicates are found, this would imply that there is similar transcriptional activity between all cell lines (and may indicate higher expression in cell lines with amplified DNA). The average of this ratio across the 16 genes tested showed a 1.36 times higher ratio in low damage sensitive cell lines compared to all other cell lines. Figure 4.8 shows that the average ratio in low damage sensitive cell lines was significantly higher than both resistant and high damage sensitive cell lines, however there was no significant difference between resistant and high damage sensitive cell lines in this region. This indicates that the genes within the amplified region may be more actively transcribed in the low damage sensitive cell lines compared to all other cell lines. To test if this increase in transcriptional activity was specific to the amplified region or if there was a genome wide increase in transcriptional activity in the low damage sensitive cell lines, we calculated the TS/ (NTS+TS) ratio for all genes in a control region of the same size directly adjacent to the amplified region. No significant difference was seen in the TS/ (NTS+TS) ratio between low damage sensitive cell lines and the resistant cell lines for this control. Moreover, the ratio in this region was significantly lower in low damage sensitive cell lines compared to high damage sensitive cell lines. To further confirm that this increase in transcriptional activity was genome wide, we compared the average TS/(NTS+TS) ration for 32 housekeeping genes between the low damage sensitive cell

lines and the resistant and high damage sensitive cell lines. While low damage sensitive cell lines did have significantly higher repair than the high damage sensitive cell lines over the housekeeping genes, the difference was less than that detected in the region of interest. Additionally, similar transcriptional activity of the housekeeping genes was detected between the low damage sensitive cell lines and the resistant cell lines. This indicates that the low damage sensitive cell lines amplified region is more transcriptionally active.

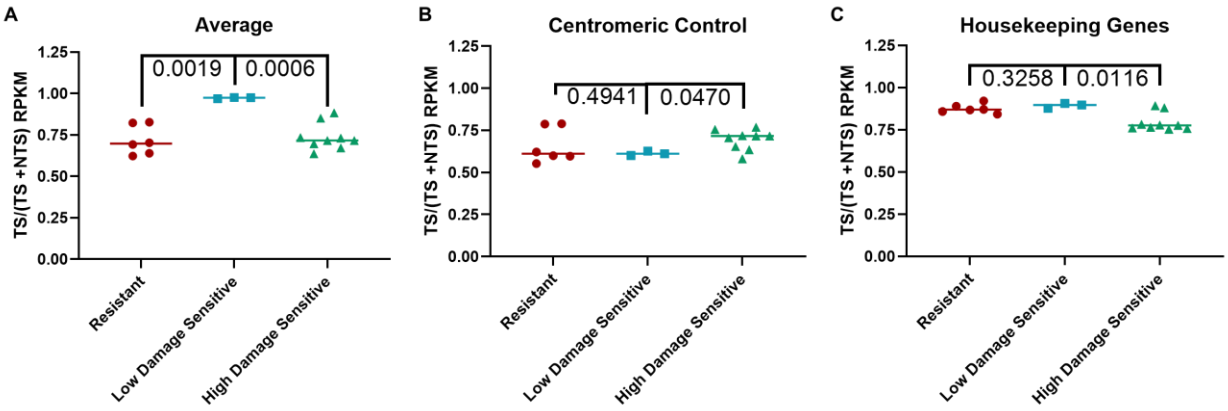

Figure 4.8: Transcriptional activity in the amplified region may be higher in low damage sensitive cell lines compared to resistant and high damage sensitive cell lines. The ratio of repair reads from the transcribed strand of genes compared to the total reads from both the transcribed and non-transcribed strand (TS/(TS+NTS)) of the gene region was calculated for each gene in the region of interest. (A) The TS/(TS+NTS) for genes in the region of interest is significantly higher in the low damage sensitive cell lines (blue) than the resistant cell lines (red; p=0.0019) and high damage sensitive cell lines (green; p=0.0006). This indicates that the amplified region is more transcriptionally active than the resistant and high damage sensitive cell lines. (B) The TS/(TS+NTS) ratio for all of the genes in the 1,592,775 base pairs immediately adjacent to the region of interest on the centromeric side shows similar transcriptional activity between the low damage sensitive cell lines and the resistant cell lines. Furthermore, there is significantly lower transcriptional activity in the low damage sensitive cell lines compared with the high damage sensitive cell lines. (C) The TS/(TS+NTS) ratio for 32 housekeeping genes once again shows similar transcriptional activity between low damage sensitive and resistant cell lines. The high damage sensitive cell lines exhibit significantly lower transcriptional activity of the housekeeping genes than the low damage sensitive cell lines, however this difference is less than the difference found from the region of interest.

The TS/ (TS+NTS) ratio for each gene in the region of interest is shown in Figure 4.9. Of the 17 genes in the region, CASC19, CASC11, and CASC21 have the most

significant increase in transcriptional activity in low damage sensitive cell lines compared to all other cell lines implicating a potential importance for these cancer associated transcripts in oxaliplatin sensitivity despite low levels of initial damage. CASC19 and CASC21 have not been implicated in altering oxaliplatin response; however siRNA knockdown of CASC11 has been shown to re-sensitize resistant cell lines to oxaliplatin making it an exciting candidate for follow-up studies (179).

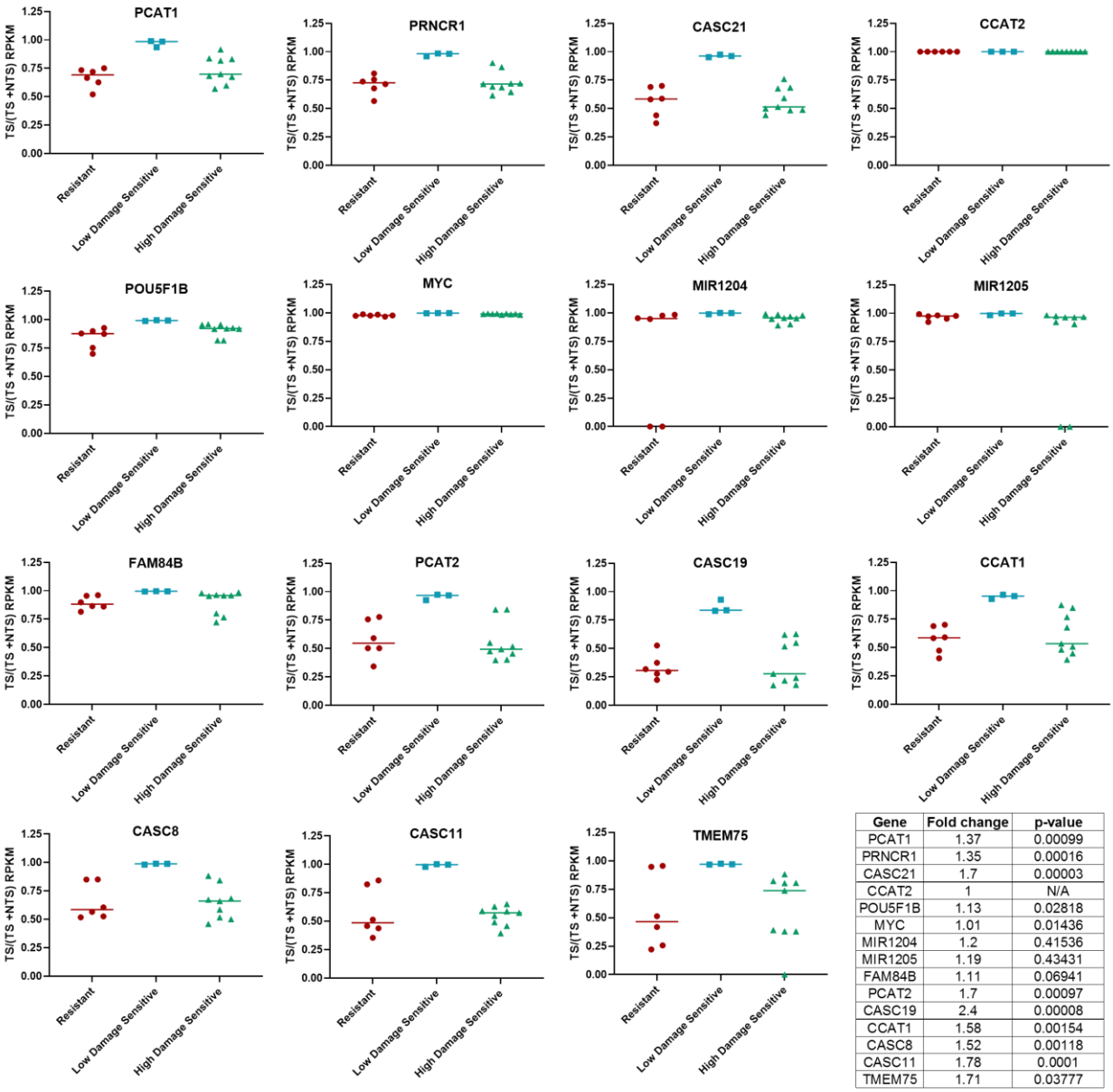

Gene	Fold change	p-value
PCAT1	1.37	0.00099
PRNCR1	1.35	0.00016
CASC21	1.7	0.00003
CCAT2	1	N/A
POU5F1B	1.13	0.02818
MYC	1.01	0.01436
MIR1204	1.2	0.41536
MIR1205	1.19	0.43431
FAM84B	1.11	0.06941
PCAT2	1.7	0.00097
CASC19	2.4	0.00008
CCAT1	1.58	0.00154
CASC8	1.52	0.00118
CASC11	1.78	0.0001
TMEM75	1.71	0.03777

Figure 4.9: Transcriptional activity of the genes within the amplified region. MIR1204, MIR1205, and FAM84B show a trend towards higher transcriptional activity in the low damage sensitive compared to the other cell lines. All other genes in this region show significantly higher transcriptional activity via repair in the low damage sensitive cell lines compared to resistant and low damage cell lines. Fold change and p-value (t-test) calculated by comparing values for low damage sensitive cell lines to all other cell lines (resistant and high damage sensitive) combined.

4.4 Discussion

In this study, we describe a new XR-seq analysis pipeline to identify differentially repaired, intergenic regions. This pipeline will enable us to better examine how different

genomic and chromatin features, both normal and pathologic, impact nucleotide excision repair. While our previous analysis focused largely on repair in transcribed regions of the genome, this pipeline enables us to better compare repair between two groups in a truly genome-wide fashion.

Using this pipeline, we were able to identify a ~1.6 mega base pair region of chromosome 8 that exhibited amplified repair in oxaliplatin sensitive cell lines that have low initial levels of oxaliplatin-DNA adduct formation. Both oxaliplatin sensitive cell lines with high initial oxaliplatin-DNA adduct levels and oxaliplatin resistant cell demonstrate normal levels of repair in this region. Further examination identified DNA amplification of this region in the low damage sensitive cell lines. This indicates that the increased repair may be due to the DNA amplification.

Surprisingly, while cancer cells often have many copy number aberrations, DNA amplifications, translocations, and other genomic instabilities (173,174,181-184), we did not identify any additional regions with this magnitude of differential repair. It is possible that there are other DNA amplifications that lack enriched repair, possibly due to the chromatin structure, or a tolerance of DNA damage in the unstable region. Further studies are needed to characterize additional amplifications and translocations in these cell lines so that we can test how repair is influenced by these genomic changes. Additionally, while we were able to use this pipeline to identify a region of possible interest for promoting oxaliplatin sensitivity in response to low levels of initial oxaliplatin damage, more work is needed to connect the significantly differentially repaired bins with possible genomic and epigenetic factors that would direct the difference in repair.

The amplified region contains a number of coding genes and non-coding RNAs that have been implicated in carcinogenesis and cancer progression; many have been specifically linked to colorectal cancer. These genes, including MYC, may be promoting higher rates of DNA replication and cell division in the face of damage leading to the increased sensitivity to oxaliplatin despite lower initial levels of damage (160,175-180). Additional studies are needed to test if knocking down the expression of genes in this region reduce sensitivity in the low damage sensitive cell lines and if overexpressing these genes in resistant cell lines increases sensitivity to oxaliplatin.

Overall, we used a novel XR-seq analysis pipeline to identify a ~1.6 mega base-pair amplified region of chromosome 8 specific to colorectal cancer cell lines that are sensitive to oxaliplatin despite low oxaliplatin damage compared to oxaliplatin resistant colorectal cancer cell lines and oxaliplatin sensitive colorectal cancer cell lines that have high oxaliplatin damage levels. In the low damage sensitive cell lines, this region displays DNA amplification, increased DNA repair, and higher transcriptional activity, none of which are found in the other cell lines. It is possible that genes in this region may play an important role in the cell death response to oxaliplatin exposure. Additional studies are needed to determine if this region can provide further insight onto determinants of oxaliplatin response.

CHAPTER 5: INFLUENCE OF CIRCADIAN RHYTHM ON TUMOR AND NORMAL TISSUE RESPONSE TO PLATINUM-BASED DRUGS

5.1 Introduction

Platinum-based drugs are one of the most commonly used drugs in solid tumor management. Platinum-based drugs can have devastating side effects including renal dysfunction, neurotoxicity, and ototoxicity (185).Despite the therapeutic strength of platinum based chemotherapeutic regimens, almost half of patients have tumors that are resistant to cisplatin and endure the toxicities from this treatment for little to no benefit (186). A better understanding of both how tumor and normal tissues respond to platinum treatment and how additional cues, such as timing of treatment, change this response may enable us to increase the therapeutic efficiency of these drugs.

The circadian clock is a transcription-translation feedback loop that regulates the daily rhythmicity of everything from an organism's biochemistry to its behavior (187). Many pathways, including nucleotide excision repair and membrane permeability, are under circadian control (126,188). Thus it is likely that tissues with a synchronized circadian rhythm would exhibit variable responses to treatment based on the time of day. This could be due to oscillations in intracellular amount of drug or in pathways that direct drug response. While our previous cell line work indicates that improved repair efficiency is not a necessary component of platinum resistance, it is possible that alterations in repair efficiency throughout the 24 hour period within a tissue could change the cellular response to platinum-based drugs. The Sancar lab has shown that excision repair and circadian rhythm are highly intertwined. XPA, a rate limiting protein

in nucleotide excision repair, has oscillatory expression in liver and brain which corresponds with a circadian pattern of cisplatin adduct removal in these tissues (189,190). XPA was shown to be a rate limiting step of nucleotide excision repair in normal human fibroblast cells thus circadian control of repair may be through the control of XPA (191). To this end, determining if tumors maintain a circadian rhythm and, if so, the extent of circadian control on both nucleotide excision repair and on gene expression could help direct better treatment plans by identifying the most effective treatment time.

Despite a number of studies exploring the role of circadian rhythm in cancer, it remains unclear if tumors maintain a circadian rhythm (192,193). Furthermore, these studies do not address the extent of circadian control, opting to only measure patterns of core circadian clock gene expression instead of testing oscillation patterns of all gene expression. Patient derived xenografts (PDXs) provide an optimal model system to further study this as we can create many identical tumors to collect at different time-points in the circadian cycle. Given that transcription-coupled repair of a gene is influenced by the oscillation of expression of that gene, we can use XR-seq and bioinformatics tools to identify all genes that display an oscillatory expression in the tumor and we can determine whether this rhythm remains in phase with normal tissue. In this study, we aim to address underlying mechanisms that alter cisplatin response and to use novel technologies to lay the foundation to identifying ways to optimize treatment timing.

5.2 Methods

5.2.1 PDX models

Twelve identical patient derived xenografts (PDXs; two per time-point, six time-points) of each unique colorectal cancer PDX models were provided by Professor Hsu of Duke Cancer Institute (Duke Medical Center approved IRB protocol Pro 00002435 and Duke University IACUC approved protocol A185-15-06). To form the PDX, 6-8 week old JAX NOD.CB17-PrkdsSCID-J mice are injected with ~one million PDX cells subcutaneously in the right flank. The size of the xenograft was measured every two days and when the tumor reached a critical mass, we proceeded with the experiments. Mice with PDXs were intraperitoneally injected with cisplatin (10 mg/Kg) at one of six time-points throughout the 24 hour circadian cycle (first collection at zeitgeber time 0, lights on, and spaced every four hours). The liver, kidney, and tumor were harvested two hours post treatment, dissociated to single cell solutions via homogenization, washed in PBS, and processed for slot blot, excision assay, or XR-seq.

5.2.2 Slot blot

The mouse liver and kidney, and the PDX were harvested and homogenized to single cell solutions. The cells in each of these samples were then lysed via homogenization in a lysis buffer (25 mM Hepes pH 7.9, 100 mM KCl, 12 mM MgCl2, 0.5 mM EDTA, 2 mM DTT, 12.5% glycerol, 0.5% NP-40). DNA was extracted from the insoluble component using the QIAamp DNA mini kit following the protocol specific to tissue processing. DNA was quantified and diluted such that 200 ng of each DNA sample was loaded into each well of a slot blot apparatus. DNA was then transferred to a membrane, and blots were blocked in PBS with 0.1% Tween (PBS-T) and 5% milk at

4°C overnight. The next day the blots were washed in PBS-T three times, and incubated in Abcam anti-platinum damage primary antibody (AbCam, 1:10000 in PBS-T) at 4°C overnight. Blots were washed and incubated in GE-Healthcare anti-Rat IgG conjugated to horse radish peroxidase for two hours. BioRad Clarity™ Western ECL Substrates were used to detect signal and signal was quantified using Image Quant. DNA loading was detected with an antibody against single stranded DNA.

5.2.3 Excision assay

The mouse liver and kidney, and the PDX were harvested and homogenized to single cell solutions. The cells in each of these samples were then lysed via homogenization in a lysis buffer (25 mM Hepes pH 7.9, 100 mM KCl, 12 mM MgCl2, 0.5 mM EDTA, 2 mM DTT, 12.5% glycerol, 0.5% NP-40). Excised oligomers were isolated from the soluble fraction of homogenates using a TFIIH immunoprecipitation (IP). PDX IP was conducted with an XPG antibody (Santa Cruz Biotechnology) while the liver and kidney IPs were conducted with p89 and p62 antibodies (Santa Cruz Biotechnology) were used for the kidney and liver IP. Excised oligomers were then extracted with phenol-chloroform, precipitated with ethanol, labeled with ^{32}P-cordecepin, and run on a sequencing gel. The gels were exposed to a phosphoimager screen and imaged with the Typhoon detection system.

5.2.4 Chronotoxicity studies

C57BL/6 mice, Cry1+/-; Cry2-/-, and Cry1-/-; Cry2-/- (Cry1Cry2 KO) were injected intraperitoneally with 10mg/Kg of cisplatin at either zeitgeber time (ZT) 01 or ZT13 on day 0 of the study. Mice were monitored regularly for survival out to four weeks post cisplatin treatment. Mouse weight was measured each day from one day prior to

treatment (day -1) to two weeks following cisplatin administration (day 14). One day before treatment (day -1) and two and four weeks post treatment (day 14 and 28), blood was collected from the mice from the submandibular vein. Blood samples were processed and Blood Urea Nitrogen (BUN) and Serum Creatinine (creatinine) were measured by the Clinical Chemistry Services of the Animal Histopathology and Lab Medicine Core at UNC.

5.3 Results

5.3.1 PDX damage and repair

To better characterize if tumors retain circadian rhythm**,** the extent of gene regulation by circadian rhythm in the tumor, and how the tumor responds to host synchronizing signals, we chose to test circadian rhythm in patient derived xenografts. These xenografts were derived from human colorectal cancer tumor samples, implanted in a mouse, and passaged a number of times until the tumor was a homogenous population of cells. While the loss of heterogeneity limits the generalizability of our findings, it enables us to test genetically identical tumors at multiple time-points. Given that many cellular properties, including membrane permeability, are under circadian regulation, we hypothesized that damage levels would differ between mice treated with 10mg/kg cisplatin at different zeitgeber times. We tested the damage level in liver, kidney, a colorectal cancer PDX, and a renal cancer PDX at four hour intervals over a twenty-four hour circadian cycle. We included renal cell carcinoma in the experiment so that we could compare tumor types. Figure 5.1 displays the damage levels at different circadian time-points for the four tissue types. We calculated the damage levels for each sample at each time point and normalized them to their single

stranded control and then to the average signal across all time-points for each tissue. To test for circadian oscillation of damage levels in each tissue we tested the amplitude and fit of a sinusoidal curve constrained to a 24 hour wavelength and a normalized damage baseline of 1 (equivalent to the average damage level across all time-points for each individual tissue). The colorectal cancer PDX demonstrated the best fit (r^2 = 0.9788) to the sinusoidal curve, however it also had the lowest amplitude. The renal PDX had the strongest amplitude and a relatively good fit (r^2=0.7463). The damage levels over circadian time exhibited a moderate fit to the sinusoidal curve in the liver and the kidney. Given that we only have one repeat for each PDX in this study, this evidence of circadian oscillation of damage formation in PDXs is anecdotal. However it does appear that damage levels do depend on treatment timing either through cell membrane permeability within the tumor or through a more systemic oscillation that impacts delivery of the drug to the tumor. Interestingly, the peak damage formation time, ZT08, is also the time of peak global nucleotide excision repair (128).

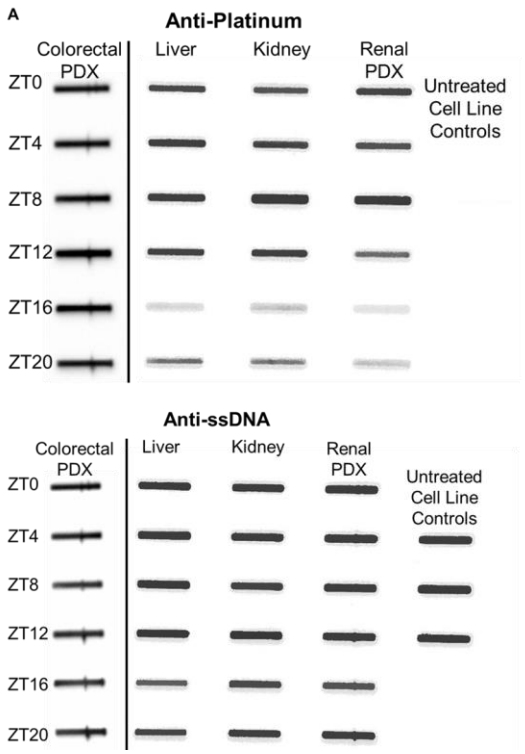

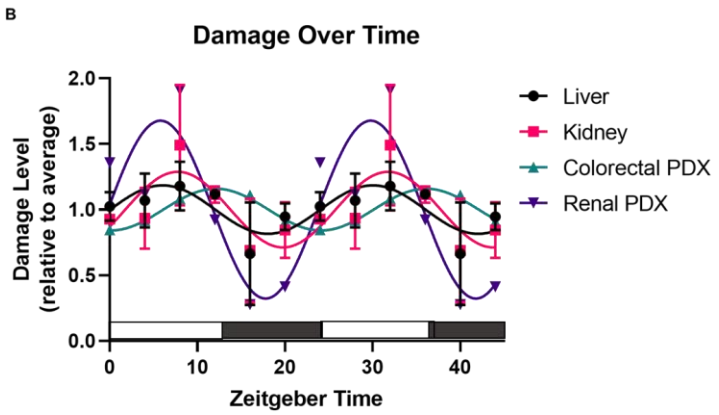

	Liver	Kidney	Colorectal PDX	Renal PDX
Best-fit values				
Amplitude	0.1845	0.2879	0.1588	0.677
PhaseShift	-0.01225	-0.4659	-1.602	0.05379
95% CI (profile likelihood)				
Amplitude	0.07316 to 0.2958	0.1327 to 0.4432	0.1424 to 0.1753	0.3989 to 0.9551
PhaseShift	-0.6601 to 0.6356	-1.035 to 0.1037	-1.706 to -1.498	-0.3695 to 0.4771
Goodness of Fit				
Degrees of Freedom	22	22	10	10
R squared	0.3493	0.402	0.9788	0.7463
Sum of Squares	0.7609	1.48	0.003274	0.9346
Sy.x	0.186	0.2593	0.0181	0.3057
Constraints				
Wavelength	Wavelength = 24	Wavelength = 24	Wavelength = 24	Wavelength = 24
Baseline	Baseline = 1	Baseline = 1	Baseline = 1	Baseline = 1

Figure 5.1: Damage levels induced by cisplatin treatment at different circadian times. (A) Mice were treated with cisplatin and sacrificed two hours later at four hour intervals to test for damage formation levels at different times. DNA from each tissue is collected and used to conduct slot blot. The top, anti-platinum panel shows damage levels at each collection time. The bottom panel shows the single stranded DNA loading control. The slot blot demonstrates that DNA damage levels vary over the circadian period. (B) The top graph shows damage levels from the slot blot experiments plotted over time (the 24 hour period is plotted twice to illustrate the sinusoidal curve fit). For each tissue type, damage levels are normalized to the average of all samples. Two repeats are averaged for the liver and kidney while both PDXs have one replicate. The bar on the X-axis indicates lights on (open) and lights off (filled). The bottom table shows the properties and goodness of fit for the sinusoidal curve. All curves were created with constraints on the wavelength (must be 24 hours) and the baseline (1).

To validate that we can extract measurable excised oligomers from PDXs, we ran an excision assay on the colorectal cancer PDX and the mouse kidney. While the PDXs require extra processing steps that lead to higher background on the excision assay, we still detect measurable excised oligomer (Figure 5.2). To further validate the possibility of conducting XR-seq in PDXs, we measured damage formation and repair in primary cell lines made from two of the colorectal cancer PDXs (119 and 057). Excision assay and slot blot (Figure 2B and C), and XR-seq (data not shown) demonstrate the

potential for moving forward with XR-seq in PDXs. We currently do not have XR-seq data from enough tumor samples to conduct accurate analysis of circadian rhythm in PDXs.

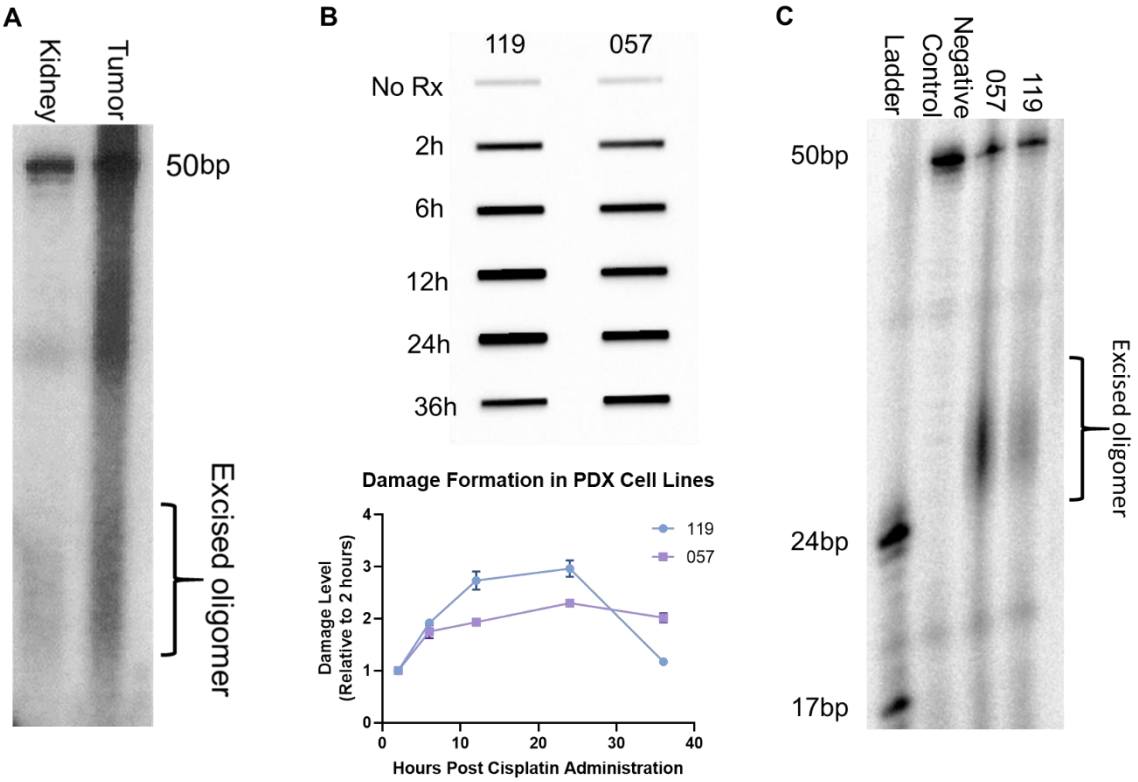

Figure 5.2: Validation of DNA damage and repair in xenografts and PDX cells. (A) Excision assay shows that PDX tumors exhibit measurable repair. The kidneys and a colorectal cancer PDX were collected from a mouse two hours post treatment with 10mg/kg cisplatin. The tissues were dissociated to single cell solution and then cells were lysed. Excised oligomers were extracted from the soluble portion of the lysed cells, purified, labeled, run on a sequencing gel, and imaged. Tumor samples require extra processing steps which increases the background seen in the excision assay compared to the kidney sample. (B) Slot blot in primary cell lines derived from two colorectal cancer PDXs (057 and 119) shows that damage levels increase over the first 24 hours post addition of cisplatin to the cell media. Repair overtakes damage formation between 24 and 36 hours post treatment as seen by the drop in damage levels. (C) Excised oligomers extracted from the two primary PDX cell lines after 1.5 hours of treatment with cisplatin validate the potential of conducting XR-seq with PDXs.

5.3.2 Impact of treatment timing on toxicity

While it is still unclear if tumors retain a synchronized circadian rhythm, administrating treatments at the most optimal time for healthy tissue may be beneficial for decreasing toxicity and increasing the therapeutic index. Furthermore, given that

oscillatory patterns in disease tissue may vary between individuals, identifying the impact of treatment timing in healthy tissue may provide a more practical and generalizable method of improving patient care.

We obtained the top 1000 genes with the strongest oscillation in expression in mouse kidney from CircaDB: Circadian Expression Profiles Database (http://circadb.hogeneschlab.org/) (194). To test if we could predict differences in response to platinum-based drugs based on gene expression, we looked for overlap between these cycling genes and the differentially expressed genes between platinum sensitive and platinum resistant colorectal cancer cell lines from our previous work with colorectal cancer cell lines. 16 genes upregulated in resistant cell lines and 21 genes upregulated in sensitive cell lines overlapped with the oscillating genes (Figure 5.3). The peak expression time for the majority of both the resistant and sensitive oscillating genes occurred around ZT20. Similarly pathway analysis of the cycling genes in mouse kidney did not identify pathways that were enriched in either sensitive or resistant cell

lines. Thus predicting treatment time based on the overlap of these gene sets does not appear to be a valid method.

A

Sensitive cycling	JTKphase
Fbxo21	7
Fnip2	10
Dgat2	12
Rbm3	13
Pck1	15
Tsc22d1	16
Cct3	19
Dnajb11	19
Spop	19
Spcs2	19.5
Cstf3	20
E2f6	20
Kbtbd7	20
Rsrc2	20
Tfrc	20
Homer1	21
Mospd2	21
Arrdc3	22
Dhx36	22
Trim2	22
Npnt	23

B

Resistant cycling	JTKphase
Slc16a7	0
Tnfaip2	0
Gmpr	4
Sh2d3c	8
Slc22a4	10
Tspan4	13
Cav1	16
Eng	18
Adra1a	20
Nrp1	20
Ptger3	20
Gucy1a2	21
Jam3	21
Hgf	23
Rhoj	23

C

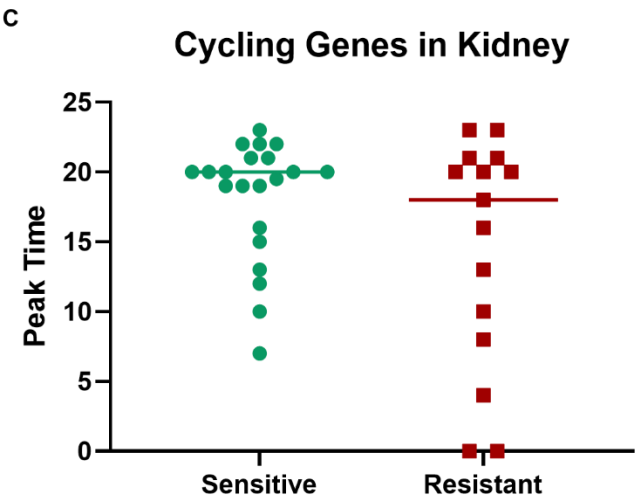

Figure 5.3: A small fraction of genes upregulated in sensitive or resistant cell lines cycle in kidneys. The top 1000 genes with the strongest circadian oscillation in mouse kidney were obtained from CircaDB: Circadian Expression Profiles Database. We next looked for the genes that overlapped between these 1000 oscillating genes and the genes that are upregulated in our (A) oxaliplatin–sensitive and (B) oxaliplatin–resistant cell lines. (C) The time of peak expression for each sensitive-oscillating gene and resistant-oscillating gene were plotted and indicate that overlap of these two gene sets cannot predict the optimal treatment time to reduce kidney damage.

Previous work has shown significant variations in cyclophosphamide toxicity based on the time of administration with mice treated at the dark to light transition (ZT02) showing highest rates of toxicity as measured by survival and weight loss while mice treated at the light to dark transition (ZT14) exhibit higher rates of survival and less weight loss (195). The dose-limiting toxicity of cisplatin is kidney damage. We have previously shown that normal kidneys in mice exhibit a strong circadian rhythm (128). Thus we hypothesized that mice treated in the morning (ZT01) will have higher levels of toxicity markers than mice treated in the evening (ZT13).

To explore the influence of treatment timing on overall toxicity, we monitored survival and weight changes in mice treated with cisplatin in the morning versus mice treated with cisplatin in the evening. Figure 5.4 shows overall survival in the morning treated mice (yellow) versus the evening treated mice (blue). Mice were treated with the highest dose allowed on our protocol (10mg/kg) however this dose was not sufficient to induce measurable differences of mortality between morning and evening treated mice. Two morning treated mice died one week after cisplatin administration, however necropsy was not conducted, thus we cannot be sure of the cause of death. We measured the weight of the mice daily; however, our treatment dose was not sufficient to induce measurable changes in mouse weight (Figure 5.4). One evening treated mouse (9208) did exhibit significant weight loss, however the mouse began regaining weight one week post cisplatin treatment.

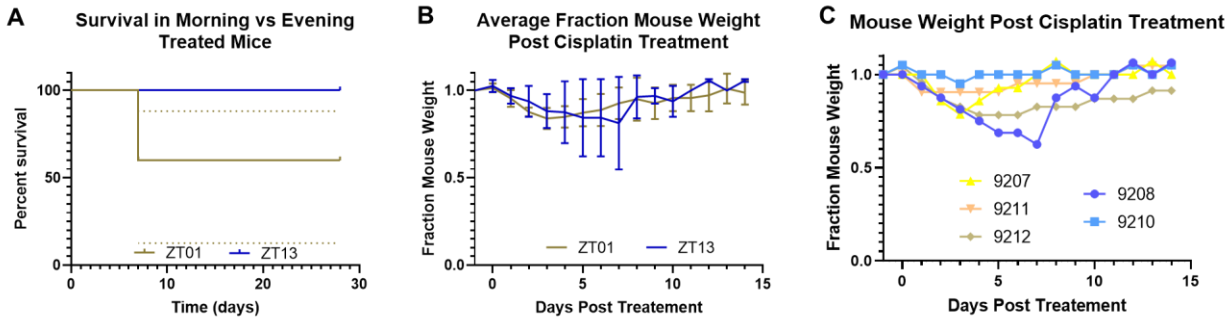

Figure 5.4: Survival and weight changes in mice treated with 10mg/Kg cisplatin at either ZT01 or ZT13. (A) Survival in mice treated at either ZT01 (n=5, yellow) or ZT13 (n=4, blue). Two mice treated at ZT01 died one week post cisplatin treatment. (B & C) The change in mouse weight following treatment (B) averaged over all morning or evening treated mice and (C) per mouse shows no significant toxicity as measured by weight changes. Weight is shown as fraction of the weight one day prior to cisplatin treatment.

Since kidney damage is the dose-limiting toxicity, we also wanted to determine if treatment timing influenced kidney specific toxicity in mice. To test this, we measured blood urea nitrogen and serum creatinine one day before and two and four weeks after cisplatin administration. In the event of kidney damage, we would expect both of these

values to rise; thus we hypothesized that mice treated in the morning would have stronger increases in blood urea nitrogen and serum creatinine levels compared to evening treated mice. However, as seen in Figure 5.5, we saw no significant changes in either blood urea nitrogen or serum creatinine. We believe our treatment dose was not adequate to induce measurable kidney damage. Another possibility is that the times we chose, ZT01 and ZT13, were not the peak and trough of toxicity but rather both around baseline. Our slot blot assay indicated that cisplatin-DNA adduct formation is strongest in mouse kidney's at ZT8, thus it is possibly that treating mice at ZT8 and ZT20 with the same dose would elucidate a difference in toxicity.

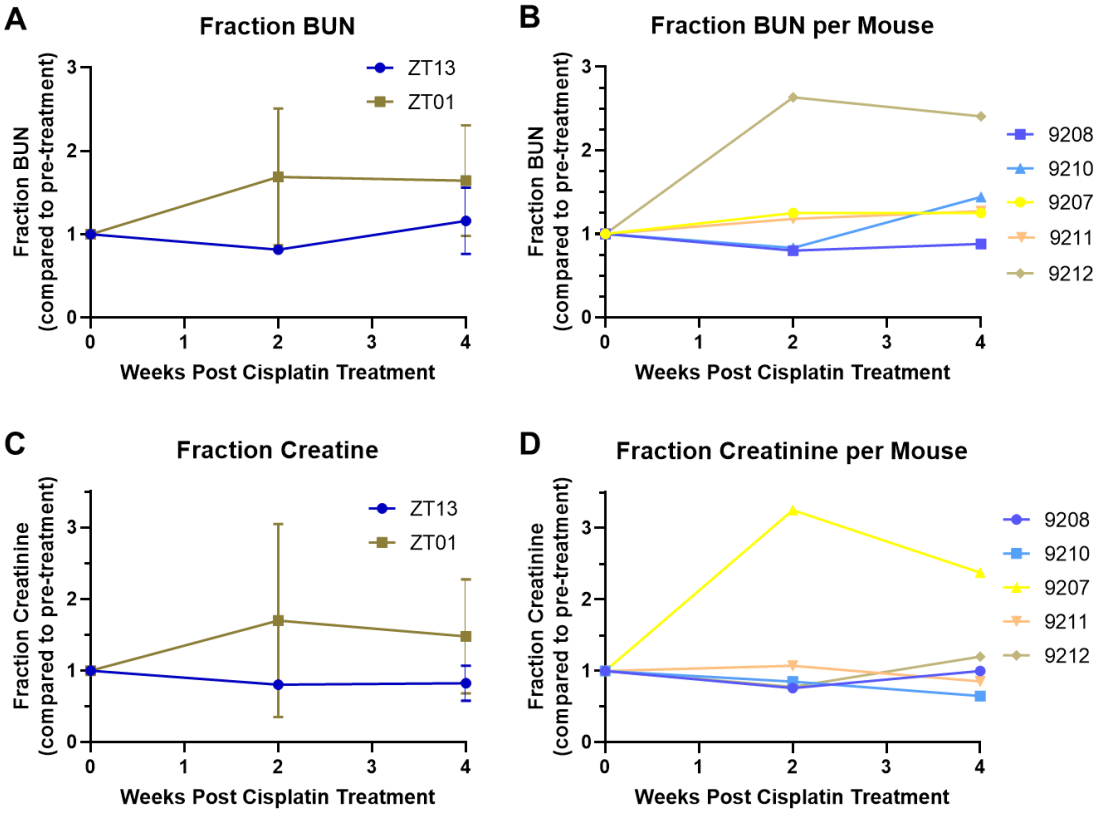

Figure 5.5: Kidney toxicity in morning vs evening treated mice. (A & B) Blood urea nitrogen levels two and four weeks following 10mg/Kg cisplatin treatment compared to the BUN level pre-cisplatin treatment level (A) averaged for all morning treated (yellow) and evening treated (blue) mice and (B) per individual mouse show no significant kidney damage. (C & D) Serum creatinine levels two and four weeks following 10mg/Kg cisplatin treatment compared to creatinine levels (C) averaged for all morning and evening mice and (D) per individual mouse show no significant kidney damage.

To confirm that any differences seen between morning and evening treated mice were due to circadian rhythm and not environmental cues, such as presence or absence of light, we tested the effect of administering cisplatin in the morning versus in the evening in CRY1/2 knock out mice and CRY1+/- CRY2-/- mice. Similar to wildtype mice, we saw no difference in any measure of toxicity between the morning treated and evening treated mice (Figure 5.6).

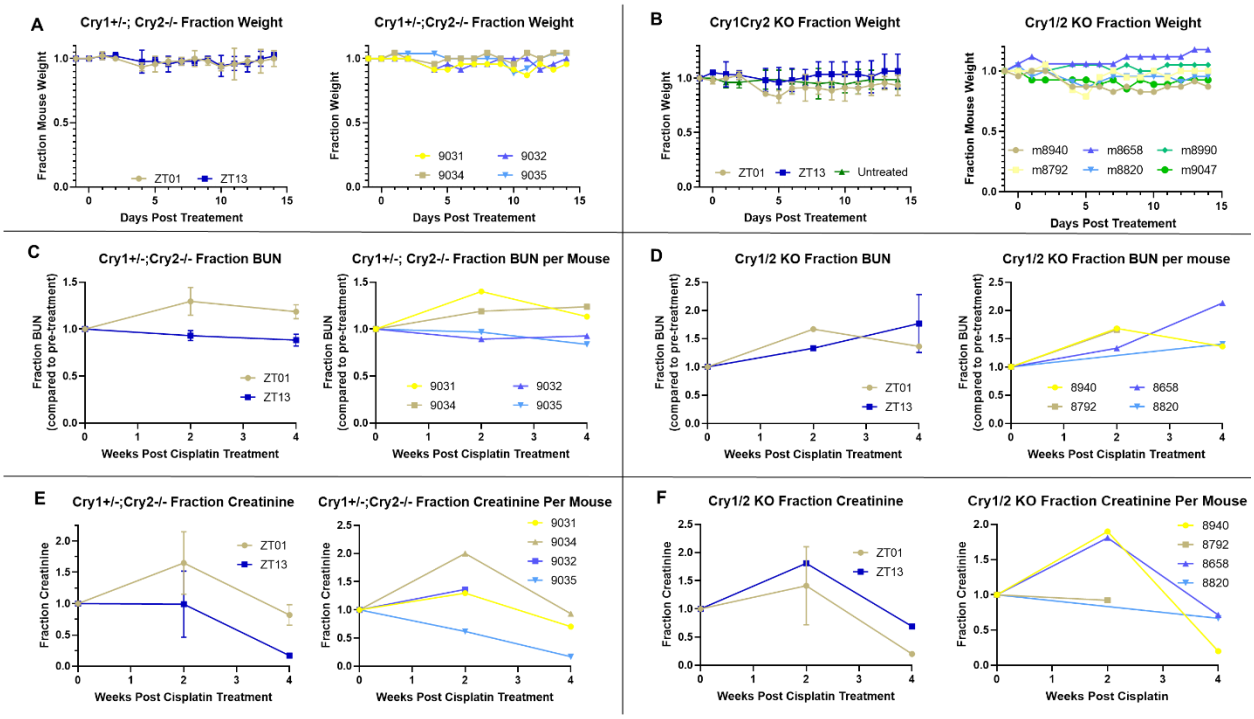

Figure 5.6: Toxicity measures in Cry1+/- Cry2-/- and Cry1-/- Cry2-/- (Cry1/2 KO) treated with 10mg/Kg cisplatin at either ZT01 (yellow) or ZT13 (blue). (A & B) Weight changes relative to weight pre-treatment, (C & D) BUN changes relative to pre-treatment BUN levels, and (E & F) serum creatinine changes relative to pre-treatment creatinine levels in (A, C, & E) Cry1+/- Cry2-/- and (B, D, & F) Cry1/2 KO show no significant toxicity averaged per morning and evening mice (left panels) or per mouse (right panels)

5.4 Discussion

Here we discuss the implications of chronotherapy and chronotoxicity for platinum-based drugs. The circadian rhythm controls many systemic and cellular factors that may influence the extent of platinum effect on diseased tissue and on normal, healthy tissue. To understand the impact of drug administration time on tumor response

to platinum, we first must characterize the presence or absences and extent of control of circadian rhythm on tumor cells. As a first step in this characterization, we measured the oscillation of damage formation in normal liver and kidney and in two types of patient derived xenografts (PDXs). The liver and kidney exhibit a moderate fit to a circadian oscillation, as measured by a sinusoidal curve, while the xenografts demonstrate a stronger fit to the curve. While the colorectal cancer PDX displays the strongest fit to the curve, it also had the smallest amplitude.

More PDXs need to be processed through XR-seq to determine if the xenografts retain a synchronized circadian rhythm. Factors that may influence the whether or not a PDX exhibits a synchronized, circadian rhythm include the initial presence or absence of a circadian rhythm in the tumor from which the PDX is derived, the extent to which the tumor responds to host synchronizers and environmental cues, and the speed at which the tumor grows. It is still unknown if human tumors maintain a synchronized, circadian rhythm and the possibility exists that this differs between tumors and individuals (196). If the circadian rhythm in a tumor is absent, we'd expect the PDX to lack a circadian rhythm as well. However, if the original tumor possess a circadian rhythm, the PDX may either demonstrate a circadian rhythm or lose its rhythm through the processing steps of creating the PDX. If tumors do retain a circadian rhythm, it remains unknown if (1) the xenograft responds to host synchronizers, such as hormones and metabolites, (2) the xenograft maintains a synchronized rhythm independent of the host through paracrine signaling, (3) individual cells demonstrate a circadian rhythm while the tumor as a whole appears to lack a rhythm due to the absence of synchronization, or (4) the tumor cells completely lack the functioning

transcriptional-translational feedback loop. Our analysis will address if the PDX as a whole exhibits a synchronized circadian rhythm and if this rhythm is in or out of synchronization with the host by comparing the PDX to the mouse liver. Additional analysis of samples from human tissue, such as experiments done with CYCLOPS (197), are needed to determine if the original tumors demonstrate a circadian rhythm. In the event that tumor-wide analysis indicates no circadian rhythm, single cell analysis of circadian rhythm in individual tumor cells will be required to determine if tumor cells lack a rhythm or a synchronization. The speed at which a tumor grows may also impact our ability to detect a synchronized rhythm as fast growing tumors may need to be processed before they have adequate time to adapt and respond to host signal. To account for this, we are using both fast and slow growing tumors. It is possible that none of the PDXs we test will have a circadian rhythm. While this would halt future studies to explore the connection between circadian rhythm and tumor response to platinum-based drugs directly related to mechanisms within the tumor cell, systemic factors that are still under circadian control may alter the tumor response to platinum as well.

Regardless of the presence or absence of a synchronized circadian rhythm in tumors, normal tissue demonstrates robust oscillation (128). Thus identifying a treatment time that decreases toxicity could hopefully improve treatment plans for patients. Additionally, rhythms in healthy tissue may be more generalizable than those of disease tissues, thus identifying an optimal treatment time based on reducing toxicity may provide a more practical translation of chronotherapy to the clinic. We tested toxicity in mice treated in the morning (ZT01) and in the evening (ZT13) by measuring survival and changes in weight, BUN, and serum creatinine. Unfortunately, no

measurable changes were identified. This is likely due to the fact that our cisplatin dose (10mg/Kg) was not high enough to induce toxicity and/or that our time-points were not at the peak and trough of toxicity. To this end, additional studies are need to test more time points and higher doses. Moreover, these studies involve a one-time dose of cisplatin which is not an accurate representation of treatment plans in human patients. Alternative dose schedules have been described for a more accurate model of patient treatment schedules (198). These involve multiple treatments with lower cisplatin doses over time; future studies should test this treatment schedule with the multiple lower doses all administrated at particular time-points in the circadian cycle.

Overall, we have provided a foundation for studying the role of circadian rhythm in directing response to platinum-based drugs in normal and xenograft tissues. While some preliminary results suggest the timing of administration may impact damage formation, additional studies are needed to identify the factors which drive these differences and the physiological implications of these variations. Additionally, it remains unknown if tumors retain a circadian rhythm, the extent of any oscillation, and the impact this may have on disease progression and drug response. Identifying optimal treatment timing provides a potential to improve patient care, however more work is needed to understand the molecular mechanisms underlying the role of circadian rhythm in disease and drug response.

CHAPTER 6: CONCLUSIONS AND FUTURE DIRECTIONS

The purpose of these studies was to better understand the molecular response of cells to platinum-based drugs and to begin to translate these responses to physiologic outcomes such that we can use our understanding of the biochemistry of treatment response to improve patient outcomes. Platinum based chemotherapy works by creating bulky DNA damage which in turn should induce cell death (5-7). Many factors have been proposed to impact this response, including improved repair efficiency of the platinum-induced damage (144,145). However the evidence supporting the role of repair in resistance is incomplete and inconsistent and thus questions still remain about the true role of nucleotide excision repair in resistance or sensitivity to the platinum-based drugs (113,114). We aimed to better understand cellular response to platinum-based drugs by focusing on characterizing the role of DNA damage formation, nucleotide excision repair, and circadian rhythm in regulating cisplatin or oxaliplatin response. In order best understand the impact of these factors individually and in combination, we studied these processes in both cell lines and patient derived xenografts. By using both of these tumor models, we can explore mechanistic processes, such as damage formation and repair, in a controlled setting and then apply our findings to a tumor model that enables us to see how tumor-host interactions and environmental cues alter the principles we defined.

In order to best characterize repair, we employed a comprehensive panel of assays. While these methods do have technical variation and limitations, as discussed in chapter 1 and in the analysis pipeline development section of chapter 4, studying repair from multiple angles creates a more complete understanding of repair efficiency. We measured repair by amount, rate, and patterns over a panel of ten colorectal cancer cell lines, creating the most comprehensive study of repair efficiency in platinum resistance to our knowledge. We first defined oxaliplatin response in these ten cell lines to identify a group of resistant cell lines and a group of sensitive cell lines. Our studies show that repair efficiency does not differ between cell lines that are oxaliplatin-sensitive and those that are oxaliplatin-resistant.

Given that platinum-based drugs are known to induce minor levels of additional DNA damages such as interstrand crosslinks and reactive oxygen species in addition to their major form of damage, intrastrand adducts, we determined cellular response to each individual damage type (162,163). To do this, we measured survival in response to three additional damaging agents and correlated response to these agents with response to oxaliplatin. Specifically, we used UV irradiation (intrastrand adducts), mitomycin C (interstrand crosslinks), and hydrogen peroxide (reactive oxygen damage) to simulate the damages formed by platinum. Interestingly, the response to oxaliplatin did not correlate with any specific damage type, indicating that factors such as the overall level of damage formation impact a cell's reaction to the drug more than the specific damage induced.

In agreement with previous studies, we found that DNA damage formation appears to play an important role in directing cellular response to platinum-based drugs

(143,164-166). Lower initial damage levels correlate with less cell death, however this correlation is not perfect. All platinum resistant cell lines in our study demonstrate low initial levels of damage. However there is more variability amongst the sensitive cell lines indicating that while low damage levels may be a necessary component of resistance, it is not sufficient to induce resistance in all cell lines. Indeed a subset of sensitive cell lines displayed initial damage levels similar to the levels seen in resistant cell lines. It is important to note that our study included seven sensitive cell lines and only three resistant cell lines, thus the higher variability seen in the sensitive cell lines may be due to the larger sample size. Regardless, the identification of sensitive cell lines with low initial damage provides a compelling model for identifying factors that lead to cell death in response to low initial damage. Identification of these pathways could provide insight into mechanisms and treatment options for re-sensitizing resistant tumors.

In effort to determine how these findings translate from cell culture to an organism, we studied damage formation in mice treated with cisplatin. We found that damage formation levels in mouse and xenograft tissue vary throughout the day, peaking around ZT8, with data moderately fitting a sinusoidal curve with a wavelength of 24 hours. In contrast, our toxicity studies, treating mice in either the morning or evening, did not identify significant time-of-day platinum-induced toxicity. We believe that this is largely due to the fact that our cisplatin dose may not be adequate to induce toxicity. However, based on our cell line work, it would fit that less cell death would occur at the time of lowest damage formation, ZT20, while conversely more cell death, and higher toxicity, would be seen at mice treated at the time of peak damage

formation, ZT08. If this is true, we may not have identified appreciable differences in toxicity as the time-points tested in our study ZT01 and ZT13 would be close to the baseline and thus exhibit similar responses to the treatment.

Through studying repair, we generated a number of XR-seq datasets that can provide insights into other molecular mechanisms, such as transcription patterns measured via transcription coupled repair, that associate with and may direct platinum response. We identified over 1000 genes with differential transcription coupled repair (indicative of differential transcription) between platinum sensitive and platinum resistant cell lines. Interestingly, the gene set with higher transcription coupled repair in platinum resistant cell lines demonstrated enrichment for plasma membrane and transport factors which may provide more insight into proteins that influence platinum influx and efflux. XR-seq data from our PDX study will enable us to test if these factors remain constant between our cell line model and xenograft model. We are collecting samples from both platinum sensitive and resistant xenografts and thus will be able to test for overlap between differentially repaired genes in both models. Genes that show up in both list will be stronger candidates for directing or predicting drug response. If we identify any oscillating genes found in the colorectal cancer xenografts, and these genes overlap with those found by our differential repair analysis, we may be able to predict how platinum response of the tumor varies over the 24 hour circadian cycle. We tested this by looking for overlap between our sensitive vs resistant genes and genes that oscillate in the kidney (194) and found that very few genes overlap. However, this may be due to the difference in tissue of origin and results may prove more promising when compared between two colorectal cancer models.

Beyond using our data to look for differences in transcription, we may also be able to use our XR-seq data to identify differences in genomic architecture. By comparing repair in intergenic regions, we identified a ~1.6 million base pair region of chromosome 8 with amplified repair specifically in these low damage sensitive cell lines using our XR-seq data. We further demonstrated that the amplified repair is due to a DNA amplification in the cell lines. This region is particularly interesting as it encodes a number of cancer related coding and non-coding RNAs that may potentially be involved in the extreme sensitivity of these cell lines, possibly by promoting cell division and replication in the face of damage or by activating alternative signaling pathways in response to the low damage levels.

Our studies have opened a number of new questions related to nucleotide excision repair, platinum response, circadian regulation of treatment response, and the overlap of these fields. First, the identification of a large DNA amplification in a subset of our colorectal cancer cell lines fueled more questions related to nucleotide excision repair efficiency in regions of genomic instability and architectural changes, specifically how do genomic architecture changes impact repair efficiency? While this finding was initially unanticipated, it was more surprising that we didn't identify more regions of major repair amplification given the prevalence of DNA amplifications and deletions in cancer cells (173,174,181-184). Characterization of the genomic architecture of each of these cell lines and integration of this data with our XR-seq data may provide a foundation for understanding how these genomic alterations impact nucleotide excision repair which in turn may help address the magnitude of repair amplification seen in this particular case.

We identified and characterized a large DNA amplification in cell lines with high sensitivity to oxaliplatin despite low levels of oxaliplatin damage. The question remains, is this a passenger alteration or do transcripts from this region impact drug response? Additional studies are needed to see if knocking down or overexpressing the genes in this region impact platinum response and, if so, the mechanism by which they do so. If this mechanism is determined, it may provide a potential target for re-sensitizing resistant tumors to platinum-based drugs.

We have shown that damage levels partially direct cellular response to platinum-based drugs. However the specific mechanisms leading to variations in damage formation remains unclear. Previous studies have implicated a role for copper transporters and organic cation transporters in platinum resistance by impacting drug influx and efflux (150-152). However in our cell line panel, gene expression of these transporters did not differ significantly between sensitive and resistant cell lines. Our analysis identified a number of plasma membrane components and transporters that may be involved in regulating initial damage amount, however validation of these factors is required to see if the variation in damage levels that we observed can be attributed to drug influx and efflux.

To determine a potential clinical relevance for our cell line work, we must test if our results are reproducible between tumor models. By conducting XR-seq on both platinum -sensitive and -resistant PDXs, we can test if the differences found by comparing platinum -sensitive and -resistant cell lines translate to an organism model. Results that are reproducible between model systems are more likely to be relevant to predicting or directing treatment outcomes and plans for patients.

We still have to determine if tumors retain synchronized circadian rhythms and how these rhythms influence response to platinum-based drugs and other drugs. Additionally, we need to address how the tumor responds to host signals and rhythms and if these systemic changes alter how tumors respond to platinum-based drugs. For instance, the differences seen in initial platinum-DNA adduct formation in mice treated with cisplatin at different time-points may be due to oscillations in cell membrane permeability (regulated by the circadian rhythm within the cells) or may be due to changes in drug delivery (regulated by more systemic rhythms). Understanding rhythms in both normal and disease tissue may provide the ability to increase the therapeutic window by both increasing the anti-tumor effect on cancer cells and decreasing the toxic effect on healthy tissue.

Lastly, all of our studies looked at treatment with a single damaging agent at a time (primarily platinum or UV). In the clinic, platinum-based drugs are given as part of combination therapy plans. Thus for our results to be clinically relevant and applicable, we must study how addition of other anti-cancer chemotherapeutic agents impacts damage formation, nucleotide excision repair, and ultimately, response to platinating agents.

Overall, drug resistance is a multifactorial process and no one phenomenon can account for all variation in treatment response. Finding trends that can be applied over multiple samples and tumor models can provide a more widespread understanding of drug response. Despite the assumption that improved nucleotide excision repair efficiency would lead to platinum resistance, we provide comprehensive evidence that it is not an essential regulator of platinum response. However, patterns of repair may

illuminate other drivers of drug response. We have also shown that damage level appears to be a critical component of platinum response, although some cell lines remain sensitive to the drug despite low damage levels. These studies build a foundation for understanding the molecular response to platinum-based drugs in colorectal cancer which will hopefully provide useful insight to ultimately improve patient care.

APPENDIX 1

Table S1: Cell line characteristics
https://www.jbc.org/content/early/2020/04/16/jbc.RA120.013347/suppl/DC1

APPENDIX 2

Table S2: Cell line experimental values.
https://www.jbc.org/content/early/2020/04/16/jbc.RA120.013347/suppl/DC1

APPENDIX 3

Table S3: Genes repaired differentially in oxaliplatin-sensitive and –resistant cell lines (positive fold change indicates higher repair levels in sensitive cell lines compared to resistant cell lines, negative fold change indicates higher repair levels in resistant cell lines compared to sensitive lines).
https://www.jbc.org/content/early/2020/04/16/jbc.RA120.013347/suppl/DC1

APPENDIX 4

Table S4: Gene set enrichment analysis (GSEA) results for genes upregulated in resistant cell lines compared to sensitive cell lines.
https://www.jbc.org/content/early/2020/04/16/jbc.RA120.013347/suppl/DC1

APPENDIX 5

Table S5: GSEA results for genes upregulated in sensitive cell lines compared to resistant cell lines.
https://www.jbc.org/content/early/2020/04/16/jbc.RA120.013347/suppl/DC1

BIBLIOGRAPHY

1. Hu, J., Selby, C. P., Adar, S., Adebali, O., and Sancar, A. (2017) Molecular mechanisms and genomic maps of DNA excision repair in Escherichia coli and humans. *The Journal of biological chemistry* **292**, 15588-15597

2. Gaddameedhi, S., Selby, C. P., Kaufmann, W. K., Smart, R. C., and Sancar, A. (2011) Control of skin cancer by the circadian rhythm. *Proceedings of the National Academy of Sciences of the United States of America* **108**, 18790-18795

3. Subramanian, A., Tamayo, P., Mootha, V. K., Mukherjee, S., Ebert, B. L., Gillette, M. A., Paulovich, A., Pomeroy, S. L., Golub, T. R., Lander, E. S., and Mesirov, J. P. (2005) Gene set enrichment analysis: A knowledge-based approach for interpreting genome-wide expression profiles. *Proceedings of the National Academy of Sciences* **102**, 15545-15550

4. Vaughn, C., and Sancar, A. (2020) Mechanisms and Maps of Nucleotide Excision Repair. in *DNA Damage, Repair, and Disease* (LLoyd, R. S., and Dizdaroglu, M. eds.), Royal Society of Chemistry, London. pp

5. Wang, D., and Lippard, S. J. (2005) Cellular processing of platinum anticancer drugs. *Nat Rev Drug Discov* **4**, 307-320

6. Reed, E., Dabholkar, M., and Chabner, B. . (1996) Platinum Analogues Cancer Chemotherapy. in *Cancer Chemotherapy*, Lippincott-Raven Publishers, Philadelphia. pp 357-378

7. Hall, M. D., Okabe, M., Shen, D. W., Liang, X. J., and Gottesman, M. M. (2008) The role of cellular accumulation in determining sensitivity to platinum-based chemotherapy. *Annu Rev Pharmacol Toxicol* **48**, 495-535

8. Ho, G. Y., Woodward, N., and Coward, J. I. (2016) Cisplatin versus carboplatin: comparative review of therapeutic management in solid malignancies. *Crit Rev Oncol Hematol* **102**, 37-46

9. Riddell, I. A., and Lippard, S. J. (2018) Cisplatin and Oxaliplatin: Our Current Understanding of Their Actions. in *Metallo-Drugs: Development and Action of Anticancer Agents* (Sigel, A., Sigel, H., Freisinger, E., and Sige, R. K. O. eds.), Walter de Gruyter co, Berlin, Germany. pp 1-42

10. Eljack, N. D., Ma, H.-Y. M., Drucker, J., Shen, C., Hambley, T. W., New, E. J., Friedrich, T., and Clarke, R. J. (2014) Mechanisms of cell uptake and toxicity of the anticancer drug cisplatin. *Metallomics*

11. Li, X. Q., Ren, J., Chen, P., Chen, Y. J., Wu, M., Wu, Y., Chen, K., and Li, J. (2018) Co-inhibition of Pol eta and ATR sensitizes cisplatin-resistant non-small cell lung

cancer cells to cisplatin by impeding DNA damage repair. *Acta Pharmacol Sin* **39**, 1359-1372

12. Ishida, S., Lee, J., Thiele, D. J., and Herskowitz, I. (2002) Uptake of the anticancer drug cisplatin mediated by the copper transporter Ctr1 in yeast and mammals. *Proceedings of the National Academy of Sciences of the United States of America* **99**, 14298-14302

13. Zhang, S., Lovejoy, K. S., Shima, J. E., Lagpacan, L. L., Shu, Y., Lapuk, A., Chen, Y., Komori, T., Gray, J. W., Chen, X., Lippard, S. J., and Giacomini, K. M. (2006) Organic cation transporters are determinants of oxaliplatin cytotoxicity. *Cancer research* **66**, 8847-8857

14. Kinoshita, Y., Kalir, T., Rahaman, J., Dottino, P., and Kohtz, D. S. (2012) Alterations in nuclear pore architecture allow cancer cell entry into or exit from drug-resistant dormancy. *Am J Pathol* **180**, 375-389

15. Basu, A., and Krishnamurthy, S. (2010) Cellular responses to Cisplatin-induced DNA damage. *J Nucleic Acids* **2010**, 201367

16. Cepeda, V., Fuertes, M. A., Castilla, J., Alonso, C., Quevedo, C., and Perez, J. M. (2007) Biochemical Mechanisms of Cisplatin Cytotoxicity. *Anti-Cancer Agents* **7**

17. Kowalski, D., Pendyala, L., Daignan-Fornier, B., Howell, S. B., and Huang, R.-Y. (2008) Dysregulation of purine nucleotide biosynthesis pathways modulates cisplatin cytotoxicity in Saccharomyces cerevisiae. *Molecular pharmacology* **74**, 1092-1100

18. Melnikov, S. V., Söll, D., Steitz, T. A., and Polikanov, Y. S. (2016) Insights into RNA binding by the anticancer drug cisplatin from the crystal structure of cisplatin-modified ribosome. *Nucleic acids research* **44**, 4978-4987

19. Hu, J., Adar, S., Selby, C. P., Lieb, J. D., and Sancar, A. (2015) Genome-wide analysis of human global and transcription-coupled excision repair of UV damage at single-nucleotide resolution. *Genes Dev* **29**, 948-960

20. Davies, N. P., Hardman, L. C., and Murray, V. (2000) The effect of chromatin structure on cisplatin damage in intact human cells. *Nucleic acids research* **28**, 2954-2958

21. Wu, B., Davey, G. E., Nazarov, A. A., Dyson, P. J., and Davey, C. A. (2011) Specific DNA structural attributes modulate platinum anticancer drug site selection and cross-link generation. *Nucleic acids research* **39**, 8200-8212

22. Sabarinathan, R., Mularoni, L., Deu-Pons, J., Gonzalez-Perez, A., and Lopez-Bigas, N. (2016) Nucleotide excision repair is impaired by binding of transcription factors to DNA. *Nature* **532**, 264-267

23. Pich, O., Muiños, F., Sabarinathan, R., Reyes-Salazar, I., Gonzalez-Perez, A., and Lopez-Bigas, N. (2018) Somatic and Germline Mutation Periodicity Follow the Orientation of the DNA Minor Groove around Nucleosomes. *Cell* **175**, 1074-1087.e1018

24. Hu, J., Adebali, O., Adar, S., and Sancar, A. (2017) Dynamic maps of UV damage formation and repair for the human genome. *Proceedings of the National Academy of Sciences of the United States of America* **114**, 6758-6763

25. Jin, L., Chun, J., Pan, C., Li, D., Lin, R., Alesi, G. N., Wang, X., Kang, H.-B., Song, L., Wang, D., Zhang, G., Fan, J., Boggon, T. J., Zhou, L., Kowalski, J., Qu, C.-K., Steuer, C. E., Chen, G. Z., Saba, N. F., Boise, L. H., Owonikoko, T. K., Khuri, F. R., Magliocca, K. R., Shin, D. M., Lonial, S., and Kang, S. (2018) MAST1 Drives Cisplatin Resistance in Human Cancers by Rewiring cRaf-Independent MEK Activation. *Cancer Cell* **34**, 315-330.e317

26. Kielbik, M., Krzyzanowski, D., Pawlik, B., and Klink, M. (2018) Cisplatin-induced ERK1/2 activity promotes G1 to S phase progression which leads to chemoresistance of ovarian cancer cells. *Oncotarget* **9**, 19847-19860

27. Zou, J., Zhu, L., Jiang, X., Wang, Y., Wang, Y., Wang, X., and Chen, B. (2018) Curcumin increases breast cancer cell sensitivity to cisplatin by decreasing FEN1 expression. *Oncotarget* **9**, 11268-11278

28. Si, H., Peng, C., Li, J., Wang, X., Zhai, L., Li, X., and Li, J. (2012) RNAi-mediated knockdown of ERK1/2 inhibits cell proliferation and invasion and increases chemosensitivity to cisplatin in human osteosarcoma U2-OS cells in vitro. *Int J Oncol* **40**, 1291-1297

29. Zhang, L., Yang, X., Li, X., Li, C., Zhao, L., Zhou, Y., and Hou, H. (2015) Butein sensitizes HeLa cells to cisplatin through the AKT and ERK/p38 MAPK pathways by targeting FoxO3a. *Int J Mol Med* **36**, 957-966

30. Zhang, F., Shen, M., Yang, L., Yang, X., Tsai, Y., Keng, P. C., Chen, Y., Lee, S. O., and Chen, Y. (2017) Simultaneous targeting of ATM and Mcl-1 increases cisplatin sensitivity of cisplatin-resistant non-small cell lung cancer. *Cancer Biol Ther* **18**, 606-615

31. Ho, I. L., Kuo, K.-L., Liu, S.-H., Chang, H.-C., Hsieh, J.-T., Wu, J.-T., Chiang, C.-K., Lin, W.-C., Tsai, Y.-C., Chou, C.-T., Hsu, C.-H., Pu, Y.-S., Shi, C.-S., and Huang, K.-H. (2015) MLN4924 Synergistically Enhances Cisplatin-induced Cytotoxicity via JNK and Bcl-xL Pathways in Human Urothelial Carcinoma. *Scientific reports* **5**, 16948-16948

32. MacKay, C., Carroll, E., Ibrahim, A. F. M., Garg, A., Inman, G. J., Hay, R. T., and Alpi, A. F. (2014) E3 ubiquitin ligase HOIP attenuates apoptotic cell death induced by cisplatin. *Cancer research* **74**, 2246-2257

33. Wang, R., Zheng, X., Zhang, L., Zhou, B., Hu, H., Li, Z., Zhang, L., Lin, Y., and Wang, X. (2017) Histone H4 expression is cooperatively maintained by IKKβ and Akt1 which attenuates cisplatin-induced apoptosis through the DNA-PK/RIP1/IAPs signaling cascade. *Scientific reports* **7**, 41715-41715

34. Almeida, L. O., Abrahao, A. C., Rosselli-Murai, L. K., Giudice, F. S., Zagni, C., Leopoldino, A. M., Squarize, C. H., and Castilho, R. M. (2013) NFκB mediates cisplatin resistance through histone modifications in head and neck squamous cell carcinoma (HNSCC). *FEBS Open Bio* **4**, 96-104

35. Wansleben, S., Davis, E., Peres, J., and Prince, S. (2013) A novel role for the anti-senescence factor TBX2 in DNA repair and cisplatin resistance. *Cell Death Dis* **4**, e846-e846

36. Zhu, Y., Regunath, K., Jacq, X., and Prives, C. (2013) Cisplatin causes cell death via TAB1 regulation of p53/MDM2/MDMX circuitry. *Genes & development* **27**, 1739-1751

37. Pouliot, L. M., Chen, Y.-C., Bai, J., Guha, R., Martin, S. E., Gottesman, M. M., and Hall, M. D. (2012) Cisplatin sensitivity mediated by WEE1 and CHK1 is mediated by miR-155 and the miR-15 family. *Cancer research* **72**, 5945-5955

38. Yan, F., Pang, J., Peng, Y., Molina, J. R., Yang, P., and Liu, S. (2016) Elevated Cellular PD1/PD-L1 Expression Confers Acquired Resistance to Cisplatin in Small Cell Lung Cancer Cells. *PloS one* **11**, e0162925-e0162925

39. Lee, Y.-S., Gregory, M. T., and Yang, W. (2014) Human Pol ζ purified with accessory subunits is active in translesion DNA synthesis and complements Pol η in cisplatin bypass. *Proceedings of the National Academy of Sciences of the United States of America* **111**, 2954-2959

40. Albertella, M. R., Green, C. M., Lehmann, A. R., and O'Connor, M. J. (2005) A Role for Polymerase η in the Cellular Tolerance to Cisplatin-Induced Damage. *Cancer Research* **65**, 9799-9806

41. Song, L., McNeil, E. M., Ritchie, A.-M., Astell, K. R., Gourley, C., and Melton, D. W. (2017) Melanoma cells replicate through chemotherapy by reducing levels of key homologous recombination protein RAD51 and increasing expression of translesion synthesis DNA polymerase ζ. *BMC cancer* **17**, 864-864

42. Sanders, M. A., Haynes, B., Nangia-Makker, P., Polin, L. A., and Shekhar, M. P. (2017) Pharmacological targeting of RAD6 enzyme-mediated translesion synthesis overcomes resistance to platinum-based drugs. *The Journal of biological chemistry* **292**, 10347-10363

43. Sancar, A. (2016) Mechanisms of DNA Repair by Photolyase and Excision Nuclease (Nobel Lecture). *Angew Chem Int Ed Engl* **55**, 8502-8527

44. Kelner, A. (1949) Effect of Visible Light on the Recovery of Streptomyces Griseus Conidia from Ultra-violet Irradiation Injury. *Proceedings of the National Academy of Sciences of the United States of America* **35**, 73-79

45. Rupert, C. S., Goodgal, S. H., and Herriott, R. M. (1958) Photoreactivation in vitro of ultraviolet-inactivated Hemophilus influenzae transforming factor. *J Gen Physiol* **41**, 451-471

46. Rupert, C. S. (1962) Photoenzymatic repair of ultraviolet damage in DNA. II. Formation of an enzyme-substrate complex. *J Gen Physiol* **45**, 725-741

47. Rupert, C. S. (1962) Photoenzymatic repair of ultraviolet damage in DNA. I. Kinetics of the reaction. *J Gen Physiol* **45**, 703-724

48. Rupert, C. S. (1960) Photoreactivation of transforming DNA by an enzyme from bakers' yeast. *J Gen Physiol* **43**, 573-595

49. Boyce, R. P., and Howard-Flanders, P. (1964) RELEASE OF ULTRAVIOLET LIGHT-INDUCED THYMINE DIMERS FROM DNA IN E. COLI K-12. *Proceedings of the National Academy of Sciences* **51**, 293-300

50. Setlow, R. B., and Carrier, W. L. (1964) THE DISAPPEARANCE OF THYMINE DIMERS FROM DNA: AN ERROR-CORRECTING MECHANISM. *Proceedings of the National Academy of Sciences* **51**, 226-231

51. Castellani, A., Jagger, J., and Setlow, R. B. (1964) Overlap of Photoreactivation and Liquid Holding Recovery in Escherichia coli B. *Science* **143**, 1170-1171

52. Rasmussen, R. E., and Painter, R. B. (1964) Evidence for Repair of Ultra-Violet Damaged Deoxyribonucleic Acid in Cultured Mammalian Cells. *Nature* **203**, 1360-1362

53. Regan, J. D., Trosko, J. E., and Carrier, W. L. (1968) Evidence for excision of ultraviolet-induced pyrimidine dimers from the DNA of human cells in vitro. *Biophys J* **8**, 319-325

54. Pettijohn, D., and Hanawalt, P. (1964) Evidence for Repair-Replication of Ultraviolet Damaged DNA in Bacteria. *J Mol Biol* **9**, 395-410

55. Sancar, A., and Rupp, W. D. (1983) A novel repair enzyme: UVRABC excision nuclease of Escherichia coli cuts a DNA strand on both sides of the damaged region. *Cell* **33**, 249-260

56. Svoboda, D. L., Taylor, J. S., Hearst, J. E., and Sancar, A. (1993) DNA repair by eukaryotic nucleotide excision nuclease. Removal of thymine dimer and psoralen monoadduct by HeLa cell-free extract and of thymine dimer by Xenopus laevis oocytes. *Journal of Biological Chemistry* **268**, 1931-1936

57. Huang, J. C., Svoboda, D. L., Reardon, J. T., and Sancar, A. (1992) Human nucleotide excision nuclease removes thymine dimers from DNA by incising the 22nd phosphodiester bond 5' and the 6th phosphodiester bond 3' to the photodimer. *Proceedings of the National Academy of Sciences* **89**, 3664-3668

58. Guzder, S. N., Habraken, Y., Sung, P., Prakash, L., and Prakash, S. (1995) Reconstitution of Yeast Nucleotide Excision Repair with Purified Rad Proteins, Replication Protein A, and Transcription Factor TFIIH. *Journal of Biological Chemistry* **270**, 12973-12976

59. Canturk, F., Karaman, M., Selby, C. P., Kemp, M. G., Kulaksiz-Erkmen, G., Hu, J., Li, W., Lindsey-Boltz, L. A., and Sancar, A. (2016) Nucleotide excision repair by dual incisions in plants. *Proceedings of the National Academy of Sciences of the United States of America* **113**, 4706-4710

60. Sibghatullah, Husain, I., Carlton, W., and Sancar, A. (1989) Human nucleotide excision repair in vitro: repair of pyrimidine dimers, psoralen and cisplatin adducts by HeLa cell-free extract. *Nucleic Acids Res* **17**, 4471-4484

61. Sancar, A. (1996) DNA excision repair. *Annu Rev Biochem* **65**, 43-81

62. Reardon, J. T., and Sancar, A. (2005) Nucleotide excision repair. *Prog Nucleic Acid Res Mol Biol* **79**, 183-235

63. Wood, R. D. (1997) Nucleotide excision repair in mammalian cells. *The Journal of biological chemistry* **272**, 23465-23468

64. Mu, D., Hsu, D. S., and Sancar, A. (1996) Reaction mechanism of human DNA repair excision nuclease. *The Journal of biological chemistry* **271**, 8285-8294

65. Mu, D., Wakasugi, M., Hsu, D. S., and Sancar, A. (1997) Characterization of reaction intermediates of human excision repair nuclease. *The Journal of biological chemistry* **272**, 28971-28979

66. Wakasugi, M., and Sancar, A. (1998) Assembly, subunit composition, and footprint of human DNA repair excision nuclease. *Proceedings of the National Academy of Sciences of the United States of America* **95**, 6669-6674

67. Hu, J., Choi, J. H., Gaddameedhi, S., Kemp, M. G., Reardon, J. T., and Sancar, A. (2013) Nucleotide excision repair in human cells: fate of the excised oligonucleotide carrying DNA damage in vivo. *The Journal of biological chemistry* **288**, 20918-20926

68. Kemp, M. G., Reardon, J. T., Lindsey-Boltz, L. A., and Sancar, A. (2012) Mechanism of release and fate of excised oligonucleotides during nucleotide excision repair. *The Journal of biological chemistry* **287**, 22889-22899

69. Kemp, M. G., and Sancar, A. (2012) DNA excision repair: where do all the dimers go? *Cell Cycle* **11**, 2997-3002

70. Choi, J. H., Gaddameedhi, S., Kim, S. Y., Hu, J., Kemp, M. G., and Sancar, A. (2014) Highly specific and sensitive method for measuring nucleotide excision repair kinetics of ultraviolet photoproducts in human cells. *Nucleic Acids Res* **42**, e29

71. Kemp, M. G., Gaddameedhi, S., Choi, J. H., Hu, J., and Sancar, A. (2014) DNA repair synthesis and ligation affect the processing of excised oligonucleotides generated by human nucleotide excision repair. *The Journal of biological chemistry* **289**, 26574-26583

72. Choi, J. H., Kim, S. Y., Kim, S. K., Kemp, M. G., and Sancar, A. (2015) An Integrated Approach for Analysis of the DNA Damage Response in Mammalian Cells: NUCLEOTIDE EXCISION REPAIR, DNA DAMAGE CHECKPOINT, AND APOPTOSIS. *The Journal of biological chemistry* **290**, 28812-28821

73. Lindsey-Boltz, L. A., Kemp, M. G., Hu, J., and Sancar, A. (2015) Analysis of Ribonucleotide Removal from DNA by Human Nucleotide Excision Repair. *The Journal of biological chemistry* **290**, 29801-29807

74. Lehmann, A. R. (2011) DNA polymerases and repair synthesis in NER in human cells. *DNA Repair (Amst)* **10**, 730-733

75. Reardon, J. T., Thompson, L. H., and Sancar, A. (1997) Rodent UV-sensitive mutant cell lines in complementation groups 6-10 have normal general excision repair activity. *Nucleic Acids Res* **25**, 1015-1021

76. Lindsey-Boltz, L. A., Kemp, M. G., Reardon, J. T., DeRocco, V., Iyer, R. R., Modrich, P., and Sancar, A. (2014) Coupling of human DNA excision repair and the DNA damage checkpoint in a defined in vitro system. *The Journal of biological chemistry* **289**, 5074-5082

77. Moser, J., Kool, H., Giakzidis, I., Caldecott, K., Mullenders, L. H., and Fousteri, M. I. (2007) Sealing of chromosomal DNA nicks during nucleotide excision repair requires XRCC1 and DNA ligase III alpha in a cell-cycle-specific manner. *Molecular cell* **27**, 311-323

78. Selby, C. P., and Sancar, A. (1997) Cockayne syndrome group B protein enhances elongation by RNA polymerase II. *Proceedings of the National Academy of Sciences of the United States of America* **94**, 11205-11209

79. Hanawalt, P. C., and Spivak, G. (2008) Transcription-coupled DNA repair: two decades of progress and surprises. *Nature reviews. Molecular cell biology* **9**, 958-970

80. Xu, J., Lahiri, I., Wang, W., Wier, A., Cianfrocco, M. A., Chong, J., Hare, A. A., Dervan, P. B., DiMaio, F., Leschziner, A. E., and Wang, D. (2017) Structural basis for the initiation of eukaryotic transcription-coupled DNA repair. *Nature* **551**, 653-657

81. Hu, J., Lieb, J. D., Sancar, A., and Adar, S. (2016) Cisplatin DNA damage and repair maps of the human genome at single-nucleotide resolution. *Proceedings of the National Academy of Sciences of the United States of America* **113**, 11507-11512

82. Hu, J., Li, W., Adebali, O., Yang, Y., Oztas, O., Selby, C. P., and Sancar, A. (2019) Genome-wide mapping of nucleotide excision repair with XR-seq. *Nat Protoc* **14**, 248-282

83. Cleaver, J. E. (1968) Defective repair replication of DNA in xeroderma pigmentosum. *Nature* **218**, 652-656

84. Halpern, J., Hopping, B., and Brostoff, J. M. (2008) Photosensitivity, corneal scarring and developmental delay: Xeroderma Pigmentosum in a tropical country. *Cases J* **1**, 254

85. Cleaver, J. E., and Bootsma, D. (1975) Xeroderma pigmentosum: biochemical and genetic characteristics. *Annu Rev Genet* **9**, 19-38

86. Bradbury, P. A., Kulke, M. H., Heist, R. S., Zhou, W., Ma, C., Xu, W., Marshall, A. L., Zhai, R., Hooshmand, S. M., Asomaning, K., Su, L., Shepherd, F. A., Lynch, T. J., Wain, J. C., Christiani, D. C., and Liu, G. (2009) Cisplatin pharmacogenetics, DNA repair polymorphisms, and esophageal cancer outcomes. *Pharmacogenet Genomics* **19**, 613-625

87. Liu, D., Wu, J., Shi, G. Y., Zhou, H. F., and Yu, Y. (2014) Role of XRCC1 and ERCC5 polymorphisms on clinical outcomes in advanced non-small cell lung cancer. *Genet Mol Res* **13**, 3100-3107

88. Zhang, R., Jia, M., Xue, H., Xu, Y., Wang, M., Zhu, M., Sun, M., Chang, J., and Wei, Q. (2017) Genetic variants in ERCC1 and XPC predict survival outcome of non-small cell lung cancer patients treated with platinum-based therapy. *Sci Rep* **7**, 10702

89. Song, X., Wang, S., Hong, X., Li, X., Zhao, X., Huai, C., Chen, H., Gao, Z., Qian, J., Wang, J., Han, B., Bai, C., Li, Q., Wu, J., and Lu, D. (2017) Single nucleotide polymorphisms of nucleotide excision repair pathway are significantly associated with outcomes of platinum-based chemotherapy in lung cancer. *Sci Rep* **7**, 11785

90. Sullivan, I., Salazar, J., Majem, M., Pallares, C., Del Rio, E., Paez, D., Baiget, M., and Barnadas, A. (2014) Pharmacogenetics of the DNA repair pathways in advanced non-small cell lung cancer patients treated with platinum-based chemotherapy. *Cancer Lett* **353**, 160-166

91. Di Francia, R., De Lucia, L., Di Paolo, M., Di Martino, S., Del Pup, L., De Monaco, A., Lleshi, A., and Berretta, M. (2015) Rational selection of predictive pharmacogenomics test for the Fluoropyrimidine/Oxaliplatin based therapy. *Eur Rev Med Pharmacol Sci* **19**, 4443-4454

92. Masuda, H., Ozols, R. F., Lai, G. M., Fojo, A., Rothenberg, M., and Hamilton, T. C. (1988) Increased DNA repair as a mechanism of acquired resistance to cis-diamminedichloroplatinum (II) in human ovarian cancer cell lines. *Cancer Res* **48**, 5713-5716

93. Scurry, J., van Zyl, B., Gulliver, D., Otton, G., Jaaback, K., Lombard, J., Vilain, R. E., and Bowden, N. A. (2018) Nucleotide excision repair protein ERCC1 and tumour-infiltrating lymphocytes are potential biomarkers of neoadjuvant platinum resistance in high grade serous ovarian cancer. *Gynecol Oncol* **151**, 306-310

94. Koberle, B., Masters, J. R., Hartley, J. A., and Wood, R. D. (1999) Defective repair of cisplatin-induced DNA damage caused by reduced XPA protein in testicular germ cell tumours. *Current biology : CB* **9**, 273-276

95. Wu, X., Fan, W., Xu, S., and Zhou, Y. (2003) Sensitization to the cytotoxicity of cisplatin by transfection with nucleotide excision repair gene xeroderma pigmentosun group A antisense RNA in human lung adenocarcinoma cells. *Clin Cancer Res* **9**, 5874-5879

96. Fang, C., Chen, Y. X., Wu, N. Y., Yin, J. Y., Li, X. P., Huang, H. S., Zhang, W., Zhou, H. H., and Liu, Z. Q. (2017) MiR-488 inhibits proliferation and cisplatin sensibility in non-small-cell lung cancer (NSCLC) cells by activating the eIF3a-mediated NER signaling pathway. *Sci Rep* **7**, 40384

97. Yu, W. K., Wang, Z., Fong, C. C., Liu, D., Yip, T. C., Au, S. K., Zhu, G., and Yang, M. (2017) Chemoresistant lung cancer stem cells display high DNA repair capability to remove cisplatin-induced DNA damage. *Br J Pharmacol* **174**, 302-313

98. Barckhausen, C., Roos, W. P., Naumann, S. C., and Kaina, B. (2014) Malignant melanoma cells acquire resistance to DNA interstrand cross-linking chemotherapeutics by p53-triggered upregulation of DDB2/XPC-mediated DNA repair. *Oncogene* **33**, 1964-1974

99. Huang, Y., Wang, X., Niu, X., Wang, X., Jiang, R., Xu, T., Liu, Y., Liang, L., Ou, X., Xing, X., Li, W., and Hu, C. (2017) EZH2 suppresses the nucleotide excision repair in nasopharyngeal carcinoma by silencing XPA gene. *Mol Carcinog* **56**, 447-463

100. Fu, X., Hu, J., Han, H. Y., Hua, Y. J., Zhou, L., Shuai, W. D., Du, W. Y., Kuang, C. M., Chen, S., Huang, W., and Liu, R. Y. (2015) High expression of XPA confers poor prognosis for nasopharyngeal carcinoma patients treated with platinum-based chemoradiotherapy. *Oncotarget* **6**, 28478-28490

101. Prochnow, S., Wilczak, W., Bosch, V., Clauditz, T. S., and Muenscher, A. (2019) ERCC1, XPF and XPA-locoregional differences and prognostic value of DNA repair protein expression in patients with head and neck squamous cell carcinoma. *Clin Oral Investig* **23**, 3319-3329

102. Modi, S., Kir, D., Giri, B., Majumder, K., Arora, N., Dudeja, V., Banerjee, S., and Saluja, A. K. (2016) Minnelide Overcomes Oxaliplatin Resistance by Downregulating the DNA Repair Pathway in Pancreatic Cancer. *J Gastrointest Surg* **20**, 13-23; discussion 23-14

103. Herath, N. I., Devun, F., Lienafa, M. C., Herbette, A., Denys, A., Sun, J. S., and Dutreix, M. (2016) The DNA Repair Inhibitor DT01 as a Novel Therapeutic Strategy for Chemosensitization of Colorectal Liver Metastasis. *Mol Cancer Ther* **15**, 15-22

104. Deng, Q., Yang, H., Lin, Y., Qiu, Y., Gu, X., He, P., Zhao, M., Wang, H., Xu, Y., Lin, Y., Jiang, J., He, J., and Zhou, J. X. (2014) Prognostic value of ERCC1 mRNA expression in non-small cell lung cancer, breast cancer, and gastric cancer in patients from Southern China. *Int J Clin Exp Pathol* **7**, 8312-8321

105. Olaussen, K. A., Dunant, A., Fouret, P., Brambilla, E., Andre, F., Haddad, V., Taranchon, E., Filipits, M., Pirker, R., Popper, H. H., Stahel, R., Sabatier, L., Pignon, J. P., Tursz, T., Le Chevalier, T., Soria, J. C., and Investigators, I. B. (2006) DNA repair by ERCC1 in non-small-cell lung cancer and cisplatin-based adjuvant chemotherapy. *N Engl J Med* **355**, 983-991

106. Pajuelo-Lozano, N., Bargiela-Iparraguirre, J., Dominguez, G., Quiroga, A. G., Perona, R., and Sanchez-Perez, I. (2018) XPA, XPC, and XPD Modulate Sensitivity in Gastric Cisplatin Resistance Cancer Cells. *Front Pharmacol* **9**, 1197

107. Weaver, D. A., Crawford, E. L., Warner, K. A., Elkhairi, F., Khuder, S. A., and Willey, J. C. (2005) ABCC5, ERCC2, XPA and XRCC1 transcript abundance levels correlate with cisplatin chemoresistance in non-small cell lung cancer cell lines. *Mol Cancer* **4**, 18

108. Kang, J., D'Andrea, A. D., and Kozono, D. (2012) A DNA repair pathway-focused score for prediction of outcomes in ovarian cancer treated with platinum-based chemotherapy. *J Natl Cancer Inst* **104**, 670-681

109. Stubbert, L. J., Smith, J. M., and McKay, B. C. (2010) Decreased transcription-coupled nucleotide excision repair capacity is associated with increased p53- and MLH1-independent apoptosis in response to cisplatin. *BMC Cancer* **10**, 207

110. Slyskova, J., Sabatella, M., Ribeiro-Silva, C., Stok, C., Theil, A. F., Vermeulen, W., and Lans, H. (2018) Base and nucleotide excision repair facilitate resolution of platinum drugs-induced transcription blockage. *Nucleic Acids Res* **46**, 9537-9549

111. Arora, S., Kothandapani, A., Tillison, K., Kalman-Maltese, V., and Patrick, S. M. (2010) Downregulation of XPF-ERCC1 enhances cisplatin efficacy in cancer cells. *DNA Repair (Amst)* **9**, 745-753

112. Arora, S., Heyza, J., Zhang, H., Kalman-Maltese, V., Tillison, K., Floyd, A. M., Chalfin, E. M., Bepler, G., and Patrick, S. M. (2016) Identification of small molecule inhibitors of ERCC1-XPF that inhibit DNA repair and potentiate cisplatin efficacy in cancer cells. *Oncotarget* **7**, 75104-75117

113. Saintas, E., Abrahams, L., Ahmad, G. T., Ajakaiye, A. M., AlHumaidi, A. S., Ashmore-Harris, C., Clark, I., Dura, U. K., Fixmer, C. N., Ike-Morris, C., Mato Prado, M., McCullough, D., Mishra, S., Scholer, K. M., Timur, H., Williamson, M. D., Alatsatianos, M., Bahsoun, B., Blackburn, E., Hogwood, C. E., Lithgow, P. E., Rowe, M., Yiangou, L., Rothweiler, F., Cinatl, J., Jr., Zehner, R., Baines, A. J., Garrett, M. D., Gourlay, C. W., Griffin, D. K., Gullick, W. J., Hargreaves, E., Howard, M. J., Lloyd, D. R., Rossman, J. S., Smales, C. M., Tsaousis, A. D., von der Haar, T., Wass, M. N., and Michaelis, M. (2017) Acquired resistance to oxaliplatin is not directly associated with increased resistance to DNA damage in SK-N-ASrOXALI4000, a newly established oxaliplatin-resistant sub-line of the neuroblastoma cell line SK-N-AS. *PLoS One* **12**, e0172140

114. Bowden, N. A. (2014) Nucleotide excision repair: why is it not used to predict response to platinum-based chemotherapy? *Cancer Lett* **346**, 163-171

115. Partch, C. L., Green, C. B., and Takahashi, J. S. (2014) Molecular architecture of the mammalian circadian clock. *Trends Cell Biol* **24**, 90-99

116. Hardin, P. E., and Panda, S. (2013) Circadian timekeeping and output mechanisms in animals. *Curr Opin Neurobiol* **23**, 724-731

117. Levi, F., and Schibler, U. (2007) Circadian Rhythms: Mechanisms and Therapeutic Implications. *Annual Review of Pharmacology and Toxicology* **47**, 593-628

118. Reppert, S. M., and Weaver, D. R. (2002) Coordination of circadian timing in mammals. *Nature* **418**, 935-941

119. Vitaterna, M. H., Selby, C. P., Todo, T., Niwa, H., Thompson, C., Fruechte, E. M., Hitomi, K., Thresher, R. J., Ishikawa, T., Miyazaki, J., Takahashi, J. S., and Sancar, A. (1999) Differential regulation of mammalian period genes and circadian rhythmicity by cryptochromes 1 and 2. *Proceedings of the National Academy of Sciences of the United States of America* **96**, 12114-12119

120. Shearman, L. P., Sriram, S., Weaver, D. R., Maywood, E. S., Chaves, I., Zheng, B., Kume, K., Lee, C. C., van der, G. T. J., Horst, Hastings, M. H., and Reppert, S. M. (2000) Interacting Molecular Loops in the Mammalian Circadian Clock. *Science* **288**, 1013-1019

121. Kume, K., Zylka, M. J., Sriram, S., Shearman, L. P., Weaver, D. R., Jin, X., Maywood, E. S., Hastings, M. H., and Reppert, S. M. (1999) mCRY1 and mCRY2 Are Essential Components of the Negative Limb of the Circadian Clock Feedback Loop. *Cell* **98**, 193-205

122. Zheng, B., Larkin, D. W., Albrecht, U., Sun, Z. S., Sage, M., Eichele, G., Lee, C. C., and Bradley, A. (1999) The mPer2 gene encodes a functional component of the mammalian circadian clock. *Nature* **400**, 169-173

123. Hughes, M., Deharo, L., Pulivarthy, S. R., Gu, J., Hayes, K., Panda, S., and Hogenesch, J. B. (2007) High-resolution time course analysis of gene expression from pituitary. *Cold Spring Harb Symp Quant Biol* **72**, 381-386

124. Ko, C. H., and Takahashi, J. S. (2006) Molecular components of the mammalian circadian clock. *Human Molecular Genetics* **15**, R271-R277

125. Kang, T. H., Reardon, J. T., and Sancar, A. (2011) Regulation of nucleotide excision repair activity by transcriptional and post-transcriptional control of the XPA protein. *Nucleic Acids Res* **39**, 3176-3187

126. Kang, T. H., Lindsey-Boltz, L. A., Reardon, J. T., and Sancar, A. (2010) Circadian control of XPA and excision repair of cisplatin-DNA damage by cryptochrome and HERC2 ubiquitin ligase. *Proceedings of the National Academy of Sciences of the United States of America* **107**, 4890-4895

127. Kang, T. H., Reardon, J. T., Kemp, M., and Sancar, A. (2009) Circadian oscillation of nucleotide excision repair in mammalian brain. *Proceedings of the National Academy of Sciences of the United States of America* **106**, 2864-2867

128. Yang, Y., Adebali, O., Wu, G., Selby, C. P., Chiou, Y. Y., Rashid, N., Hu, J., Hogenesch, J. B., and Sancar, A. (2018) Cisplatin-DNA adduct repair of transcribed genes is controlled by two circadian programs in mouse tissues. *Proceedings of the National Academy of Sciences of the United States of America* **115**, E4777-E4785

129. Choi, J.-H., Gaddameedhi, S., Kim, S.-Y., Hu, J., Kemp, M. G., and Sancar, A. (2014) Highly specific and sensitive method for measuring nucleotide excision repair kinetics of ultraviolet photoproducts in human cells. *Nucleic acids research* **42**, e29-e29

130. Choi, J.-H., Kim, S.-Y., Kim, S.-K., Kemp, M. G., and Sancar, A. (2015) An Integrated Approach for Analysis of the DNA Damage Response in Mammalian Cells: NUCLEOTIDE EXCISION REPAIR, DNA DAMAGE CHECKPOINT, AND APOPTOSIS. *Journal of Biological Chemistry* **290**, 28812-28821

131. Kemp, M. G., Gaddameedhi, S., Choi, J.-H., Hu, J., and Sancar, A. (2014) DNA repair synthesis and ligation affect the processing of excised oligonucleotides

generated by human nucleotide excision repair. *The Journal of biological chemistry* **289**, 26574-26583

132. Canturk, F., Karaman, M., Selby, C. P., Kemp, M. G., Kulaksiz-Erkmen, G., Hu, J., Li, W., Lindsey-Boltz, L. A., and Sancar, A. (2016) Nucleotide excision repair by dual incisions in plants. *Proceedings of the National Academy of Sciences* **113**, 4706-4710

133. Lindsey-Boltz, L. A., Kemp, M. G., Hu, J., and Sancar, A. (2015) Analysis of Ribonucleotide Removal from DNA by Human Nucleotide Excision Repair. *The Journal of biological chemistry* **290**, 29801-29807

134. Vaughn, C. M., Selby, C. P., Yang, Y., Hsu, D. S., and Sancar, A. (2020) Genome-wide single-nucleotide resolution of oxaliplatin–DNA adduct repair in drug-sensitive and -resistant colorectal cancer cell lines. *Journal of Biological Chemistry*

135. Vaughn, C. M., Selby, C. P., Yang, Y., Hsu, D. S., and Sancar, A. (2020) Genome-wide single-nucleotide resolution of oxaliplatin-DNA adduct repair in drug-sensitive and -resistant colorectal cancer cell lines. *The Journal of biological chemistry*

136. Benson, A. B., 3rd, Venook, A. P., Cederquist, L., Chan, E., Chen, Y. J., Cooper, H. S., Deming, D., Engstrom, P. F., Enzinger, P. C., Fichera, A., Grem, J. L., Grothey, A., Hochster, H. S., Hoffe, S., Hunt, S., Kamel, A., Kirilcuk, N., Krishnamurthi, S., Messersmith, W. A., Mulcahy, M. F., Murphy, J. D., Nurkin, S., Saltz, L., Sharma, S., Shibata, D., Skibber, J. M., Sofocleous, C. T., Stoffel, E. M., Stotsky-Himelfarb, E., Willett, C. G., Wu, C. S., Gregory, K. M., and Freedman-Cass, D. (2017) Colon Cancer, Version 1.2017, NCCN Clinical Practice Guidelines in Oncology. *J Natl Compr Canc Netw* **15**, 370-398

137. de Gramont, A., Schmoll, H. J., Cervantes, A., and Tournigand, C. (2003) The evolving role of oxaliplatin in the management of colorectal cancer. *Colorectal disease : the official journal of the Association of Coloproctology of Great Britain and Ireland* **5 Suppl 3**, 10-19

138. Riou, L., Eveno, E., van Hoffen, A., van Zeeland, A. A., Sarasin, A., and Mullenders, L. H. F. (2004) Differential Repair of the Two Major UV-Induced Photolesions in Trichothiodystrophy Fibroblasts. *Cancer Research* **64**, 889-894

139. Yang, Y., Liu, Z., Selby, C. P., and Sancar, A. (2019) Long-term, genome-wide kinetic analysis of the effect of the circadian clock and transcription on the repair of cisplatin-DNA adducts in the mouse liver. *The Journal of biological chemistry* **294**, 11960-11968

140. Deger, N., Yang, Y., Lindsey-Boltz, L. A., Sancar, A., and Selby, C. P. (2019) Drosophila, which lacks canonical transcription-coupled repair proteins, performs transcription-coupled repair. *J Biol Chem* **294**, 18092-18098

141. Ahmed, D., Eide, P. W., Eilertsen, I. A., Danielsen, S. A., Eknæs, M., Hektoen, M., Lind, G. E., and Lothe, R. A. (2013) Epigenetic and genetic features of 24 colon cancer cell lines. *Oncogenesis* **2**, e71-e71

142. Novakovic, P., Stempak, J. M., Sohn, K.-J., and Kim, Y.-I. (2005) Effects of folate deficiency on gene expression in the apoptosis and cancer pathways in colon cancer cells. *Carcinogenesis* **27**, 916-924

143. Unger, F. T., Klasen, H. A., Tchartchian, G., de Wilde, R. L., and Witte, I. (2009) DNA damage induced by cis- and carboplatin as indicator for in vitro sensitivity of ovarian carcinoma cells. *BMC Cancer* **9**, 359

144. Mezencev, R., Matyunina, L. V., Wagner, G. T., and McDonald, J. F. (2016) Acquired resistance of pancreatic cancer cells to cisplatin is multifactorial with cell context-dependent involvement of resistance genes. *Cancer Gene Ther* **23**, 446-453

145. Massari, F., Santoni, M., Ciccarese, C., Brunelli, M., Conti, A., Santini, D., Montironi, R., Cascinu, S., and Tortora, G. (2015) Emerging concepts on drug resistance in bladder cancer: Implications for future strategies. *Crit Rev Oncol Hematol* **96**, 81-90

146. Fang, Y., Zhang, C., Wu, T., Wang, Q., Liu, J., and Dai, P. (2017) Transcriptome Sequencing Reveals Key Pathways and Genes Associated with Cisplatin Resistance in Lung Adenocarcinoma A549 Cells. *PLoS One* **12**, e0170609

147. Oztas, O., Selby, C. P., Sancar, A., and Adebali, O. (2018) Genome-wide excision repair in Arabidopsis is coupled to transcription and reflects circadian gene expression patterns. *Nature communications* **9**, 1503

148. Li, W., Adebali, O., Yang, Y., Selby, C. P., and Sancar, A. (2018) Single-nucleotide resolution dynamic repair maps of UV damage in Saccharomyces cerevisiae genome. *Proc Natl Acad Sci U S A* **115**, E3408-e3415

149. Guffanti, F., Fratelli, M., Ganzinelli, M., Bolis, M., Ricci, F., Bizzaro, F., Chilà, R., Sina, F. P., Fruscio, R., Lupia, M., Cavallaro, U., Cappelletti, M. R., Generali, D., Giavazzi, R., and Damia, G. (2018) Platinum sensitivity and DNA repair in a recently established panel of patient-derived ovarian carcinoma xenografts. *Oncotarget* **9**, 24707-24717

150. Howell, S. B., Safaei, R., Larson, C. A., and Sailor, M. J. (2010) Copper transporters and the cellular pharmacology of the platinum-containing cancer drugs. *Molecular pharmacology* **77**, 887-894

151. Katano, K., Kondo, A., Safaei, R., Holzer, A., Samimi, G., Mishima, M., Kuo, Y. M., Rochdi, M., and Howell, S. B. (2002) Acquisition of resistance to cisplatin is accompanied by changes in the cellular pharmacology of copper. *Cancer Res* **62**, 6559-6565

152. Samimi, G., Safaei, R., Katano, K., Holzer, A. K., Rochdi, M., Tomioka, M., Goodman, M., and Howell, S. B. (2004) Increased expression of the copper efflux transporter ATP7A mediates resistance to cisplatin, carboplatin, and oxaliplatin in ovarian cancer cells. *Clin Cancer Res* **10**, 4661-4669

153. Love, M. I., Huber, W., and Anders, S. (2014) Moderated estimation of fold change and dispersion for RNA-seq data with DESeq2. *Genome Biology* **15**, 550

154. Meynard, D., Le Morvan, V., Bonnet, J., and Robert, J. (2007) Functional analysis of the gene expression profiles of colorectal cancer cell lines in relation to oxaliplatin and cisplatin cytotoxicity. *Oncol Rep* **17**, 1213-1221

155. Szklarczyk, D., Morris, J. H., Cook, H., Kuhn, M., Wyder, S., Simonovic, M., Santos, A., Doncheva, N. T., Roth, A., Bork, P., Jensen, L. J., and von Mering, C. (2017) The STRING database in 2017: quality-controlled protein-protein association networks, made broadly accessible. *Nucleic acids research* **45**, D362-D368

156. Zhang, J., Jiang, Y., Zhu, J., Wu, T., Ma, J., Du, C., Chen, S., Li, T., Han, J., and Wang, X. (2017) Overexpression of long non-coding RNA colon cancer-associated transcript 2 is associated with advanced tumor progression and poor prognosis in patients with colorectal cancer. *Oncol Lett* **14**, 6907-6914

157. Ozawa, T., Matsuyama, T., Toiyama, Y., Takahashi, N., Ishikawa, T., Uetake, H., Yamada, Y., Kusunoki, M., Calin, G., and Goel, A. (2017) CCAT1 and CCAT2 long noncoding RNAs, located within the 8q.24.21 'gene desert', serve as important prognostic biomarkers in colorectal cancer. *Ann Oncol* **28**, 1882-1888

158. Chen, S., Wu, H., Lv, N., Wang, H., Wang, Y., Tang, Q., Shao, H., and Sun, C. (2016) LncRNA CCAT2 predicts poor prognosis and regulates growth and metastasis in small cell lung cancer. *Biomedicine & pharmacotherapy = Biomedecine & pharmacotherapie* **82**, 583-588

159. Ling, H., Spizzo, R., Atlasi, Y., Nicoloso, M., Shimizu, M., Redis, R. S., Nishida, N., Gafa, R., Song, J., Guo, Z., Ivan, C., Barbarotto, E., De Vries, I., Zhang, X., Ferracin, M., Churchman, M., van Galen, J. F., Beverloo, B. H., Shariati, M., Haderk, F., Estecio, M. R., Garcia-Manero, G., Patijn, G. A., Gotley, D. C., Bhardwaj, V., Shureiqi, I., Sen, S., Multani, A. S., Welsh, J., Yamamoto, K., Taniguchi, I., Song, M. A., Gallinger, S., Casey, G., Thibodeau, S. N., Le Marchand, L., Tiirikainen, M., Mani, S. A., Zhang, W., Davuluri, R. V., Mimori, K., Mori, M., Sieuwerts, A. M., Martens, J. W., Tomlinson, I., Negrini, M., Berindan-Neagoe, I., Foekens, J. A., Hamilton, S. R., Lanza, G., Kopetz, S., Fodde, R., and Calin, G. A. (2013) CCAT2, a novel noncoding RNA mapping to 8q24, underlies metastatic progression and chromosomal instability in colon cancer. *Genome Res* **23**, 1446-1461

160. Gong, W. J., Yin, J. Y., Li, X. P., Fang, C., Xiao, D., Zhang, W., Zhou, H. H., Li, X., and Liu, Z. Q. (2016) Association of well-characterized lung cancer lncRNA

polymorphisms with lung cancer susceptibility and platinum-based chemotherapy response. *Tumour biology : the journal of the International Society for Oncodevelopmental Biology and Medicine* **37**, 8349-8358

161. Hahne, J. C., and Valeri, N. (2018) Non-Coding RNAs and Resistance to Anticancer Drugs in Gastrointestinal Tumors. *Front Oncol* **8**, 226-226

162. Johnson, S. W., Perez, R. P., Godwin, A. K., Yeung, A. T., Handel, L. M., Ozols, R. F., and Hamilton, T. C. (1994) Role of platinum-DNA adduct formation and removal in cisplatin resistance in human ovarian cancer cell lines. *Biochemical pharmacology* **47**, 689-697

163. Preston, T. J., Henderson, J. T., McCallum, G. P., and Wells, P. G. (2009) Base excision repair of reactive oxygen species-initiated 7,8-dihydro-8-oxo-2'-deoxyguanosine inhibits the cytotoxicity of platinum anticancer drugs. *Mol Cancer Ther* **8**, 2015-2026

164. Kim, E. S., Lee, J. J., He, G., Chow, C. W., Fujimoto, J., Kalhor, N., Swisher, S. G., Wistuba, II, Stewart, D. J., and Siddik, Z. H. (2012) Tissue platinum concentration and tumor response in non-small-cell lung cancer. *Journal of clinical oncology : official journal of the American Society of Clinical Oncology* **30**, 3345-3352

165. Veal, G. J., Dias, C., Price, L., Parry, A., Errington, J., Hale, J., Pearson, A. D., Boddy, A. V., Newell, D. R., and Tilby, M. J. (2001) Influence of cellular factors and pharmacokinetics on the formation of platinum-DNA adducts in leukocytes of children receiving cisplatin therapy. *Clin Cancer Res* **7**, 2205-2212

166. Wang, S., Scharadin, T. M., Zimmermann, M., Malfatti, M. A., Turteltaub, K. W., de Vere White, R., Pan, C.-X., and Henderson, P. T. (2018) Correlation of Platinum Cytotoxicity to Drug-DNA Adduct Levels in a Breast Cancer Cell Line Panel. *Chem Res Toxicol* **31**, 1293-1304

167. Hu, J., Selby, C. P., Adar, S., Adebali, O., and Sancar, A. (2017) Molecular mechanisms and genomic maps of DNA excision repair in Escherichia coli and humans. *The Journal of biological chemistry* **292**, 15588-15597

168. Li, W., Hu, J., Adebali, O., Adar, S., Yang, Y., Chiou, Y. Y., and Sancar, A. (2017) Human genome-wide repair map of DNA damage caused by the cigarette smoke carcinogen benzo[a]pyrene. *Proceedings of the National Academy of Sciences of the United States of America* **114**, 6752-6757

169. Reardon, J. T., and Sancar, A. (2005) Nucleotide Excision Repair. in *Progress in Nucleic Acid Research and Molecular Biology*, Academic Press. pp 183-235

170. Michelini, F., Jalihal, A. P., Francia, S., Meers, C., Neeb, Z. T., Rossiello, F., Gioia, U., Aguado, J., Jones-Weinert, C., Luke, B., Biamonti, G., Nowacki, M., Storici, F., Carninci, P., Walter, N. G., and d'Adda di Fagagna, F. (2018) From "Cellular"

RNA to “Smart” RNA: Multiple Roles of RNA in Genome Stability and Beyond. *Chemical Reviews* **118**, 4365-4403

171. Sharma, V., and Misteli, T. (2013) Non-coding RNAs in DNA damage and repair. *FEBS Lett* **587**, 1832-1839

172. d’Adda di Fagagna, F. (2014) A direct role for small non-coding RNAs in DNA damage response. *Trends in Cell Biology* **24**, 171-178

173. Tsafrir, D., Bacolod, M., Selvanayagam, Z., Tsafrir, I., Shia, J., Zeng, Z., Liu, H., Krier, C., Stengel, R. F., Barany, F., Gerald, W. L., Paty, P. B., Domany, E., and Notterman, D. A. (2006) Relationship of Gene Expression and Chromosomal Abnormalities in Colorectal Cancer. *Cancer Research* **66**, 2129-2137

174. Platzer, P., Upender, M. B., Wilson, K., Willis, J., Lutterbaugh, J., Nosrati, A., Willson, J. K. V., Mack, D., Ried, T., and Markowitz, S. (2002) Silence of Chromosomal Amplifications in Colon Cancer. *Cancer Research* **62**, 1134-1138

175. Biliran, H., Banerjee, S., Thakur, A., Sarkar, F. H., Bollig, A., Ahmed, F., Wu, J., Sun, Y., and Liao, J. D. (2007) c-Myc–Induced Chemosensitization Is Mediated by Suppression of Cyclin D1 Expression and Nuclear Factor-κB Activity in Pancreatic Cancer Cells. *Clinical Cancer Research* **13**, 2811-2821

176. Elbadawy, M., Usui, T., Yamawaki, H., and Sasaki, K. (2019) Emerging Roles of C-Myc in Cancer Stem Cell-Related Signaling and Resistance to Cancer Chemotherapy: A Potential Therapeutic Target Against Colorectal Cancer. *Int J Mol Sci* **20**, 2340

177. Gong, W.-J., Peng, J.-B., Yin, J.-Y., Li, X.-P., Zheng, W., Xiao, L., Tan, L.-M., Xiao, D., Chen, Y.-X., Li, X., Zhou, H.-H., and Liu, Z.-Q. (2017) Association between well-characterized lung cancer lncRNA polymorphisms and platinum-based chemotherapy toxicity in Chinese patients with lung cancer. *Acta Pharmacol Sin* **38**, 581-590

178. Lv, Z., Wei, J., You, W., Wang, R., Shang, J., Xiong, Y., Yang, H., Yang, X., and Fu, Z. (2017) Disruption of the c-Myc/miR-200b-3p/PRDX2 regulatory loop enhances tumor metastasis and chemotherapeutic resistance in colorectal cancer. *J Transl Med* **15**, 257-257

179. Shen, F., Feng, L., Zhou, J., Zhang, H., Xu, Y., Jiang, R., Zhang, H., and Chen, Y. (2019) Overexpression of CASC11 in ovarian squamous cell carcinoma mediates the development of cancer cell resistance to chemotherapy. *Gene* **710**, 363-366

180. Zhang, Y., Li, Q., Yu, S., Zhu, C., Zhang, Z., Cao, H., and Xu, J. (2019) Long non-coding RNA FAM84B-AS promotes resistance of gastric cancer to platinum drugs through inhibition of FAM84B expression. *Biochemical and Biophysical Research Communications* **509**, 753-762

181. Ried, T., Knutzen, R., Steinbeck, R., Blegen, H., Schröck, E., Heselmeyer, K., du Manoir, S., and Auer, G. (1996) Comparative genomic hybridization reveals a specific pattern of chromosomal gains and losses during the genesis of colorectal tumors. *Genes, Chromosomes and Cancer* **15**, 234-245

182. Bomme, L., Bardi, G., Pandis, N., Fenger, C., Kronborg, O., and Heim, S. (1994) Clonal karyotypic abnormalities in colorectal adenomas: Clues to the early genetic events in the adenoma-carcinoma sequence. *Genes, Chromosomes and Cancer* **10**, 190-196

183. He, Q.-J., Zeng, W.-F., Sham, J. S. T., Xie, D., Yang, X.-W., Lin, H.-L., Zhan, W.-H., Lin, F., Zeng, S.-D., Nie, D., Ma, L.-F., Li, C.-J., Lu, S., and Guan, X.-Y. (2003) Recurrent genetic alterations in 26 colorectal carcinomas and 21 adenomas from Chinese patients. *Cancer Genetics and Cytogenetics* **144**, 112-118

184. Bardi, G., Sukhikh, T., Pandis, N., Fenger, C., Kronborg, O., and Heim, S. (1995) Karyotypic characterization of colorectal adenocarcinomas. *Genes, Chromosomes and Cancer* **12**, 97-109

185. Ho, G. Y., Woodward, N., and Coward, J. I. G. (2016) Cisplatin versus carboplatin: comparative review of therapeutic management in solid malignancies. *Critical Reviews in Oncology/Hematology* **102**, 37-46

186. von der Maase, H., Hansen, S. W., Roberts, J. T., Dogliotti, L., Oliver, T., Moore, M. J., Bodrogi, I., Albers, P., Knuth, A., Lippert, C. M., Kerbrat, P., Sanchez Rovira, P., Wersall, P., Cleall, S. P., Roychowdhury, D. F., Tomlin, I., Visseren-Grul, C. M., and Conte, P. F. (2000) Gemcitabine and cisplatin versus methotrexate, vinblastine, doxorubicin, and cisplatin in advanced or metastatic bladder cancer: results of a large, randomized, multinational, multicenter, phase III study. *Journal of clinical oncology : official journal of the American Society of Clinical Oncology* **18**, 3068-3077

187. Sancar, A., Lindsey-Boltz, L. A., Gaddameedhi, S., Selby, C. P., Ye, R., Chiou, Y.-Y., Kemp, M. G., Hu, J., Lee, J. H., and Ozturk, N. (2015) Circadian Clock, Cancer, and Chemotherapy. *Biochemistry* **54**, 110-123

188. Hussain, M. M., and Pan, X. (2015) Circadian Regulation of Macronutrient Absorption. *Journal of Biological Rhythms* **30**, 459-469

189. Kang, T.-H., Lindsey-Boltz, L. A., Reardon, J. T., and Sancar, A. (2010) Circadian control of XPA and excision repair of cisplatin-DNA damage by cryptochrome and HERC2 ubiquitin ligase. *Proceedings of the National Academy of Sciences of the United States of America* **107**, 4890-4895

190. Kang, T.-H., Reardon, J. T., Kemp, M., and Sancar, A. (2009) Circadian oscillation of nucleotide excision repair in mammalian brain. *Proceedings of the National Academy of Sciences of the United States of America* **106**, 2864-2867

191. Kang, T.-H., Reardon, J. T., and Sancar, A. (2011) Regulation of nucleotide excision repair activity by transcriptional and post-transcriptional control of the XPA protein. *Nucleic Acids Research* **39**, 3176-3187

192. Comas, M., Kuropatwinski, K. K., Wrobel, M., Toshkov, I., and Antoch, M. P. (2014) Daily rhythms are retained both in spontaneously developed sarcomas and in xenografts grown in immunocompromised SCID mice. *Chronobiol Int* **31**, 901-910

193. Hussain, M. M., and Pan, X. (2015) Circadian Regulation of Macronutrient Absorption. *J Biol Rhythms* **30**, 459-469

194. Pizarro, A., Hayer, K., Lahens, N. F., and Hogenesch, J. B. (2013) CircaDB: a database of mammalian circadian gene expression profiles. *Nucleic acids research* **41**, D1009-D1013

195. Gorbacheva, V. Y., Kondratov, R. V., Zhang, R., Cherukuri, S., Gudkov, A. V., Takahashi, J. S., and Antoch, M. P. (2005) Circadian sensitivity to the chemotherapeutic agent cyclophosphamide depends on the functional status of the CLOCK/BMAL1 transactivation complex. *Proceedings of the National Academy of Sciences of the United States of America* **102**, 3407-3412

196. Yu, E. A., and Weaver, D. R. (2011) Disrupting the circadian clock: gene-specific effects on aging, cancer, and other phenotypes. *Aging (Albany NY)* **3**, 479-493

197. Anafi, R. C., Francey, L. J., Hogenesch, J. B., and Kim, J. (2017) CYCLOPS reveals human transcriptional rhythms in health and disease. *Proceedings of the National Academy of Sciences of the United States of America* **114**, 5312-5317

198. Sharp, C. N., and Siskind, L. J. (2017) Developing better mouse models to study cisplatin-induced kidney injury. *Am J Physiol Renal Physiol* **313**, F835-F841